IMPROVING SERVICEABILITY OF CONCRETE INFRASTRUCTURE USING PRESTRESSING TECHNIQUE

A Dissertation

by

SUN HEE PARK

Submitted to the Office of Graduate and Professional Studies of
Texas A&M University
in partial fulfillment of the requirements for the degree of

DOCTOR OF PHILOSOPHY

Chair of Committee,	Stefan Hurlebaus
Co-Chair of Committee,	John B. Mander
Committee Members,	Anna C. Birely
	Steve C. Suh
Head of Department,	Robin Autenrieth

May 2020

Major Subject: Civil Engineering

ABSTRACT

The evaluation of existing concrete infrastructure is needed as design approaches have changed and load demands have increased due to traffic volume increase over the decades. The concrete structures experience increasing crack widths as well as unexpected new cracks especially on bridge structure and railroad ties. These cracks may decrease service life and are possible signs of structural deficiencies. This study is focused on two particular structures that experiencing such cracks: (i) inverted-T bent caps and (ii) railroad ties. Concepts for improving the performance of these structures are developed and experimentally validated.

For inverted-T bent caps, to address the ledge flexure, hanger, and/or punching shear deficiencies, which are identified in previous studies based on the current design specification, a conceptual design of eighteen alternative retrofit solutions are developed. The solutions include both metallic and fiber reinforced polymer materials, which are applied either with or without prestress. To identify which retrofit solutions are most viable for further investigation, a weighted sum decision making model is used based on six criteria: (i) strength, (ii) cost, (iii) constructability, (iv) dimensional/clearance constraints, (v) durability/longevity, and (vi) ease of monitoring. Among the most highly ranked solutions, the solutions utilizing prestressing techniques are selected: through-web post-tensioning threadbar with catcher channel (and end-region stiffener) and load balancing post-tensioning solutions. Based on one-half scale experimental tests, results demonstrate that the specimens are strengthened and the solutions are capable of

restraining any pre-existing cracks thereby delaying failure. Design and retrofit recommendations are provided, including their limitations.

For prestressing concrete railroad ties (sleepers), use of non-metallic aramid fiber reinforced polymer instead of the usual steel strands is explored. Such a switch in prestress materials may help in reducing electric leakage and corrosion issue when in service; however, the strength, stiffness, and crack resistance due to the material change should not be inferior. Test results on sleepers prestressed by aramid fiber reinforced polymer strands demonstrate that the strands are capable of providing sufficient strength and stiffness. Recommendations are made on how the performance could be improved by using smaller diameter strands to delaying further cracking beneath the rail seats.

ACKNOWLEDGEMENTS

I would like to express my deepest gratitude to my advisor, Dr. Stefan Hurlebaus, and co-advisor, Dr. John B. Mander, for or providing invaluable insight, expertise and guidance throughout the course of this research. I am grateful to Dr. Anna C. Birely for her support and valuable advice during entire research periods as a committee member. I also wish to thank Dr. Suh, serving on my committee.

I would like to thank Dr. Tevfik Terzioglu and Jilong Cui for their contribution and partnership and for being great friends. I am grateful to Charles Droddy, who provided advice and assistance during testing at High Bay Structural Laboratory. I also wish to thank the many graduate and undergraduate students who assisted in experimental tests.

Most importantly, I would like to express my heartfelt gratitude to my parents, Chong Yoon Park and Shook Tsoo Lim. None of this would have been possible without their love and continuous support. Also, thank you to my brilliant and loving husband Jinho Kim, and my little girl, Sua Kim. Without your support, I never would have accomplished this tremendous goal. Thank you for all your love, trust, and support throughout my entire academic career.

CONTRIBUTORS AND FUNDING SOURCES

Contributors

This work was supervised by a dissertation committee consisting of Professors Stefan Hurlebaus, John B. Mander, Anna C. Birely of the Department of Civil and Environmental Engineering and Professor Steve C. Suh of the Department of Mechanical Engineering.

All other work conducted for the dissertation was completed by the student independently.

Funding Sources

Graduate study was supported by the Dawn 92' & Dennis Wittry 91' Non-Endowed Fellowship from Texas A&M University.

This research was also supported by grants from the Federal Highway Administration (FHWA) and the Texas Department of Transportation (TxDOT) under Project 0-6893, and from the Association of American Railroads (AAR). The project was conducted at Texas A&M University (TAMU) through the Texas A&M Transportation Institute (TTI). The findings and opinions presented herein are those of the authors and are not necessarily those of the sponsoring agency.

TABLE OF CONTENTS

Page

LIST OF FIGURES

Page

LIST OF TABLES

Page

1. INTRODUCTION

1.1. Background and Motivation

In-service concrete infrastructure commonly faces problems related to increasing load demands by high volume of traffic and/or heavy haul traffic. Such concrete structures especially bridge structures and railroad tie experience unexpected cracks. This study focused on an inverted-T bent cap and railroad tie which are mainly experiencing such cracks as shown in Figure 1.1. These cracks may decrease service life and are possible signs of structural deficiencies. Deterioration of such deficient concrete infrastructure is one of the major problems faced by civil engineers.

The potential needs to strengthen inverted-T bent caps are the result of (a) changes in design provisions since the time construction in the late 1960s, and (b) interest in increasing the number of lanes on the bridge, thereby increasing the load demands. To improve the serviceability and ultimate strength of such inverted-T bent caps in accordance with current design codes, replacement or retrofitting is necessary, and retrofitting the bent caps may be an effective and economical solution as an alternative to replacement.

In the railroad tie industry, an increase of heavy track hauls causes significant stress increments on the railroad ties and results in serious cracks on the ties. Since such cracks on railroad ties may cause serviceability issues such as corrosion of prestressing steel or a track signal disturbance, the railroad ties with cracks need to be repaired and replaced to keep use the rail track.

The replacement of a damaged structure is not always practical on account of cost, interruption to traffic, and the acceptable condition of other parts of the structure. Improving the serviceability and ultimate strength of deficient concrete structures is essential to reduce the maintenance costs associated with demolishing and reconstructing these structures. Therefore, concepts for improving the performance of inverted-T bent caps and railroad ties are developed and experimentally validated in this study.

(a) Cracks on inverted-T bent cap in Austin, Texas

(b) Crack on concrete railroad ties. Reprinted from [1]

Figure 1.1. Cracks found on concrete infrastructure

1.2. Literature Review

To identify relevant technical information, this section reviews previous studies related to inverted-T bent caps and railroad ties in general and then strengthening methods to improve performance of inverted-T bent caps and railroad ties especially that using prestressing techniques.

1.2.1. Inverted-T Bent Caps

A bridge is divided broadly into three parts: superstructure, substructure, and foundation. Bent cap is a part of substructure that transfers the load from the girders to the columns. The main types of bent caps are drop bent cap, integral bent cap, and inverted-T bent cap, which is investigated this study. Figure 1.2 illustrates an inverted-T bent cap consisted of two parts: (1) stem (or web); and (2) ledges (or brackets). Girder loads are applied to the ledges and transferred to the web.

This section comprehensively reviewed previous studies on the behavior of inverted-T beams and then strengthening methods for inverted-T beams, standard-T beams, and rectangular bent caps.

1.2.1.1. Behavior of Inverted-T Beams

Many bridges with inverted-T bent caps were built in Texas during 1960s to provide increased clearance beneath bridges while providing lower overall height of a bridge. However, the bridges often experience undesirable cracking at the web-to-ledge interface of inverted-T bent caps (see Figure 1.1(a)) [2-7]. One major reason for the cracking may be the bridges were built when there was a general lack of understating of the inverted-T

beam behavior. For better understanding of behavior of the inverted-T beams, several studies to investigate behavior of inverted-T beams have been conducted.

Furlong et al. [2] experimentally investigated the difference between the behavior of inverted-T beams and T-beams. Figure 1.3 shows four major behaviors of inverted-T beams where must be given special consideration: (I) the web with increase of diagonal tension which is already considered in T-beams; (II) loads are supported by stirrups to transmit vertical forces into the web, called hanger tension; (III) bracket (or ledge) serves the beam itself as part of the tension portion (positive moment region) or the compression portion (negative moment region) of the beam, called as bracket flexure; and (IV) loads create a problem due to the small twisting suggested by the bracket shear.

Furlong and Mirza [3] investigated the behavior of the flanges (ledges) of the inverted-T beams and conducted experimental tests. They identified the six failure mechanisms of the inverted-T bent caps including three entire cross-section failure modes and three local failure modes. Conventional RC beams, which shaped in rectangular and/or standard-T, fail in entire cross-section; flexure, shear, torsion, or flexure-shear. On the other hand, inverted-T RC beams could fail due to other local causes such as hanger failure, punching shear in the flange, and bracket (ledge) failure in addition to the entire cross-section failure modes. Figure 1.4 shows local failure modes that are the critical failure modes in inverted-T bent caps. Based on the test results, they provided details of reinforcement and advice for design procedures applicable to the flanges as well as the shear and flexural strength of the inverted-T beams.

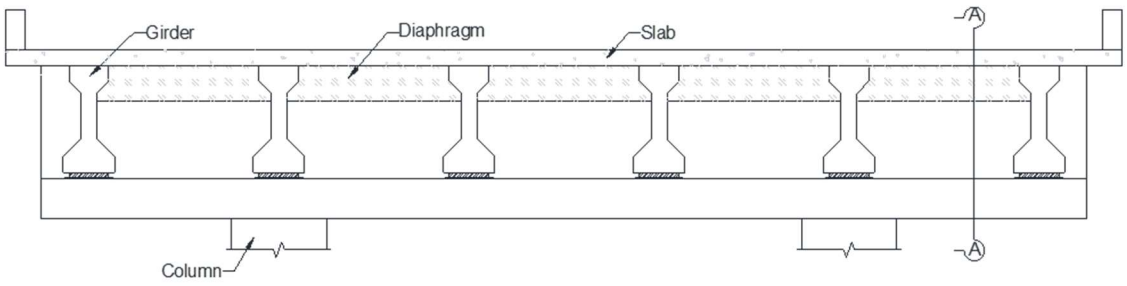

(a) Elevation

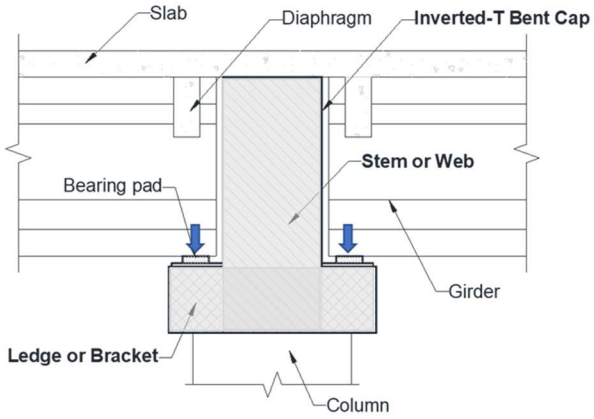

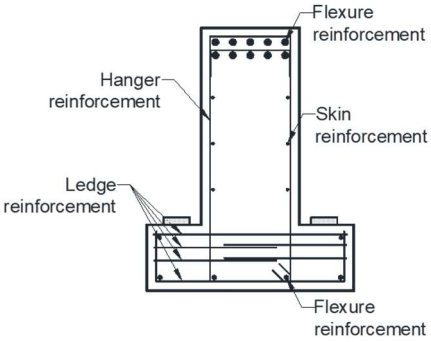

(b) Section A-A *(c) Reinforcement details*

Figure 1.2. Inverted-T bent cap geometry and reinforcement

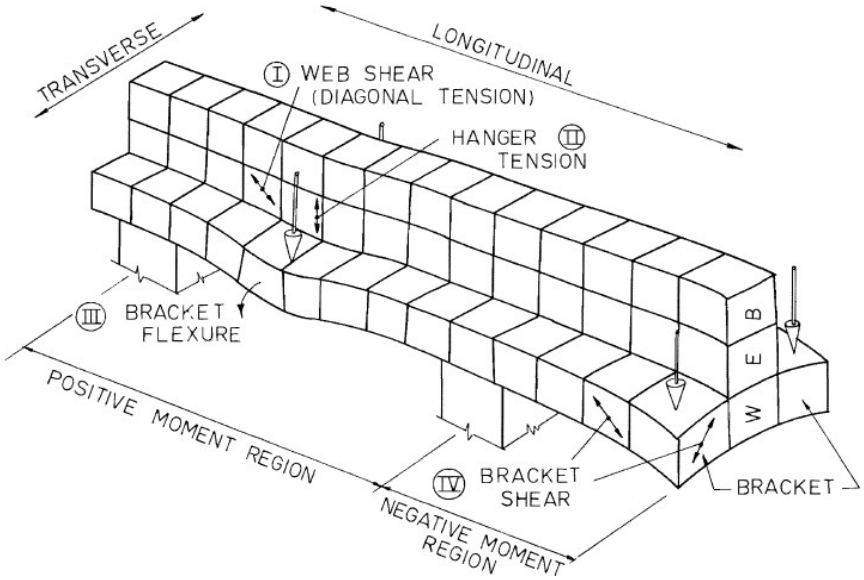

Figure 1.3. Structural behavior of inverted-T beams. Reprinted from reference [2]

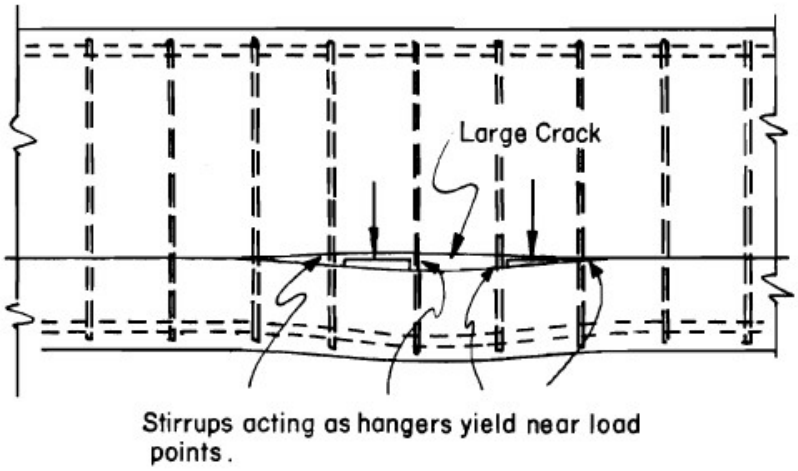

(a) Hanger failure

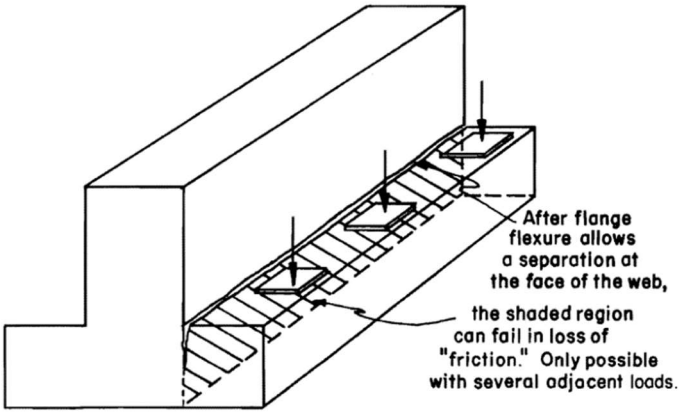

(b) Bracket (Ledge) failure

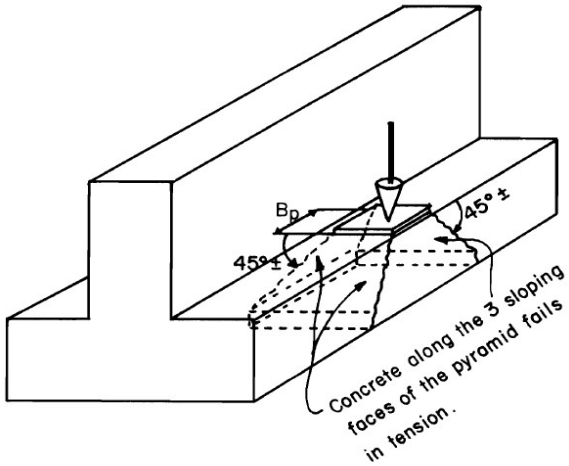

(c) Punching failure

Figure 1.4. Local failure modes of inverted-T bent caps. Reprinted from reference [3]

With a better understanding of the behavior of inverted-T beams, researchers have explored behavior of inverted-T beam ledges. Zhu et al. [4] investigated crack control for ledges in inverted-T bent caps. They addressed that the current design guidelines do not address the problem of crack control at service load adequately, and developed design provisions for cracking. Based on the investigation, they concluded that (a) diagonal bars were an effective way of controlling the crack widths in the interior spans, (b) diagonal bars were not as effective at the end-face of the cantilever span, and the distance of the farthest exterior load from the end face was the most important factor to control the crack widths, and (c) service load was limited to check the crack widths in the end faces.

Larson et al. [5] experimentally investigated the behavior of reinforced concrete inverted-T straddle bent specimens to identify the causes of diagonal cracking in the ledges of these bents. A strut-and-tie model was used to achieve the final specimen design that was designed to fail by web-shear. The large-scale specimens were tested as an upside-down simply-supported beam. During the tests, it was observed that most of the specimens displayed a web-shear failure. However, flexural failure, diagonal strut failure, punching shear, and ledge shear friction failures were also observed. From the experimental tests, increasing the ledge length along the length of the straddle bent increased the shear strength of the inverted-T beams, whereas increasing the ledge depth did not have any significant effect on the strength. The authors also theoretically evaluated existing inverted-T beam structures and found that they had already been subjected to approximately 70-85 percent of their capacity and need to be strengthened.

As a consequent study, Garber et al. [8] developed a 3-dimensional strut-and-tie model (STM) to estimate capacity of inverted-T beams. They compared estimated capacities to the test results conducted by Larson et al. [5] to evaluate the accuracy and conservativeness of empirical design approaches as well as the strut-and-tie model. Based on the analysis, the use of STM for cross-section resulted in more accurate estimation of the inverted-T ledge capacities which fails in punching shear. However, the use of STM for the cross section did not allow for the prediction of the true failure mode for the specimens subjected to ledge failure.

Deifalla and Ghobarah [9] also studied behavior and analysis of inverted-T shaped RC beams under shear and torsion to suggest to unify approach for the design for RC inverted-T shaped beams. They proposed an analytical model to predict shear and torsional behavior of the inverted-T beams by dividing inverted-T shape into three rectangular subdivisions and adopting rectangular RC beam model. Shear and torsional behavior prediction using the model agreed with the experimental results for the shear and torsional behavior of flanged beams.

With deeper understanding of the behavior of inverted-T bent caps, better design guidelines were established for inverted-T bent cap (or beam) ledges. AASHTO [10], a governing bridge design specification in U.S., provides design methods for D-regions in Section 5.8. Especially for beam ledges, AASHTO [10] specified that beam ledges may be designed in accordance with either the strut-and-tie model (STM) specified in Section 5.8.2 or the sectional stress analysis method specified in Section 5.8.4.3. Two dimensional STM is adopted for inverted-T beam ledge design. For the sectional stress

analysis method, potential cracks are used. Figure 1.5 shows such cracks and their locations on the ledge of an inverted-T bent cap. The cracks are referred to as "ledge shear friction and flexure ①," "hanger ②," "punching shear ③," and "bearing ④" in Figure 1.5. AASHTO [10] indicates that the beam ledges must resist (a) flexure, shear, and horizontal forces (Crack ①); (b) tension force in the supporting element (Crack ②); (c) punching shear at points of loading (Crack ③); and (d) bearing force (Crack ④). Requirements to address the specific conditions of the inverted-T beam ledge component are outlined in Articles 5.8.4.3.2 through 5.8.4.3.6.

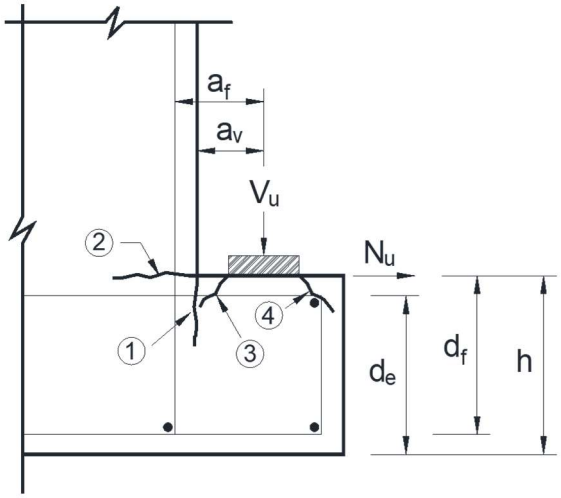

Figure 1.5. Notation and potential crack locations for ledge beams.

Hurlebaus et al. [6] theoretically evaluated capacities of in-service (existing) inverted-T bent caps in Austin, Texas including both multi- and single-column bents in accordance with AASHTO [11]. To evaluate the capacity of the bent caps, expected future load demands (V_u as depicted in Figure 1.6) with an increased number of lanes were determined. Figure 3.1 illustrates how a live load was calculated for inverted-T bent caps.

As the most critical condition, the girder reaction model was used to determine a load demand for a ledge. The estimated capacity of each ledge of the inverted-T ben caps was also determined by using the stress analysis methods and compared to the expected future load demand. Based on the expected future load demands with an increased number of lanes, the authors determined that the ledge flexure and hanger capacities of bent caps are insufficient, and the bent caps need to be strengthened for future load demands.

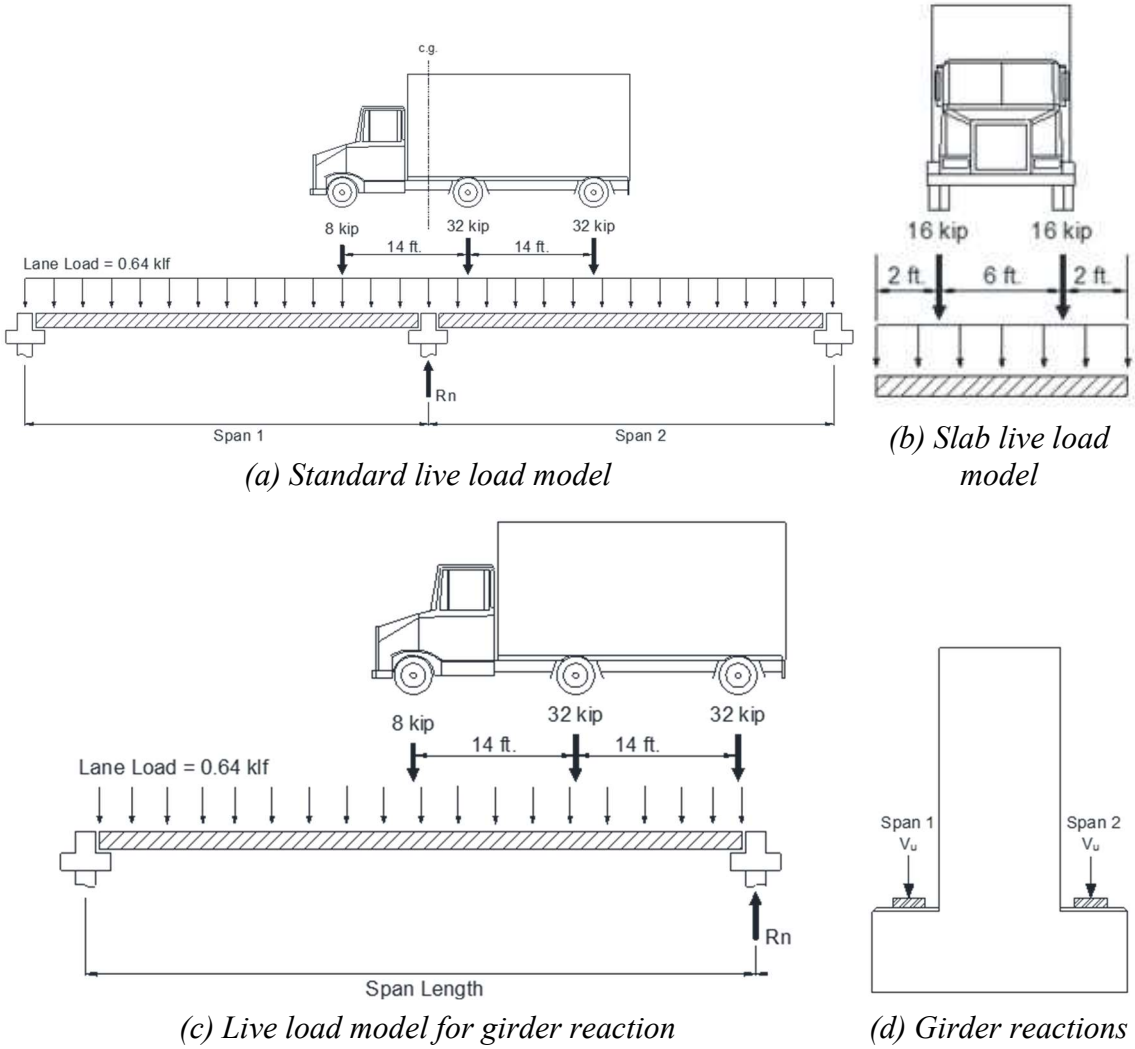

(a) Standard live load model

(b) Slab live load model

(c) Live load model for girder reaction

(d) Girder reactions

Figure 1.6. Live Load models on girder used for the computation of girder reaction

1.2.1.2. Strengthening of Inverted-T Beam

As aforementioned, many researchers have investigated the behavior of inverted-T beams and suggested design guidelines [2-5, 7-9, 12-18]. However, most of such research was focused on the design and behavior of inverted-T beams but not strengthening of in-service inverted-T bent caps experiencing cracks.

Most recently, Galal and Sekar [19] experimentally investigated the effectiveness of using anchored carbon fiber-reinforced polymer (CFRP) sheets to eliminate the brittle failure mechanism of the hanger, web, or flange and improve the strength of the inverted-T bent caps. Eight tests were conducted on four of one-third scaled specimens. The reinforcement arrangement for the specimens was selected to simulate three different nonductile failure mechanisms and to avoid having two or more failure modes. As shown in Figure 1.7, the CFRP sheets were wrapped in two different configurations to investigate their effectiveness in rehabilitating the hanger, web, and ledge zone: (a) thread rod anchors at the web with the curved angle plate with concave grout to avoid debonding, particularly near reentrant corners; and (b) CFRP fan-type anchor at the loading points. Experimental results indicated that the anchored CFRP sheets were effective in improving the displacement ductility and the load-carrying capacity of the inverted-T bent cap. However, the weakness of this method is the anchors used to prevent debonding of the FRP sheets were applied at the web-to-ledge interface where the cracks are mainly observed (see Figure 1.1(a)).

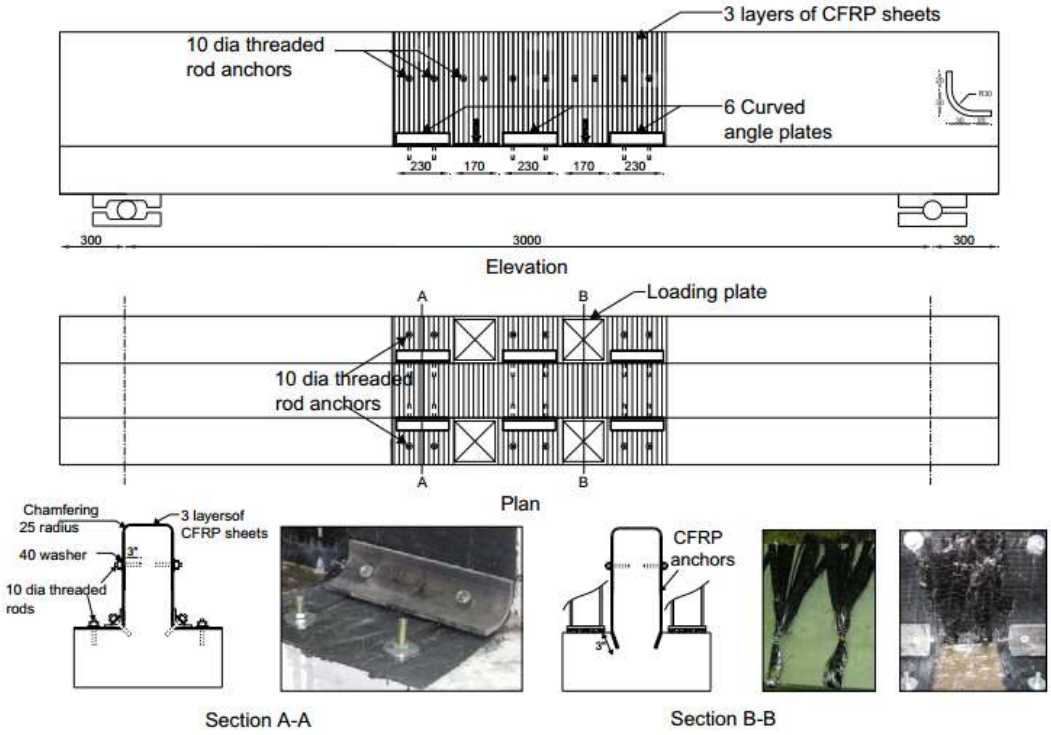

(a) Rehabilitation of hanger zone with fiber anchors

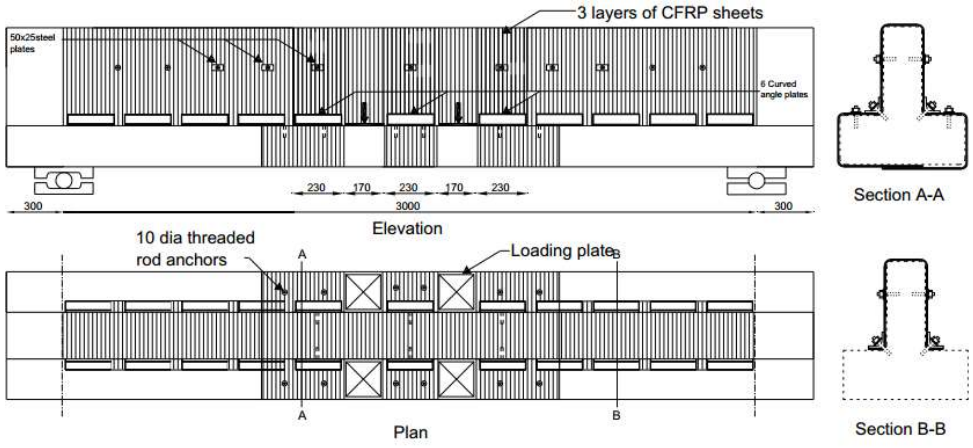

(b) Rehabilitation of hanger zone without fiber anchors

Figure 1.7. Anchored carbon fiber reinforced polymers rehabilitation schemes using angle plate. Reprinted with permission from Elsevier [19][12]

---

[1] Reprinted from Composites Part B: Engineering, 39(4), Khaled Galal and Mukesh Sekar, Rehabilitation of RC inverted-T girders using anchored CFRP sheets, 604-617, Copyright 2008, with permission from Elsevier

[2] Reprinted from The Lancet, Vol. 39, Khaled Galal and Mukesh Sekar, Rehabilitation of RC inverted-T girders using anchored CFRP sheets, 604-617, Copyright 2008, with permission from Elsevier.

Since there are a few studies on strengthening of inverted-T bent caps (or beams), research related to strengthening standard-T shape beams and rectangular shape bent caps are also reviewed in the following subsections.

1.2.1.3. Strengthening of Standard-T Shape Beam

Higgins et al. [20] experimentally investigated the effect of various shear strengthening techniques on the performance of reinforced T-shape girders. Fifteen full-scale T-shape beam specimens were tested under four-point bending. The inverted-T beam specimens, designed to fail in shear, had an overall height of 48 in., a flange width of 36 in., a web width of 14 in., and a flange thickness of 6 in. The specimen length was 26 ft. The specimens were loaded incrementally on the top of the web to produce initial cracking. After the crack initiation, the specimens were strengthened for shear with epoxy injection, external steel stirrups, internal steel stirrups, surface-bonded CFRP stirrups, or NSM FRP. The retrofitted specimens were then loaded to failure. Based on the experimental results, it was evident that the external steel strips, internal steel strips, and surface-bonded CFRP strips were effective in improving the shear capacity of the specimens, while the epoxy injection and FRP NSM retrofit solution was found to be ineffective. To increase shear capacity of the specimens, the authors suggested a reduction of FRP strip spacing. The effect of internal steel strips on the long-term service life performance of the structure was found to be relatively outstanding among these retrofit solutions. No specific recommendation for a single retrofit solution was made.

Goebel et al. [21] investigated the effectiveness of NSM CFRP as a method to strengthen the shear capacity of girders. Ten full-sized specimens were built. One side of

each was over-reinforced in shear to induce failure in the side retrofitted with NSM CFRP. The specimens were tested in four-point bending while loads were applied at the top of the web. After the crack initiation, the load was removed, and the same loading sequence was repeated to obtain baseline behavior of the specimen under the fully cracked condition. Then specimens were loaded to failure after vertical-oriented NSM-CFRP strips were installed for shear strengthening. Test results indicated that NSM-CFRP transverse reinforcing significantly affected the shear capacity of specimens. The performance of the NSM-CFRP retrofit under fatigue loading and environmental exposure had minimal impact on the shear capacity of the specimen. Recommendations for the design of shear strength with NSM CFRP were provided.

Chaallal et al. [22] noted that the FRP strengthening methods for shear strengthening may have high potential for debonding and require surface preparation, and there is high uncertainty in the FRP-to-concrete bond. The authors tested the embedded through-section (ETS) FRP method wherein vertical holes were drilled through the middle of the cross-section, after which the holes were cleaned and filled two-thirds with epoxy adhesive. The CFRP rods were also coated with a thin layer of epoxy and installed in the hole. The authors tested externally bonded (EB) CFRP and NSM FRP rods in which grooves were made on both sides of the web, cleaned, and filled two-thirds with epoxy, and then FRP bars coated with a thin layer of epoxy were installed in the grooves. T-beam specimens with and without transverse reinforcement were considered for this experimental study. From the experimental tests, it was evident that the ETS FRP system significantly enhanced the shear capacity of the beam even with limited amounts of

transverse reinforcement. Flexure failure occurred in beams with the ETS FRP system, whereas sheet debonding and separation of side concrete were observed in the EB FRP and NSM FRP solutions, respectively. Because the FRP rods in the ETS method were embedded in the core concrete, the contribution of ETS FRP did not decrease in the presence of transverse steel reinforcement, whereas the contributions of EB FRP and NSM FRP were negligible in beams with transverse reinforcement.

Breveglieri et al. [23] experimentally investigated the effectiveness of ETS steel bars and CFRP rods on the shear strengthening of RC T-beams. Nineteen specimens were tested under three-point bending with a shear span of 35.4 in. The specimens were 14.2 in. high and 8 ft. 8 in. long. The ETS bars at a spacing of either 7.1 in. or 11.8 in. were placed in between existing stirrups to increase the effectiveness of the strengthening technique. From the experimental tests, it was evident that the ETS strengthening technique significantly enhanced the load-carrying capacity of the specimens. The inclined ETS bars were found to be more effective for capacity increase than the vertical ETS bars. It was also noted that the contribution of the ETS strengthening technique decreased with the increase in internal transverse reinforcement ratio.

1.2.1.4. Strengthening of Rectangular Bent Cap using Prestressing Techniques

Woods [24] and Aravinthan and Suntharavadivel [25] carried out a project to strengthen the bent cap of the Tenthill Creek Bridge in Gatton, Queensland, Australia. Growing volume of heavy transportation across the bridge has caused shear and flexural cracking in the bent cap. The author properly repaired cracks with epoxy injection, then the external post-tensioning has been applied to achieve maximum efficiency of the strengthening. He

also conducted laboratory tests on three specimens that used as a model of bent caps of the Tenthill Creek Bridge. The performance of epoxy crack injection and/or external PT to rehabilitate a concrete member in shear has been evaluated. The applying external PT only on the concrete member, it increased the load carrying capacity of the member. In addition, if the initial cracks repaired by epoxy injection prior to install external PT, the substantial capacity increase was achieved.

In the United States, an example of shear strengthening of the bent cap using external post-tensioning is Hawthorne and Morrison Bridges [26]. Based on the Oregon Department of Transportation, some of the bents were under-strength for current traffic loadings. Thus, an engineering firm recommended a system of externally mounted post-tensioned bars to increase the load carrying capability of the bents. A set of four rods were required for a bent in Morrison Avenue, while bents in Hawthorne Avenue only required two rods per bent. A steel I-beam used as an anchoring block on each end of the bent cap, and the rods are protected by protective caps from corrosion.

(a) Hawthorne Avenue bent cap *(b) Morrison Avenue bent cap*

Figure 1.8. Hawthorne and Morrison Bridge Bent Cap Strengthening. Reprinted from reference [26]

Many research have been conducted to strengthen concrete beams including literatures reviewed in this section [12, 19-24, 27-34], and ACI Committee 364.2T [35] provides methods to increase the shear capacity of existing reinforced concrete structures. Several alternatives are discussed: (a) external reinforcement provided by steel rods, reinforcement bars, post-tensioning, or steel plates; (b) section enlargement using concrete, shotcrete, reinforced concrete, or mortar bonded to the concrete element; (c) internal reinforcement provided by steel or fiber-reinforced polymer (FRP) reinforcement installed by drilling holes, and the dowels being effectively grouted; (d) near-surface-mounted reinforcement provided by steel or FRP rods into grooves; (e) supplemental members; and (f) externally bonded FRP plates and strips. Factors to include in selecting a retrofit method are purpose, magnitude of strength increase required, cost, in-service conditions, dimensional and clearance constraints, aesthetics, material, and equipment availability.

Based on the literatures reviewed in this section, a series of retrofit solutions for inverted-T bent caps to improve serviceability and ultimate strength is developed and experimentally validated in this study.

1.2.2. Railroad Ties

In the railroad tie industry, an increase of heavy track hauls causes significant stress increments on the concrete railroad ties. The American Railway Engineering and Maintenance-of-Way Association (AREMA) has reported that prestressed concrete ties have failed with cracks under service load conditions. This failure of concrete ties results in significant economic losses, due to maintenance, and causes considerable downtime resulting in reduced line capacity [36]. AREMA [37] noted that if a concrete tie cracks, it must be repaired and replaced to keep use the rail track.

To gather technical information related to improving performance of railroad ties, previous studies are reviewed in terms of the serviceability of railroad concrete ties in general and strengthening methods that are applicable to railroad ties.

1.2.2.1. Serviceability of Concrete Railroad Ties

Venuti [38] detailed the history of concrete railroad ties; why they became used, how they were designed, fabricated, and installed, and how they're currently being used on modern railroads. The author states that concrete railroad ties began becoming popular in the 1950s in post-World War II. As the use of concrete ties has been settled, the American Railway Engineering Association (AREA), now named as American Railway Engineering and Maintenance Association (AREMA) developed a series of specifications for concrete ties. In the specifications, there are limitations on positive and negative moments of ties in design point of view, and the ties life expectancy is expected to be 50 years when designing concrete ties [37].

The concrete ties installed in the rail system generally have two critical positions that affect strength and durability: the rail seat and the center of the ties as shown in Figure 1.9. Subsequently, it was found that pre-tensioning the tendons by setting the eccentricity at the center enhances the strength of the ties by balancing the positive moment on the rail seat and the negative moment on the center of the tie. These ties were designed to hold a wheel load of 40 kips which is then factored to account for the dynamic effects of the moving train. With approximately 160,000 miles of heavy haul track hauling 1.9 trillion ton-miles annually, the United States has one of the most extensive systems of railroads in the world [39]. These high loads can cause serious stress on the rail ties,

requiring maintenance and increasing the cost. It needs to be aware that prestressed concrete ties are much more advantageous in the aspects of strength and durability than timber, but there are still issues to be investigated and improved to draw their full potential.

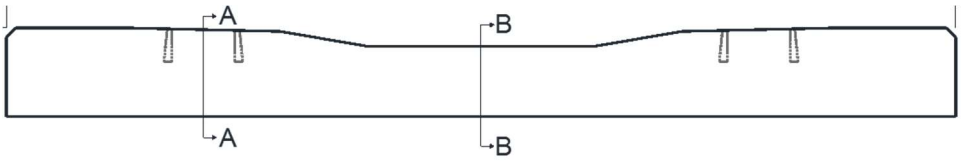

Figure 1.9. Typical concrete railroad tie elevation view showing critical region; rail seat (section A-A); and center (section B-B).

Van Dyk et al. [40] surveyed issues pertaining to prestressed concrete railroad ties among the several U.S. railroad companies. The survey results indicated that concrete cracks near the rail seats and at the center of ties remain an ongoing critical issue affecting tie performance. AREMA [37] defined that the tie is failed if it was cracked under service load state, and thus, maintenance, including either repairing or replacement, is required to keep using. The ties without repairing or replacement will result in derailment. The National Transportation Safety Board (NTSB) [41] reported that the accident was caused by excessive track gauge due to the deterioration of ties. It was determined that the tie deterioration was caused by cracks that allowed water penetration and corrosion [41].

Based on the study of Zeman et al. [42] and Ferdous and Manalo [43], the main cause of failure of concrete railroad ties is rail seat abrasion (RSA). This occurs when the tie experiences a high amount of axle-load, and especially moisture is present underneath the rail seat. If the rail seat is damaged, there may be an interruption of the signal in the rail gauges, which may damage the tie or derail the train. The standard railway system

uses a direct current (DC) circuit to signal the presence of trains within a circuit block to other trains in another block. A power source passes current through the rail to a relay point, and the relay point sends the signal back to the power source through the opposite rail. If there is no train, the relay is energized and the "Clear" signal is displayed, while the train enters the rail, the steel axle interrupts the current flowing from the relay to the power supply and displays the "Stop" signal. The problem arises when an insulator pad, which installed to isolate the steel shoulder from the rail, allows current flow into the concrete and connects the signals of the two rails. This connection results in a false short circuit that de-energizes the relay and greatly reduces the track capacity. If these problems have found, they must be repaired, and it will cost money.

Along with the electric signal disturbance, another main concern is the corrosion of the prestressing steel in the tie, which results in a large loss in the prestressing force and the overall strength of the tie. Corrosion of prestressing steel can occur when water penetrates through the cracks and the steel is oxidized; thereby a loss of prestress and hence the overall strength of the tie [44, 45]. Corrosion in reinforcing bars and false signaling in the railroad system can become more prevalent than expected if wet concrete becomes a semiconductor, or rebars become a high electrical conductor. In addition, freeze-thaw cycles accelerate moisture penetration and corrosion [46].

1.2.2.2. Strengthening Concrete Railroad Ties

To overcome the serviceability issues caused by cracks on the railroad ties, many studies have been conducted on improvement of durability and overall performance of concrete ties; therefore, the total maintenance cost can be lowered and used economically.

Mindess et al. [47] studied fiber reinforced concrete to increase the impact resistance of the tie. Three types of concrete were tested including plain concrete without fibers, a wrinkled steel fiber concrete, and a monofilament polypropylene fiber concrete. Several ties were made for each concrete matrix and tested under static loads directly applied to the rails and impact loads applied at various heights. In the case of plain concrete ties, cracks were generated from the bottom of the ties, where the load was applied. Failure occurred along with the slippage of the prestressing steels. The fiber concrete ties can withstand larger peak loads and absorb more energy before failure occurs than the plain concrete ties. As a result, the use of fiber concrete has been found to increase the toughness and durability of concrete ties. However, there was no indication of corrosion resistance and electrical conductivity improvement.

Donovan [48] investigated concrete railroad tie designs to improve their durability. The author evaluated four commercial tie designs which had different concrete mixes and material sources. The most viable tie design with the highest strength at the most reasonable cost was identified. With the tie design, the author also reviewed and selected a possible source of aggregate to be used in the concrete mix. Eleven aggregate producers were compared using a series of tests: Alkali Silica Reactivity (ASR), freeze-thaw cycles, abrasion resistance, and shape. Based on the evaluation, the aggregate was selected and the mix design was established using multiple factors including type of cement, use of plasticizers and fly ash, air entrainment, and method in which it is cured. Finally, this research provided an optimized concrete railroad tie, but it was for one specific purpose,

a short line railroad in Nevada. A durable, corrosion resistant design needs to be established for more general use.

Recently, Zeitouni et al. [49] investigated the use of the high strength reduced modulus (HSRM) prestressed concrete railroad ties to overcome premature cracking near the central region of the tie. The authors conducted the four points bending tests and 3-dimensional finite element (FE) analysis using ABAQUS, a commercial FE software, to investigate the performance of the HSRM ties. They compared and contrast the experimental test and the FE analysis results to predict the behavior of the HSRM ties. Based on the results, the HSRM ties delayed the initiation of tensile cracks with better stress distribution and decreased width and length of the cracks. However, there has been no indication of electrical conductivity and corrosion resistance improvement.

Li et al. [50] developed a hybrid GFRP-concrete beam consisting of a rectangular hollow GFRP pultruded profile filled with concrete. The hybrid GFRP-concrete beam designed to provide tensile strength and to protect the concrete block inside from suffering chemical attacks. The authors conducted numerical analysis using finite element model to analyze the impact behavior of the hybrid concrete. The analysis revealed that the hybrid beam outperforms the conventional prestressed concrete railroad ties.

1.2.2.3. Application of Fiber Reinforced Polymer (FRP) to Concrete Structure

Although research on strengthening concrete railroad ties has been conducted, the strengthening techniques could not overcome potential corrosion and electrical leakage. To eliminate the corrosion issue on the concrete structures, the research on FRP started during the mid-nineteenth century to replace steel in corrosion-prone RC structures.

Because FRP materials are nonmagnetic and noncorrosive, the problem of electromagnetic interference and steel corrosion can be avoided with FRP bars. Currently, FRP bars are extensively used in major infrastructure projects considering its non-corrosive, high strength to weight proportion and fatigue properties [51]. In addition, FRP bars have the advantages of high strength and lightweight, and a number of design guides and national standards have been published to provide recommendations for the analysis, design, and construction of concrete structures reinforced with FRP bars. However, due to the substantial differences in the physical and mechanical properties between FRP and conventional steel, the use of FRP bars is still a formidable challenge for engineers [29].

The elastic modulus of FRP bars is much less than that of steel bars. Glass fiber-reinforced polymer (GFRP) bars and aramid fiber-reinforced polymer (AFRP) bars have an elastic modulus of between 5076 and 7252 ksi, and the elastic modulus of carbon fiber reinforced polymer (CFRP) bars is between 17400 and 21756 ksi. This low elastic modulus leads to higher deflection and larger crack width in FRP bar-reinforced concrete beams that have an equivalent reinforcement ratio to steel-reinforced concrete beams; therefore, both deflection and crack width must be checked for the serviceability limit state. In addition, while steel bars behave inelastically after yield strength, FRP bars show perfect elastic behavior up to failure. Since FRP bars are linear elastic to failure and fail in a brittle manner, a ductile steel-like failure does not occur in FRP bar-reinforced concrete beams. To avoid brittle failure over-reinforced beams, failure by concrete crushing, which is generally not considered in steel-reinforced concrete design, is preferred in FRP bar reinforced concrete design [27].

Lutch et al. [52] and Harris et al. [53] theoretically investigated concrete ties to identify an optimal layout design by using different combinations of concrete strengths, prestressing loads, and prestressing materials. Four different concrete compressive strengths were used in the project: 7 ksi, 9.5 ksi, 12 ksi, and 15 ksi. For each concrete strength, three different prestressing materials were used: 0.21 in. diameter wire; 0.25, 0.3125, and 0.375 in. diameter 7-wire strands; and 0.25 and 0.3125 in. diameter CFRP strands. CXT 505S-50 tie, a commercial heavy haul tie, was used as the basis for the optimization design. Following the guidelines set by ACI Committee 440 [54], a tie using 0.25 in. diameter CFRP strands resulted in having the highest flexural capacity for high strength concrete. Although this project shows the best resemblance of this proposed research, it is only a theoretical application with no physical testing performed.

Noël and Soudki [55] conducted to investigate fatigue behavior of GFRP, the results showed that GFRP bars embedded in concrete have shorter fatigue lives than similar bars tested in the air by approximately a full order of magnitude. Preliminary fatigue test results carried out by El Refai [56] showed that the fatigue limit of basalt FRP (BFRP) bars was about 4% of their ultimate capacity. However, the fatigue limit of GFRP bars was about 3% of their ultimate capacity. Furthermore, the results showed that BFRP has a low sensitivity to water moisture and is a durable material. Therefore, BFRP would be suitable for use as prestressing or non-prestressing. Compared to steel, the BFRP materials possess a considerable higher strength-to-weight and modulus-to-weight ratios. These properties can be very useful and advantageous for different applications. Chemical and mechanical properties of the BFRP material can serve both structural and functional

issues pertinent to the particular structure. Therefore, BFRP materials are a good candidate for prestressing and non-prestressing applications. However, a lack of studies on basalt bar reinforced concrete beams in fatigue applications has limited the use of this type of bars in the construction industry [57].

AFRP bars have shown to be the more applicable material due to their greater deflection and curvature under pre-stressed applications compared to carbon, and greater strength and moment capacity compared to glass [58]. McKay and Erki [59] demonstrated three pre-stressing concrete beams with AFRP bars on the bottom and conventional steel on the top.

The AFRP bars were pre-stressed to 80% of the ultimate strength. Each beam was subjected to a different loading condition: beam 1 was loaded to near ultimate, released, and loaded again until failure; beam 2 was loaded until cracking then set under a cyclic loading of 4 Hz and failed after 1.96 million cycles; and beam 3 was loaded in the same fashion as beam 2 but with a more consistent cycle of loading to minimize elastic recovery. The results of this experiment showed the AFRP having a higher relaxation than steel at 10-20% over 50 years, yet near equal fatigue strength under service conditions to that of steel. Another major finding was that AFRP should be used in fully pre-stressed applications to prevent the need for rod fretting which leads to a decrease in bond strength decreasing the capacity of the concrete beam.

Current research on the use of AFRP bars in prestressed concrete structures primarily focuses on bridge girders and decks. Gar [60] considered the use of pre-stressed AFRP bars on a two-way bridge deck with precast panels. The deck consisted of two

panels and pre-stressed with AFRP bars spaced about 5 in. on center in the direction of traffic and reinforced with AFRP bars spaced about 6 in. on center in the transverse direction. The entire deck was supported by three reinforced beams equally spaced with equal tributary areas for each. The deck was loaded with a factored HS20 truck load equating to approximately 22.5 tons and was applied through a steel plate representative of the tire footprint. It was found that the deck resisted the maximum factored wheel loads in all locations. Failure was governed by flexure, the tandem axle load governed the flexural failure, and shear requirements were met. It was also discovered that although AFRP bars are a brittle material with no clear yield point, the deck underwent noticeable deformation before failure due to the low modulus of elasticity of AFRP, about 1/3 that of steel.

Gar et al. [58] also used AFRP pre-stressing tendons in an AASHTO I-girder Type I with a conventional bridge deck and compared to conventional pre-stressed steel girder with the same decking. Both experimental and a finite element analysis were performed resulting in a 5%-7% error in the prediction of cracking moments and material failure. They demonstrated that pre-tensioned AFRP both meets serviceability requirements and maintains adequate flexural strength. It was seen that the curvature at failure was approximately 18 times greater than the curvature at cracking, yet the mode of failure was tendon rupture in the tension face. This increase in curvature showed that although the tendons may fail suddenly in rupture, there is sufficient ductility present to provide an appropriate warning prior to failure. Deflection of the girder was also measured during the load testing. It was found that the AFRP girder deflected half the allowable under service

loading and half the deflection of a comparable prestressed steel girder at failure. This is due to the higher ductility of steel after yielding compared to AFRP. However, this research does not review the corrosion resistance of the AFRP girder in comparison to the prestressed steel girder and how it affects serviceability. Due to the environmental similarities shown by both railroad ties and bridge girders, the success of AFRP in concrete railroad ties should reveal similar results.

Gar et al. [61] also conducted flexure and shear tests on full-scaled AASHTO I-girder Type I with prestressed and non-prestressed AFRP tendons. They used AFRP specimens with partially prestressed because of the limited capacity of the prestressing anchorage system. With the flexural test, the deflection of the girder and cracking moment has been evaluated based on current design specification. Based on the flexure test result, the AFRP specimen showed brittle failure with tendon rupture while the control specimen failed with concrete crushing which provides enough ductility. For the partially prestressed AFRP beam, the deflection under service load is the most critical for design. Through two shear tests, the sear capacity of the AFRP prestressed girder was almost twice greater than factored shear load. Shear failure mode was crushing of the web due to compressive stresses, and it was similar to the control specimen.

1.2.3. Summary

In light of the foregoing literature review, the following key research questions related to the strengthening of concrete infrastructure arose:

Q1. Is the concrete infrastructure such as in-service inverted-T bent caps and railroad ties able to be retrofitted (or repaired)? What are the options?

Q2. Is prestressing technique applicable to the concrete infrastructure to improve serviceability and ultimate strength? What are the pros and cons of use of prestressing techniques?

Q3. For inverted-T bent caps, what are the criteria that need to be considered to select retrofit solutions for in-service bent caps?

Q4. Can corrosion and electric signal disturbance issues on railroad ties be solved simultaneously? What are the solutions?

Q5. Is fiber reinforced polymer able to replace the conventional prestressing steel with promise structural behavior?

1.3. Objectives

The primary objective of this study is to develop solutions to improve serviceability of the concrete infrastructure. Although there are various strategies to improve performance of in-service concrete infrastructure, this study focuses on the methods utilizing prestressing techniques. The objectives of this study are to

1) Review and analyze concrete infrastructure that currently used in the industries; inverted-T bent cap and railroad tie;
2) Develop the solutions to improve serviceability of inverted-T bent caps;
3) Assess the applicability of the solutions and identify the most viable solutions using the weighted sum model (WSM);
4) Evaluate performance of the selected viable solutions in terms of serviceability and ultimate strength limits;

5) Design a class of prestressed concrete tie using aramid fiber reinforced polymer (AFRP) strands; and
6) Evaluate AFRP strands as a substitute of prestressing steels in railroad ties

These objectives are expected to benefit the industry through increased durability, safety, and reliability of concrete infrastructure over its service life. Along with improved serviceability, the total cost is expected to decrease due to the decreased cost of maintenance and replacing the structure in the future.

1.4. Significance

As the cracks representing deficient capacity of concrete structures in terms of serviceability and strength have been found, developing solutions are needed to improve serviceability of the inverted-T bent cap. There are several methods to improve concrete structures. This research especially focuses on improving performance of in-service inverted-T bent caps and railroad ties.

First, a conceptual design of various retrofit solutions is proposed to address the critical sectional shear failure modes; ledge flexure, hanger, and punching shear. A framework to evaluate the alternative retrofit solutions using the Weighted Sum Model was developed to rate and rank based on six criteria; thereby providing engineers in different regions options to select a solution that applies to the structure in their region. With a set of weight factors given by an asset owner, most viable retrofit solutions were identified for further validation and their robustness was validated. To validate the effectiveness of the solutions utilizing prestressing techniques including both vertical (local) and horizontal (overall) post-tensioning in terms of improving serviceability and

ultimate strength, this study conducted experimental investigations. These solutions may eliminate potential debonding issues that may be observed from the strengthening methods using FRP sheets as well as restrain existing cracks.

Second, this research proposes a solution to overcome major issues that may occur in conventional railroad ties prestressed by steel wires. The solution completely replaces prestressing steel wires with aramid fiber reinforced polymer (AFRP) tendons to eliminate the concern of steel corrosion and reduce electric leakage. Thus, the complete replacement of prestressing steel with AFRP tendons would significantly reduce the need to repair and replace the ties in the future. Consequently, designing new ties using AFRP, which is noncorrosive and nonconductive material, is suitable for the continual improvement and widespread use of concrete railroad ties.

1.5. Dissertation Organization

Following this introduction, Section 2 presents evaluation using a weighted sum model (WSM) for a set of alternative retrofit solutions to improve serviceability and ultimate strength of inverted-T bent caps and the results of the sensitivity analysis. Based on the analysis results, most viable solutions were identified. Among the identified solutions, the solutions utilizing prestressing techniques were experimentally investigated in this study. Section 3 addresses design concepts, experimental test program, and recommendations for the supplemental steel retrofitting methods. Section 4 delivers preliminary design concepts and design recommendations based on the experimental test results for the load balancing PT solution. Code-based capacity predictions were also evaluated in this section. Section 5 describes details of the prestressed concrete railroad ties using AFRP tendons. Finally,

Section 6 summarizes and provides conclusion of the study and recommendations for future research. Appendix A provides detailed information that is used for evaluating solutions using WSM.

2. SENSITIVITY ANALYSIS OF MULTI-CRITERIA DECISION-MAKING METHOD DEVELOPED FOR SELECTION OF RETROFITTING SOLUTIONS FOR EXISTING INVERTED-T BENT CAPS

2.1. Section Summary

Bridges with inverted-T bent caps benefit from providing increased clearance beneath the bent cap beams. However, diquietening cracks are often observed at the re-entrant corners of the beam ends. When judged against current standards, such bent caps have also been formed to be deficient in terms of either hanger or ledge capacity. Therefore, eighteen alternative retrofit solutions are developed to improve performance. Among the solutions, the most viable solutions are determined for further investigation by evaluating the solutions based on six criteria using a multi-criteria decision making methods. A multi-criteria decision making methods allow designers to identify a preferred alternative, classify alternatives in a small number of categories, and/or rank alternatives in a subjective preference order. The weighted sum model is applied to make a selection of retrofitting solutions for existing inverted-T bent caps. The major limitation of multi-criteria decision making methods is the subjectivity of assigned criteria weights. Sensitivity analyses are conducted to determine how the selection of retrofit solutions varies when the relative importance (weight) of the criteria considered in the process is changed. Based on the analyses, most alternative designs are somewhat sensitive to '*Strength*' and '*Cost*' criteria weights. Analysis results give options for assigning weight factors to the criteria depending on the evaluation purpose.

2.2. Introduction

Inverted-T bent caps are generally used to reduce the overall elevation of bridges, to improve the available vertical clearance beneath the beams, and to reduce the overall approach earthworks. Many of such bridges have experienced undesirable cracks at the web-to-ledge interface of inverted-T bent caps as shown in Figure 1.1(a). Such cracks may potentially reduce the service life of the substructure and are a sign of potential structural deficiency. If most of the superstructure of the bridge is in acceptable condition, replacing a deficient bent cap is impractical either due to high cost or disruption to traffic. Hurlebaus et al. [6] proposed eighteen retrofit solutions for in-service bent caps. The retrofit solutions were developed for inverted-T bent caps deficient per current design codes and specifications.

In this study, a framework to evaluate and to identify the most viable solutions to retrofit in-service inverted-T bent caps are developed. There are many decision analysis tools available to evaluate the alternatives in multi-criteria systems. In this study, the method used should be simple to apply, yet sufficiently robust to take into account different considerations of the problem at hand. The current problem and objective are to rate and rank a diversity of retrofit solutions to improve serviceability of structural concrete infrastructure in terms of the six criteria: (i) strength increase, (ii) total cost, (iii) constructability, (iv) dimensional and clearance constraints, (v) durability, and (vi) ease of monitoring. The decision analysis process considers all six criteria while providing flexibility to consider different weight factors for each criterion depending on their importance. Therefore, *Weighted Sum Model* (WSM) was adopted due to its characteristics of simplicity and robustness.

This paper first reviews MCDM methods specifically the WSM in terms of the evaluation criteria. The retrofit solutions are briefly introduced The WSM is then applied to the eighteen retrofit solutions designed for retrofitting in-service inverted-T bent caps. The robustness of the solution selection is then investigated through a sensitivity analysis. The results compared and contrasted with the initial rank of solutions. Finally, the most viable nine of the eighteen designs are established and conclusions regarding the robustness of the decision are drawn.

2.3. Weighted Sum Model (WSM)

MCDM methods are generic approaches to assist the decision making process according to preferences of a decision maker when there is more than one criterion [62]. MCDM methods cover a wide range of quite distinct approaches; they can be broadly classified into two categories: discrete MCDM (or *Multi-attribute Decision-Making*, MADM), and continuous *Multi-objective Decision-Making* (MODM) methods [63, 64]. Recently, numerous publications have been published to provide information about MCDM methods, their development, and application in different fields [65].

The WSM may be used to evaluate several alternatives in terms of various criteria and permits the assignment of different weight factors for different criteria [66]. The WSM defines the optimal alternative solution as that solution corresponds to the "best" value of the weighted sum. The model is formulated for problems in which all variables have the same physical dimensions based on the "additive utility" assumption. The WSM is the most widely-used for normalized multi-dimensional problems. While other models may

incorporate more parameters for effective decision-making, the additional information makes the process cumbersome with doubtful utility.

Peng [67] conducted regional earthquake vulnerability assessment using a combination of MCDM methods including the WSM. The author evaluated the earthquake vulnerability of 31 regions in China using real-life data. Based on the assessment, the 31 regions were categorized into four regions: high, relatively high, relatively low, and low vulnerability level regions. The evaluation result provided requirements at different aspects of earthquake planning, responding, mitigation, and recovery for each vulnerability level region.

Terzioglu et al. [68] used the WSM to evaluate the nondestructive evaluation (NDE) techniques for the inspection of a particular defect condition in post-tensioning (PT) and stay cable system based on five criteria: precision, accuracy, ease of use, inspection requirements, and cost. They considered two different scenarios (cost-driven and accuracy-driven) by varying weight factors. Their work provided the end-user with necessary tools for choosing the most viable NDE methods. They also provided preliminary results for inspecting the PT and stay cable specimens; magnetic methods determined as the most viable to detect strand defects. They noted that this framework they provided is extendable to other scenarios such as inspection of bridge deck, buildings, and historic structures.

Herein the WSM is formulated as

$$S_{\mathrm{i}} = \sum_{k=1}^{N} W_k a_{ik} \text{ , for } i = 1, 2, 3, \dots M \tag{2.1}$$

in which S_i = the total score for alternative i; W_k = the relative weight factor for criteria k; and a_{ik} = the individual score for alternative i when evaluated in terms of criteria k. The above general formula considers a total of M alternative retrofit solutions in terms of N criteria.

The WSM provides an overall score for the considered alternatives (retrofit solutions) by summing individual scores under each criterion multiplied by its associated weight factor. The individual scores for each criterion must be normalized, so as to not lose meaning when summed to calculate the total score. The weight factors must be selected such that the desired influence of each criterion is reflected relative to the others. The WSM has been applied to civil engineering problems and provided flexibility for bridge owners and engineers for future modification of the decision analysis process by changing weight factors or adding new criteria to the list.

2.4. Description of Alternative Retrofit Solutions

In this study, eighteen alternative retrofit solutions for in-service inverted-T bent caps to improve structural performance proposed by Hurlebaus et al. [6] were evaluated. Figure 2.1 shows a conceptual design for the solutions that was used to determine score for the solutions. This section briefly provides a concept of the solutions with the preliminary design. Table 2.1 summarizes purpose of the solutions and applicability. Most of the solutions may strengthen all three major sectional capacities and applicable for multi-column bent; whereas some cannot strengthen hanger or cannot be applicable for single-column bent.

Table 2.1. Eighteen alternative solutions developed to address critical failure modes

Soln. No.	Description of Solution	Purpose of Solution			Applied Bent Type	
		Ledge Flexure	Hanger	Punching Shear	Single Column	Multi Column
1	Prestressed high strength threadbar	O		O		O
2	Steel hanger bracket	O		O		O
3	End region stiffener	O	O	O	O	O
4	Clamped cross threadbar	O	O	O		O
5	Grouted cross threadbar	O	O	O		O
6	Upper seat brackets	O		O		O
7	Threadbar hanger with steel bracket	O		O		O
8	Through-web PT threadbar with catcher channel	O	O	O	O	O
9	Grouted threadbar anchored with catcher channel	O		O		O
10	Anchored FRP wrap	O	O	O	O	O
11	Concrete infill with prestressing threadbar	O		O		O
12	Concrete infill with hanger threadbar	O	O	O		O
13	Concrete masonry piers	O	O	O		O
14	Load balancing post-tensioning (PT)	O	O	O	O	O
15	Concrete infill with FRP anchored by FRP anchors	O		O	O	O
16	Concrete infill with partial-depth FRP anchored by steel waling	O		O	O	O
17	Concrete infill with full-depth FRP anchored by steel waling	O	O	O	O	O
18	Enlarged bearing pad			O	O	O

Solution 1 (prestressed high strength threadbars) was designed to provide an additional ledge flexure and punching shear capacities. Horizontal prestress forces are applied to the ledge of the inverted-T bent cap using externally anchored high-strength threadbars. Existing ledge cracks are restrained, and girder loads are actively distributed by the alternative load paths by inducing prestressing forces.

Solution 2 (steel hanger bracket) provide a complementary load path that reduces load demand on the ledge by allowing girders sit on steel brackets anchored to the web.

The steel bracket is designed to transfer loads, and the anchors are designed to carry shear and tension loads.

Solution 3 (end-region stiffener), which an anchored steel plate is applied to the end of the bent cap, is applied to strengthen the end region where distress often typically observed as crack emanating from the re-entrant corner. The solution is only applicable to the end region and may be used in conjunction with other retrofit solutions. The solution enhances hanger, ledge flexure, and punching shear capacity of the end region of the inverted-T bent cap.

Solution 4 (clamped cross prestressing threadbar) designed to address ledge flexure and punching shear deficiencies. The anchored threadbars provide supplementary load path to transfer the girder loads to the web. Pre-existing cracks at the re-entrant corners may be restrained by prestressing the threadbars.

Solution 5 (grouted cross threadbar) is similar to that of the clamped cross prestressing threadbar. Instead of using an external anchoring system in the web, threadbars are grouted to provide anchorage. The grouted threadbars terminate at a location higher than the clamped cross; thereby suitable for augmenting an inverted-T bent with a ledge flexure or punching shear deficiency by transferring the loads into the existing hanger reinforcement.

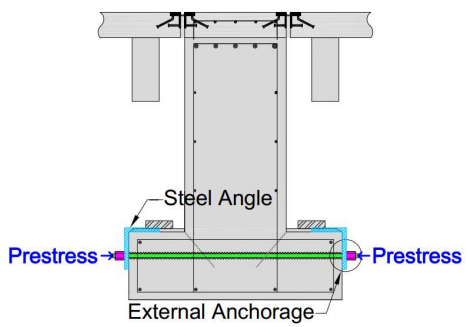

1. Prestressed high strength threadbar

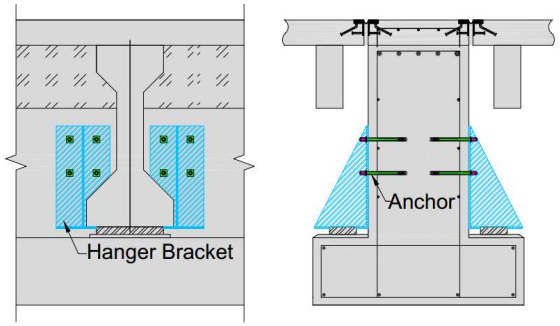

2. Steel hanger bracket

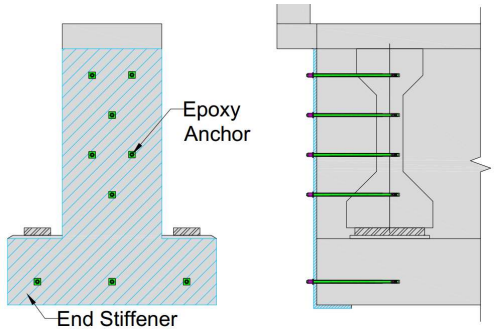

3. End region stiffener

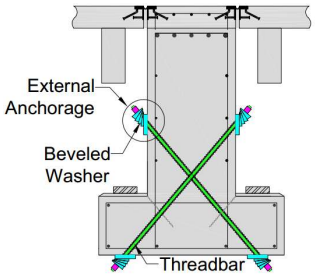

4. Clamped cross threadbar

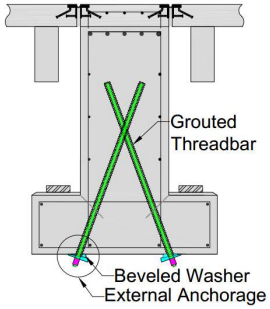

5. Grouted cross threadbar

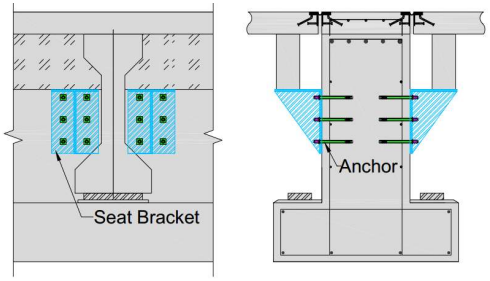

6. Upper seat brackets

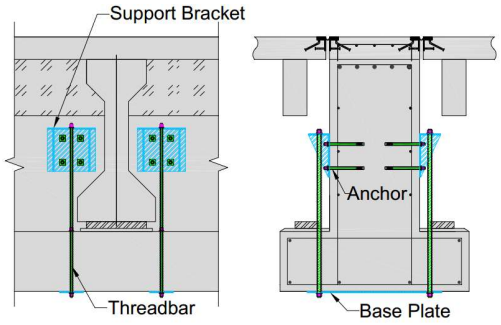

7. Threadbar hanger with steel bracket

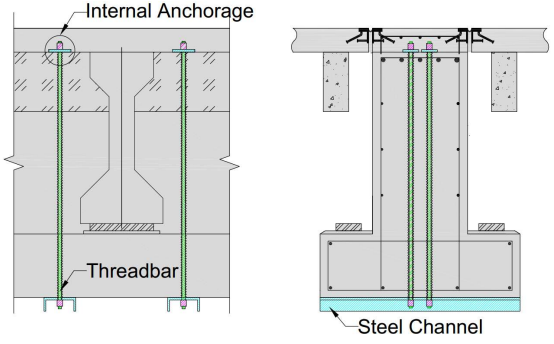

8. Through-web post-installed PT threadbar with catcher channel

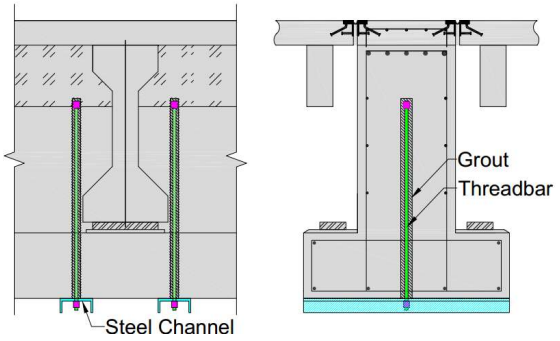

9. Grouted threadbar anchored with channel

Figure 2.1. Schematic view of alternative retrofit solutions for in-service inverted-T bent caps

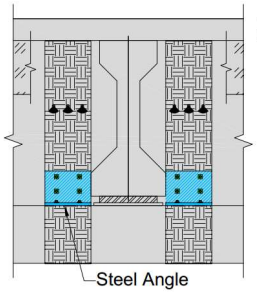

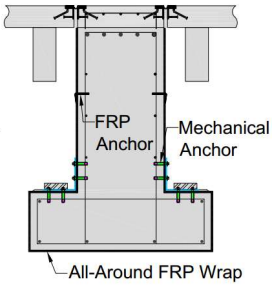

10. Anchored FRP wrap

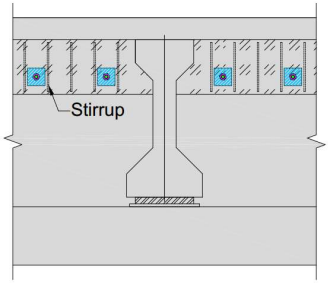

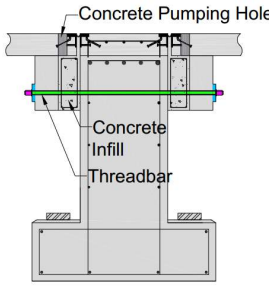

11. Concrete infill with prestressing threadbar

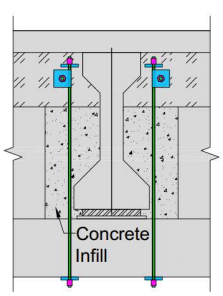

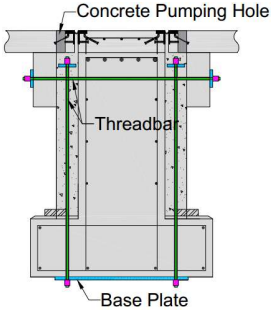

12. Concrete infill with hanger threadbar

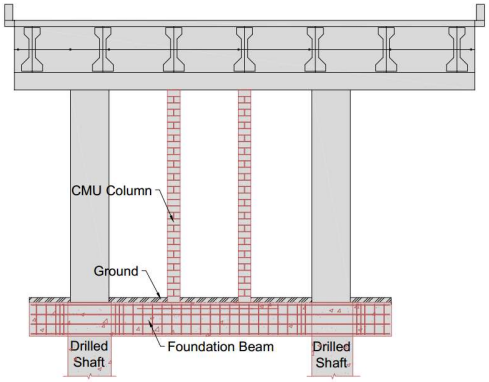

13. Concrete masonry piers

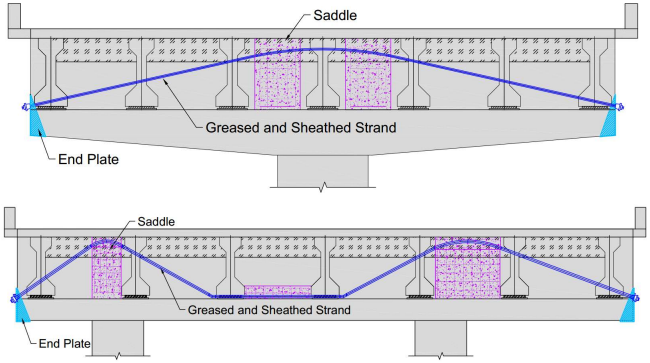

14. Load balancing post-tensioning (PT)

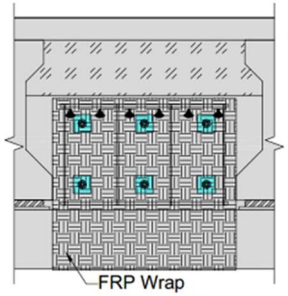

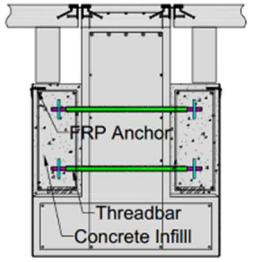

15. Concrete infill with FRP anchored wrap

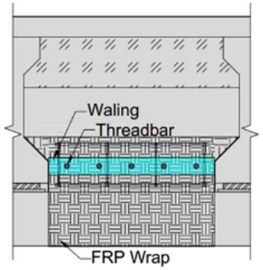

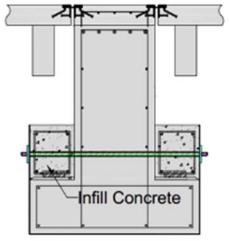

16. Concrete infill with partial-depth FRP anchored by steel waling

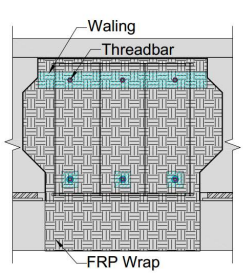

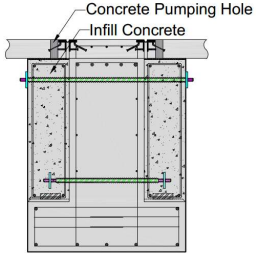

17. Concrete infill with full-depth FRP anchored by steel waling

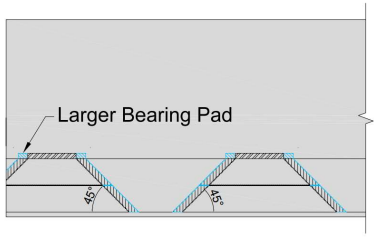

18. Enlarged bearing pad

Figure 2.1. Schematic view of alternative retrofit solutions for in-service inverted-T bent caps (Cont.)

Solution 6 (upper seat brackets) is designed to provide supporting elements below the diaphragm to provide a complementary load path directly form the bridge deck slab. As an additional load path is provided to reduce the loads from the slab to the girder, the load demand on the ledge of the inverted-T bent cap is reduced. This solution will indirectly account for the insufficient shear resistance of the ledge. The load from the brackets must be transferred into the web of the inverted-T bent cap beam, and in turn, the shear carried by the hangers as before.

Solution 7 (threadbar hanger with steel bracket) provides supplementary load paths to transfer the girder loads to the web at mid depth, therefore it is expected to enhance only the punching shear and ledge flexure capacity. The threadbars are designed to transfer the girder loads and the steel brackets are designed to provide support to the threadbars.

Solution 8 (through-web PT threadbar with catcher channel) designed to provide additional hanger capacity as well as ledge flexure and/or punching shear capacity. This solution results in transferring the loads from the ledge into the web via a series of threadbars with the load paths, and the threadbars may be torqued to induce prestress. The prestressing force should inhibit cracking in the web and ledges.

Solution 9 has a similar concept as Solution 8 but with partial depth grouted threadbars. The bonded threadbars shall be used as internally anchored bars within the web when there is not sufficient gap or access for top-down hole boring. This solution transfers the loads on the ledge into the web, thereby strengthening the hanger, ledge flexure, and punching shear capacity of the inverted-T bent cap.

Solution 10 (anchored FRP wrap) is for wrapping the side of the web and the ledges of the inverted-T section in critical regions. This solution strengthens the bent cap for ledge, punching, and hanger by providing additional multiple load paths to the girder loads. The FRP sheets are anchored at the termination region by FRP anchors and a steel angle is mechanically anchored at the corner between the web and ledge to reduce the potential for FRP debonding.

Solution 11 (concrete infill with prestressing threadbar) applies the attribute of providing extra support capacity to a bridge deck system by providing a measure of the total girder reaction being taken by the deck slab (the flange) of the overall deck slab flange-girder system. In this way, the ledge of the inverted-T beam can release some of the total support reaction of the bridge deck. By placing infill concrete between the diaphragms, the diaphragms are clamped to the web of the inverted-T bent cap member to provide reaction support to the deck slab.

Solution 12 (concrete infill with hanger threadbars) locally thicken the web with concrete infill, and the hanger threadbars are embedded within the concrete infill to effectively transfer the girder loads to the top of the web. The girder loads then may be effectively transferred by struts (arch action) directly to the column to address ledge flexure and hanger deficiencies.

Solution 13 (concrete masonry piers) provides additional supports to the inverted-T bent cap by concrete masonry piers beneath each interior girder. The masonry piers are seated on a reinforced concrete foundation cast between the existing drilled shafts. This

solution strengthens the interior of bent cap for ledge, punching, and hanger by providing additional multiple load paths to the girder loads.

Solution 14 (load balancing post-tensioning) uses a post-tensioning (PT) solution that retrofits the entire inverted-T bent at once while all solutions provide local sections of the inverted-T bent cap with increased seating capacity for individual girders. The PT strands strengthen the hanger capacity of the bent cap by providing upward forces, by lifting the cantilever parts with the end-region stiffener.

Solution 15 (concrete infill with FRP anchored by FRP anchors) uses infill concrete to transform the inverted-T cross-section to a rectangular cross-section and the FRP sheets to provide an alternative load path for the girder load by wrapping the overall section. The FRP sheet cannot be applied beyond the diaphragm since the depth of the infill concrete is limited by the presence of the diaphragm. Therefore, the solution only works for punching shear and ledge flexure deficiencies. By placing infill concrete with minimum reinforcement on the ledge, FRP sheets may be installed without concern for debonding at the edge of the ledge. The embedded threadbars are used to connect the web and infill concrete. The FRP sheets are anchored at the termination regions by FRP anchors.

Solution 16 (concrete infill with partial-depth FRP anchored by steel waling) is similar to Solution 15 but with shallower infill concrete and different FRP anchoring scheme. A shallower infill concrete is used for the solution and the FRP sheet is anchored at termination region by steel waling. The solution is intended for inverted-T bent caps with a diaphragm and provides an increase in the ledge flexure and punching shear

capacity. Through threadbars are used for the solution to connect the web and infill concrete and also to provide a location for attachment of the waling. Steel waling is used on each side of the beam to provide end anchorage to the FRP sheets.

Solution 17 (concrete infill with full-depth FRP anchored by steel waling) is intended for inverted-T bent caps without a diaphragm. With full depth infill concrete and the FRP sheet, the solution provides an increase in the hanger, ledge flexure, and punching shear capacities. Threadbars are placed in two layers with the steel waling at the top layer. FRP sheet is anchored at the end by steel waling.

Solution 18 (enlarged bearing pad) is proposed to improve punching shear capacity using different sizes of the bearing pads. Punching shear capacity is dependent on edge distance, spacing between the girders, depth of the ledge, and width of the bearing pad. While the spacing between the girders, distance from the edge, or depth of the ledge are not changeable for the real structure, the size of bearing pads can be changed by replacing. To increase the punching shear capacity, replacing the original bearing pads to larger bearing pads are suggested using a hydraulic jack to lift girders.

2.5. Description of Considered Criteria

Six criteria including strength increase, total cost, constructability, clearance constraints, durability, and ease of monitoring were considered for the assessment of retrofit solutions for inverted-T bent caps. These criteria were selected according to their specific importance in the decision-making process for selecting the potential retrofit solutions. Each alternative may have an individual score for each criterion.

Table 2.2 presents the score chart for the six criteria with short descriptions. The score range changes from 0 to 10, where 0 represents *the lowest (undesirable) score* possible, and 10 represents *the highest (desirable) score*. The retrofit solutions that provide high strength increase, low cost, less dimensional and clearance constraints, high durability/longevity, ease of construction, and ease of monitoring are assigned high scores. The details of each criterion are described in the following subsections.

2.5.1. Strength Increase

Ability to provide sufficient increase in strength is the most important criterion to evaluate the retrofit solutions. In this study, all 18 alternatives are designed to provide sufficient strength increase; therefore, the strength increases criteria focus on two subcategories: (a) the location and deficiency addressed, and (b) the effectiveness and robustness of the given solution.

Retrofit solutions were first evaluated based on the location (internal or external) strengthened and the primary purpose of the proposed solution. Six subcategories are defined for strength increase in terms of location and deficiency: (a) interior ledge flexure deficiency, (b) interior punching shear deficiency, (c) interior hanger deficiency, (d) exterior ledge flexure deficiency, (e) exterior punching shear deficiency, and (f) exterior hanger deficiency. Full scores for these six subcategories sum to 15. The total score for the location and deficiency addressed is normalized to 10 to combine with the score for another subcategory of the retrofit system that has a full score of 10.

Table 2.2. Scoring Definitions for Six Criteria.

Score	Strength Increase		Cost	Constructability					Dimensional and Clearance Constraints (in.)	Durability/Longevity			Ease of Monitoring
	F/S/H deficiency* for int. [for ext.]	Retrofit system	Total cost (K)	Risk of. damaging reinf.	Access req.	Total weight (kips)	Lane closure (day)			Corrosion	Debonding	Risk of fatigue and fracture	Method
							Below bridge	Above bridge					
0	No strengthening		>$100	Very high	Diaphragm and web	>10	>30	>30	>9	Directly exposed to environment	FRP w/o anchors	Very high	Not possible
1	1 int. girder [Partial ext.]	—	$91–$100	—	—	9 – 10	27–29	27–29	8–9	—	—	—	—
2	2 int. girders [Full ext.]	—	$81–$90	High	Behind the girders	8 – 9	24–26	24–26	7–8	Directly exposed to environment below bridge	Anchored FRP using epoxy	High	NDT
3	3 int. girders	—	$71–$80	—	—	7 – 8	21–23	21–23	6–7	—	—	—	—
4	—	Passive support	$61–$70	Medium	Deck and/or bottom	6 – 7	18–20	18–20	5–6	Partially enclosed	Grouted threadbars	Medium	Borescope testing
5	—	—	$51–$60	—	—	5 – 6	15–17	15–17	4–5	—	—	—	—
6	—	Strengthening	$41–$50	Low	Web and/or ledges	4 – 5	12–14	12–14	3–4	Fully enclosed	Large epoxy anchor	Low	Hands-on inspection
7	—	—	$31–$40	—	—	3 – 4	9–11	9–11	2–3	—	—	—	—
8	—	Alt. load path	$21–$30	Very low	Bottom	2 – 3	6–8	6–8	1–2	Enclosed and grouted	Small epoxy anchor	Very low	Visual inspection w/ lift
9	—	—	$11–$20	—	—	1 – 2	3–5	3–5	0–1	—	—	—	—
10	—	Active support	$0–$10	No risk	Sides and/or ends	0 – 1	0–2	0–2	0 (No changes)	Noncorrosive material	No risk	None	Visual inspection from ground

**F = Ledge flexure, S = Punching shear, H = Hanger deficiency*

The effectiveness and robustness of the proposed retrofit solution is another important strength consideration. Retrofit solutions are categorized as one of four retrofit systems: (a) active support system, (b) passive support system, (c) alternate load path system, and (d) strengthening system.

An *active support system* actively supports a share of the total load prior to any potential overload being applied. A *passive support system* is supplementary to the original structure and its associated load paths. For a passive system to work under overload, the primary structure will need to start failing by incurring greater-than-normal structural deformation. As deformations markedly increase, the passive system begins engaging by providing a supplementary load path. An *alternate load path system* relieves some of the girder reaction on the bearing pad and directs it elsewhere by providing an alternative load path. The standard design of an existing inverted-T bent system applies the reaction of the girder onto the bearing seat on the ledges of the inverted-T beam. Any system that provides a new load path relieving the load from the ledge and providing an alternative path to the web of the inverted-T bent cap may be considered an alternative load path system. A *strengthening system* enhances the capacity of the primary resistance mechanism to provide greater overall capacity. In contrast, active and passive support systems are *augmentation systems* that are new to the structure.

2.5.2. Cost

The total construction cost of each retrofit solution was estimated using the unit costs based on the contractor's prices for materials, labor, and equipment. Details of the required work items and bill of quantities for each alternative are described in Hurlebaus et al. [6].

The required work items are decomposed as primary activities (drilling holes, welding steel plates, etc.), major items (steel angle, steel bracket, threadbar, anchor bolts, etc.), and their ancillary items that support the primary activities such as equipment rental and operator costs. The costs of required items are categorized as material, labor, and equipment costs, and calculated using the unit cost method. The unit prices of each work item are estimated mainly based on the contractor's prices for materials, labor, and equipment. The cost data are established based on E-base and historical data from previous TxDOT projects. Adjustments are made to unit prices to reflect specific conditions such as quantity (unit prices for larger quantities of a material are less than smaller quantities), availability (if the complete unit is available), and commonality of the items.

Among the work items, a boom lift is considered as a general requirement item since the bent caps are elevated around 8 m from the ground. The labor cost of construction workers is also common to all cases. It is assumed that three construction workers will engage in the whole construction process. A telehandler with an operator is considered if the weight of a component exceeds 230 kg (500 lb).

Drilling of concrete may also be considered as a common operation since most of the proposed retrofit solutions require drilling and anchoring into the concrete. There are several drilling methods that can be used to drill the concrete depending on the depth and diameter of the hole. Hammer drills may be used for drilling shallow and small diameter holes at a fairly low cost. Concrete core drills or rock-bolt drills may be used for drilling relatively deep holes and various diameters that can go up to 1.5 m for the core drill. The

drilling depth was considered as the critical factor in this study, and the concrete drilling method was selected based on the required drilling depth.

Hammer drills can be selected to drill a hole that has a drilling depth smaller than 610 mm; otherwise, core drills can be considered for estimating the relative cost. Rock-bolt drills can also be used for deep concrete drilling operations and can be more cost effective if there are a large number of holes to be drilled. For the hammer drills, the cost of hammer drill bits is considered as an ancillary item. For the core drills, which require relatively higher expertise, labor cost for a core drill specialist, rental cost for a core drill rig, and material cost for a diamond core drill bit are considered. The same drilling speed rate is assumed for all solutions for estimating the work hours required for concrete drilling.

Steel components (steel angle, steel bracket, etc.) are another major item that may significantly contribute to the total cost. The unit price of A36 steel is estimated based on the provided contractor's price, and a markup of 30 percent is applied to consider the wastage cost. Plasma cutting of the steel plate, welding, and corresponding labor costs, if any, are considered as ancillary items of steel components.

In the case of grouted and epoxy anchored bolts and rods, the cost of grout and epoxy resin is considered as the material cost, and equipment cost includes specific epoxy guns, grouting mixer, and pump. The cost of the grouted threadbars that are longer than 1.5 m considers the use of hollow bars with grout inlet holes. For the FRP application, the costs of grinding and epoxy resin are considered as ancillary items. For PT bars, extra costs of a post-tension jack and post-tension specialist are also included in the total cost.

The mobilization cost is estimated as a lump sum bid item and added to the total cost. The mobilization cost is conservatively taken as 20 percent of the total cost. A 20 percent contingency sum is added to the subtotal to account for uncertainties in quantities of work items, unit prices, and potential risk events during the construction of retrofits.

2.5.3. Constructability

Constructability is considered as the successful implementation of all operations. The constructability of each alternative is evaluated based on the difficulty of required operations and certain risk factors involved during the application of these operations. The constructability considerations include (i) risk of damaging reinforcement, (ii) accessibility requirements, (iii) possible lane closures, (iv) the weight that must be lifted, and (v) overall ease of construction. Since there is a possible lane closure above and below the bridge, five categories are defined for constructability with the considerations. The average of the scores from these five subcategories is taken as the constructability score of the considered retrofit method.

Most retrofit solutions require some drilling and anchoring into the concrete, which may create a risk of damaging the existing mild steel reinforcement in the bent. This risk is greater as the drilling depth and diameter increase. Although it is possible to identify the location of reinforcement accurately, there may still be some level of risk associated with drilling holes at an angle. For example, the clamped cross threadbar solution requires drilling a long diagonal hole from the bottom of the ledge through the web, which has a high risk of damaging hanger stirrups. On the other hand, the steel hanger brackets having several anchor bolts have a low risk of damaging existing reinforcement since the short-

distance horizontal drilling operation has to avoid just one layer of stirrups. The retrofit options are rated relative to each other in terms of the risk involved in damaging the existing reinforcement.

Another difficulty is the accessibility requirement for the installation of various steel and bar components on the inverted-T bents. Each retrofit solution has different steel plates, threaded bars, steel brackets, etc., and the size of these components necessitates different accessibility requirements. Each retrofit solution is rated such that solutions that use smaller components and require less accessibility are assigned a higher score. One of the major operations is lifting and installing heavy steel components on the bent. Most of these operations require a telehandler, which increases the time and cost of operations. The retrofit solution can be considered as less attractive as the number of heavyweight components increases.

Lane closure is an important consideration for evaluating the viability of retrofit solutions. Lane closures cause some level of disturbance to the public, creating direct and indirect costs. Direct costs include workers, additional traffic signs to reroute traffic, and the like. Indirect costs incurred by the public include extra gasoline consumption and delay due to congestion. The solution that creates a minimum disturbance to the public and requires minimum lane closures gets the highest score (Solution 8). The total lane closure times for the lanes above and below the bridge are estimated to provide quantifiable information, which provides objective guidance for rating the retrofit solutions. The solutions that require less lane closure time are assigned a higher score.

Total weight of the components that need to be lifted up is an important factor to assess the constructability of each solution since the bent caps are located approximately 8 m from the ground, and the heavier components are more difficult to lift up. Therefore, the highest score of 10 is assigned for the solution with a component under 450 kg (1 kip), and the lowest score of 0 is assigned for solution components over 4.5 ton (10 kips).

2.5.4. Dimensional and Clearance Constraints

In most practical applications, dimensional and vertical clearance constraints beneath the bridge are more critical than horizontal clearances at the sides of the bents. Therefore, only the dimensional and clearance constraints beneath the bridge are considered, which can easily be quantified based on the amount of protrusion beneath the bent. The highest score of 10 indicates that there are no changes in vertical clearance due to retrofitting.

2.5.5. Durability/Longevity

Durability is the ability of the material/retrofit to resist any long-term deterioration such as corrosion, wear, fatigue, and/or disintegration due to cyclic moisture and temperature changes that may compromise the life expectancy of the retrofitted structure. Longevity of a structure can be defined as the ability of the structure to have a longer life span under continuous service. It is imperative to select appropriate construction material for durable construction, which simply provides longevity by increasing the life cycle of the structure. Therefore, the durability of the proposed solutions is also considered while rating the viability and effectiveness of the retrofit solution. The durability of the retrofit solution may increase the overall long-term economic efficiency while assuring sufficient capacity throughout the intended lifetime of the structure.

One of the most common durability concerns is corrosion of the steel components used for the retrofit. Corrosion causes degradation of the metallic area by chemical reactions with the environment, especially when the moisture content is high. Substructure components are particularly susceptible to corrosion due to runoff through expansion joints, potentially leading to rapid corrosion in that substructure region. The proposed retrofit solutions on inverted-T bent caps are generally in such critical high-risk regions where they can be exposed to moisture more often. Although there may be solutions to provide additional corrosion protection, such as galvanizing or epoxy coating, these solutions are not considered in scoring the retrofit solutions because they can be applied to all steel components and do not affect the relative score. Instead, the retrofit solutions are evaluated based on the materials used, the concrete or grout cover provided for the steel components, and whether they are directly exposed to the environment or enclosed within a drilled hole.

Another parameter that affects the durability and longevity of the retrofit solution is the effectiveness of the bond between concrete and epoxy. The mechanical properties and short-term behavior of such systems have been well studied, but the long-term performance remains largely unknown. The concrete-epoxy interface may experience debonding due to moisture ingress, freeze-thaw cycles, or thermal loading coupled with mechanical loading. Although epoxy anchored bolts may experience debonding, moisture-affected debonding failures in FRP retrofitted systems may be a more critical issue in terms of durability of the retrofit system. These differences and risk levels require consideration while scoring retrofit solutions.

2.5.6. Ease of Monitoring and Inspection

Monitoring, inspection, and condition assessment of critical components, and of the entire retrofit solution, is also an important consideration. Condition assessment allows bridge owners or engineers to take timely, proactive action to mitigate or prevent further deterioration and unanticipated failure of structural components.

Although corrosion protection methods and construction practices have improved over time, there remains the possibility of some degree of corrosion. The consequences may be significant if inspection, maintenance, and repairs are not performed in a timely fashion.

It is possible to use a relatively inexpensive visual inspection method for external retrofit solutions where corrosion distress can be identified visually in terms of staining, cracking, or spalling of the concrete cover. However, these distress indicators are typically not visible when threadbars are enclosed or embedded in concrete. In such cases, inspectors may need to use relative time-consuming (expensive) *nondestructive testing* (NDT) methods such as a borescope. It is desirable that a retrofit solution be easily inspected; thus, retrofit solutions are rated based on the difficulty of inspection.

2.6. Applying WSM for Selecting Retrofit Solutions for In-service Inverted-T Bent Caps

As noted in the introduction, Hurlebaus et al. [6] proposed eighteen unique solutions (illustrated in Figure 2.1) to retrofit in-service inverted-T bent caps to improve serviceability and ultimate strength capacities. The details of the retrofit solutions and evidence of scores for each solution are provided in Hurlebaus et al. [6]. Figure 2.2 shows a complete set of unweighted scores measured by following scoring definition of each criterion. Detail scores of each solution for individual criteria are provided in Appendix A.

Table 2.3 lists the weights assigned in this study. Each criterion is weighted to emphasize the desired influence among the remaining criteria; the sum of all the individual weights must be unity. The weights were established based on discussions with recommendations from the asset owner's priorities. Clearly, the owner valued most a strength-driven approach by emphasizing the strength category with a 50 percent weight.

The decision matrix is a representation of ratings and rankings for all retrofit solutions, in which the overall scores for each retrofit solution are collected and summarized in a more concise and practical format (see Table 2.4). The decision matrix must rely on quantitative metrics that relate the rehabilitation needs of the structure and the performance of the proposed retrofit solution. Having quantifiable metrics enables the decision matrix to be repeat and general enough for the inclusion of new retrofit alternatives.

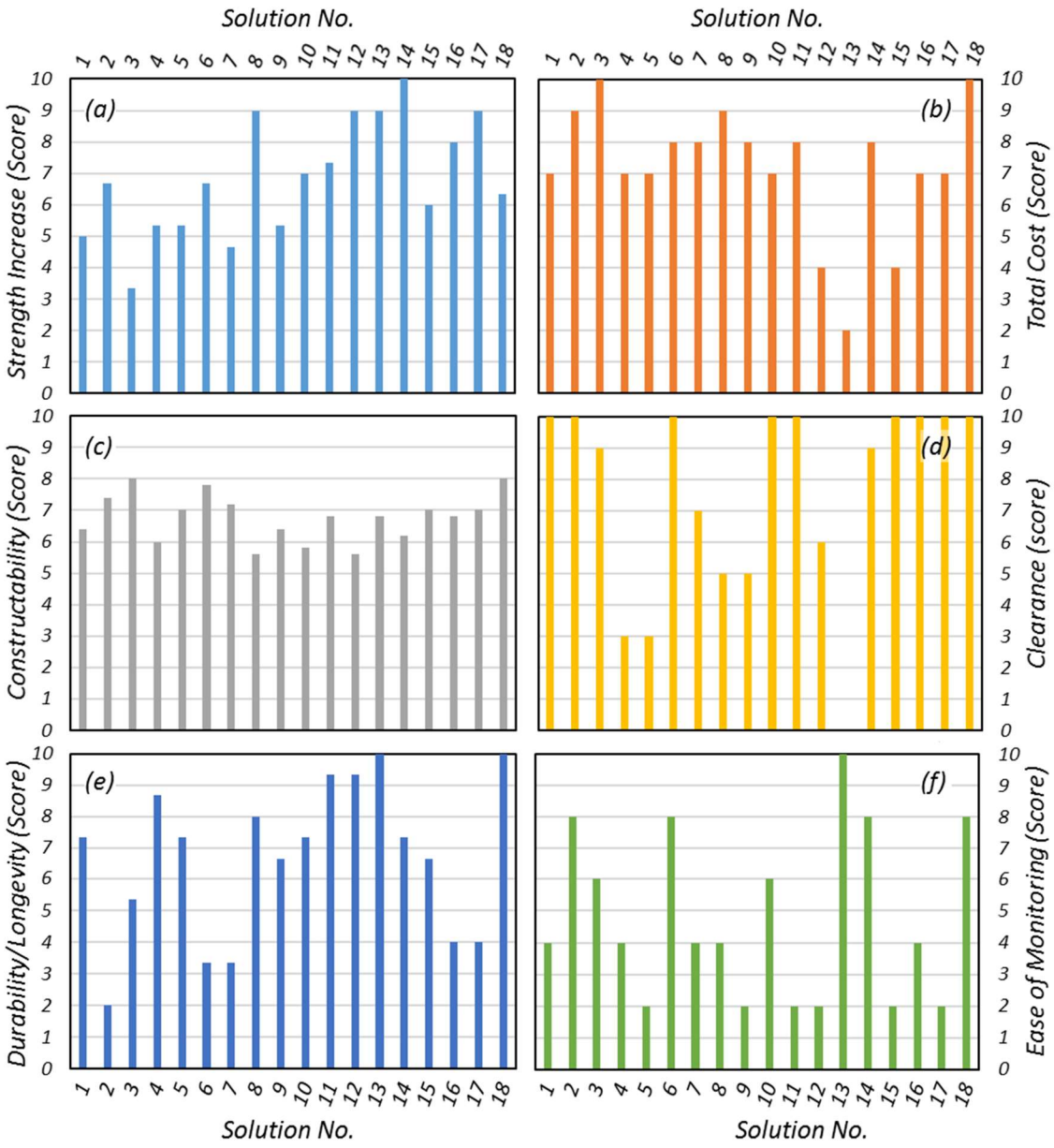

Figure 2.2. Comparison of retrofit solutions in terms of six criteria. The highest (most favorable) score is 10, the most desirable; 0 is the lowest score.

Table 2.3. Weight factors for considered criteria.

Criteria		Weight Factors	
C_1	Strength increase	W_1	50%
C_2	Total cost	W_2	15%
C_3	Constructability	W_3	10%
C_4	Clearance constraints	W_4	15%
C_5	Durability/longevity	W_5	5%
C_6	Ease of monitoring	W_6	5%

Systematic evaluation of retrofit options requires rating and ranking based on their ability to provide sufficient strength at a lower cost while creating minimum clearance and constructability issues. In order to create a systematic procedure for developing the decision matrix, scoring definitions are provided for each criterion in the previous section. Most of the definitions provide measurable benchmarks for the assigned scores such as in the case of strength and cost criteria. Although for most of the considered criteria it is possible to identify some measurable outcomes, it may not be always possible to establish a quantifiable benchmark such as in the case of durability criterion. In that case, relatively subjective evaluation categories were created based on engineering judgment.

The scoring system using weights is straightforward for engineers to apply as well as easy to modify using the decision matrix. If the bridge engineer wants to add a new retrofit solution or modify existing solutions, the engineer can do so by simply inserting a new row to the individual scoring tables as defined in the previous sections. Similarly, a new criterion (such as aesthetics) can be added by preparing the scoring definitions and rating table for this new criterion. Then the weight factor table should be modified to incorporate the new criterion, with the sum of all factors equal to unity.

Table 2.4. Decision matrix for the evaluation of retrofit methods

			Criteria						Score
			C_1, Strength Increase	C_2, Total Cost	C_3, Constructability	C_4, Clearance	C_5, Durability / Longevity	C_6, Ease of Monitoring	
Weight Factor:			w_1	w_2	w_3	w_4	w_5	w_6	
Retrofit Alternatives	1	Prestressed high strength threadbar	$a_{1,1}$	$a_{1,2}$	$a_{1,3}$	$a_{1,4}$	$a_{1,5}$	$a_{1,6}$	S_1
	2	Steel hanger bracket	$a_{2,1}$	$a_{2,2}$	$a_{2,3}$	$a_{2,4}$	$a_{2,5}$	$a_{2,6}$	S_2
	3	End region stiffener	$a_{3,1}$	$a_{3,2}$	$a_{3,3}$	$a_{3,4}$	$a_{3,5}$	$a_{3,6}$	S_3
	4	Clamped cross threadbar	$a_{4,1}$	$a_{4,2}$	$a_{4,3}$	$a_{4,4}$	$a_{4,5}$	$a_{4,6}$	S_4
	5	Grouted cross threadbar	$a_{5,1}$	$a_{5,2}$	$a_{5,3}$	$a_{5,4}$	$a_{5,5}$	$a_{5,6}$	S_5
	6	Upper seat brackets	$a_{6,1}$	$a_{6,2}$	$a_{6,3}$	$a_{6,4}$	$a_{6,5}$	$a_{6,6}$	S_6
	7	Threadbar hanger with steel bracket	$a_{7,1}$	$a_{7,2}$	$a_{7,3}$	$a_{7,4}$	$a_{7,5}$	$a_{7,6}$	S_7
	8	Through-web PT threadbar with catcher channel	$a_{8,1}$	$a_{8,2}$	$a_{8,3}$	$a_{8,4}$	$a_{8,5}$	$a_{8,6}$	S_8
	9	Grouted threadbar anchored with channel	$a_{9,1}$	$a_{9,2}$	$a_{9,3}$	$a_{9,4}$	$a_{9,5}$	$a_{9,6}$	S_9
	10	Anchored FRP wrap	$a_{10,1}$	$a_{10,2}$	$a_{10,3}$	$a_{10,4}$	$a_{10,5}$	$a_{10,6}$	S_{10}
	11	Concrete infill with prestressing threadbar	$a_{11,1}$	$a_{11,2}$	$a_{11,3}$	$a_{11,4}$	$a_{11,5}$	$a_{11,6}$	S_{11}
	12	Concrete infill with hanger threadbar	$a_{12,1}$	$a_{12,2}$	$a_{12,3}$	$a_{12,4}$	$a_{12,5}$	$a_{12,6}$	S_{12}
	13	Concrete masonry piers	$a_{13,1}$	$a_{13,2}$	$a_{13,3}$	$a_{13,4}$	$a_{13,5}$	$a_{13,6}$	S_{13}
	14	Load balancing post-tensioning	$a_{14,1}$	$a_{14,2}$	$a_{14,3}$	$a_{14,4}$	$a_{14,5}$	$a_{14,6}$	S_{14}
	15	Concrete infill with FRP anchored by FRP anchors	$a_{15,1}$	$a_{15,2}$	$a_{15,3}$	$a_{15,4}$	$a_{15,5}$	$a_{15,6}$	S_{15}
	16	Concrete infill with partial-depth FRP anchored by steel waling	$a_{16,1}$	$a_{16,2}$	$a_{16,3}$	$a_{16,4}$	$a_{16,5}$	$a_{16,6}$	S_{16}
	17	Concrete infill with full-depth FRP anchored by steel waling	$a_{17,1}$	$a_{17,2}$	$a_{17,3}$	$a_{17,4}$	$a_{17,5}$	$a_{17,6}$	S_{17}
	18	Enlarged bearing pad	$a_{18,1}$	$a_{18,2}$	$a_{18,3}$	$a_{18,4}$	$a_{18,5}$	$a_{18,6}$	A_{18}

Figure 2.3 shows comparative bar charts for average unweighted scores and weighted scores for all solutions. Based on the unweighted total scores of solutions (see Figure 2.3(a)), Enlarged bearing pad solution (Solution 18) scored the highest value followed by a load balancing post-tensioning (PT) solution (14) and upper seat bracket solution (6). These results did not reflect relative importance between the criteria.

To emphasize importance of a criterion, weight factors were then assigned. Figure 2.3(b) illustrates weighted scores for all retrofit solutions. The top five solutions are load balancing (14), concrete infill with full-depth FRP anchored by steel waling (17), enlarged bearing pad (18), through-web PT threadbar with catcher channel (8), and concrete infill with partial-depth FRP anchored by steel waling (16). However, the ranking can still be changeable by varying weight factors. To investigate the effects of the weights for each criterion, sensitivity analyses were conducted.

2.7. Sensitivity Analysis

Sensitivity analysis is a basic analysis method for the effective use and implementation of an MCDM method. There are numerous methodologies that can be used to conduct sensitivity analysis for an MCDM method. In this study, two commonly used sensitivity analysis techniques, which are applicable for most MCDM methods, were adopted: (i) the simulation approaches proposed by Butler et al. [69]; and (ii) the deterministic method developed by Triantaphyllou and Sánchez [70]. The simulation approaches were used to discover the sensitivity of alternatives to the weight factors, while the deterministic methods were used to determine the most critical criteria.

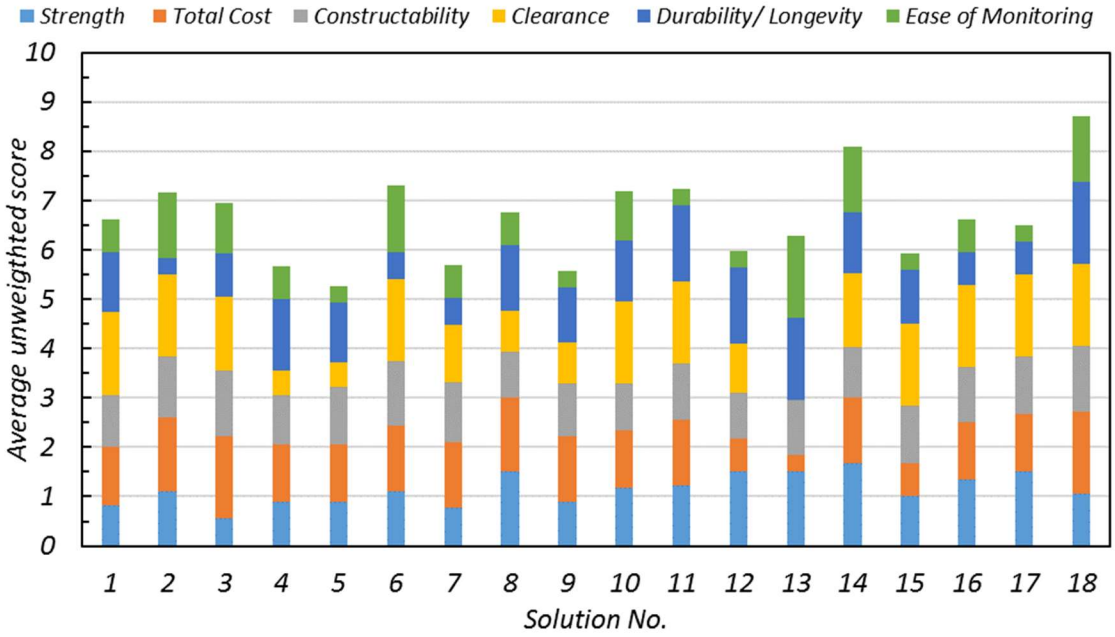

(a) Average unweighted scores (the possible highest score is 10)

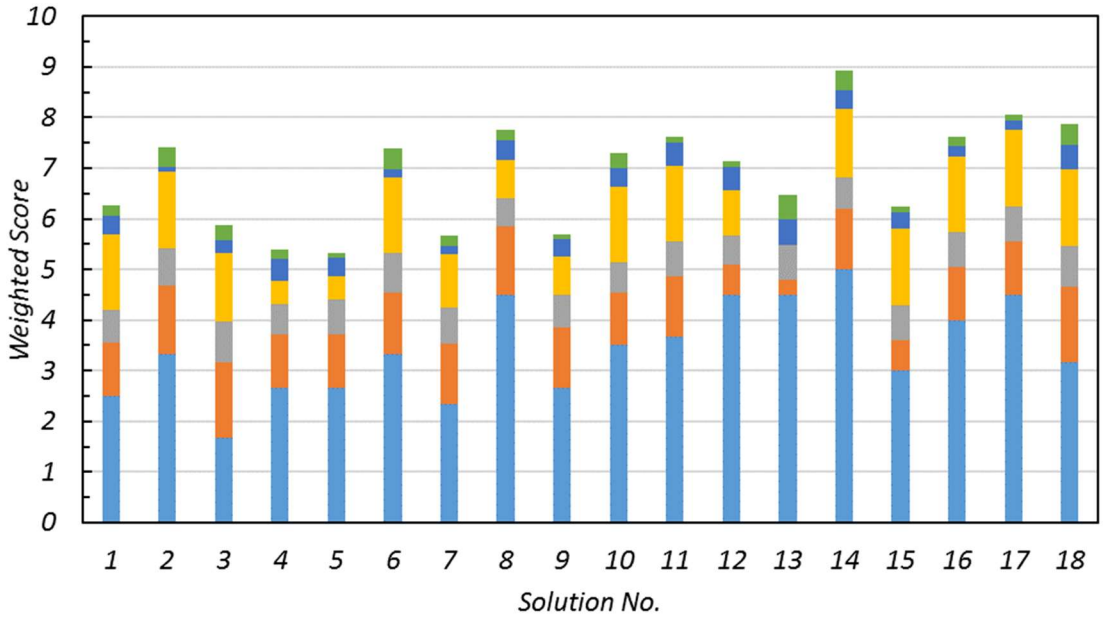

(b) Weighted scores (the possible highest weighted score is 10)

Figure 2.3. Total unweighted and weighted scores for retrofit solutions.

2.7.1. Simulation Approaches

Butler et al. [69] proposed three classes of the simulation approaches based on the information on the weights: no information (*random weights*), importance order information (*rank-order weights*), and partial information (*response distribution weights*). However, Butler et al. [69] noted that the approach with *response distribution weights* requires weight assessment, but these assessed weights may be subjected to response error. These errors allow for the selection of weights that violate the rank-order of the weights. Therefore, in this study, simulation approaches with *random weights* and *rank-order weights* were conducted.

The ranking of the retrofit solutions (or alternatives) was obtained from simulated WSM scores with 5000 independent sets of both weights (*random* and *rank-order*). The weights can be generated by a computer simulation program; in this study, MATLAB (2018) was used.

Figure 2.4 presents the results of the simulation with both *random weights* and *rank-order weights* using the box-and-Whisker plots. The plots include the boxes representing quartile limits with the median (red lines), upper and lower 1.5 interquartile ranges (1.5IQR, dashed lines), and outliers (blue dots beyond 1.5IQR).

2.7.1.1. Random Weights

As an extreme case, weights for each criterion may be generated completely randomly (*random weights*). This approach implies no prior knowledge of the relative importance of the criterion. Simulated *random weights* were used to determine the statistics for the ranking of the alternatives.

Figure 2.4(a) shows the potential rankings of the alternatives with *random weights*. The rankings are widely distributed for the most alternatives. Based on the rank distribution of the solutions, potential top and bottom solutions could also be determined. It is also determined sensitivity level of the weights; the alternative with wider ranking distribution is more sensitive to the weights of the criteria.

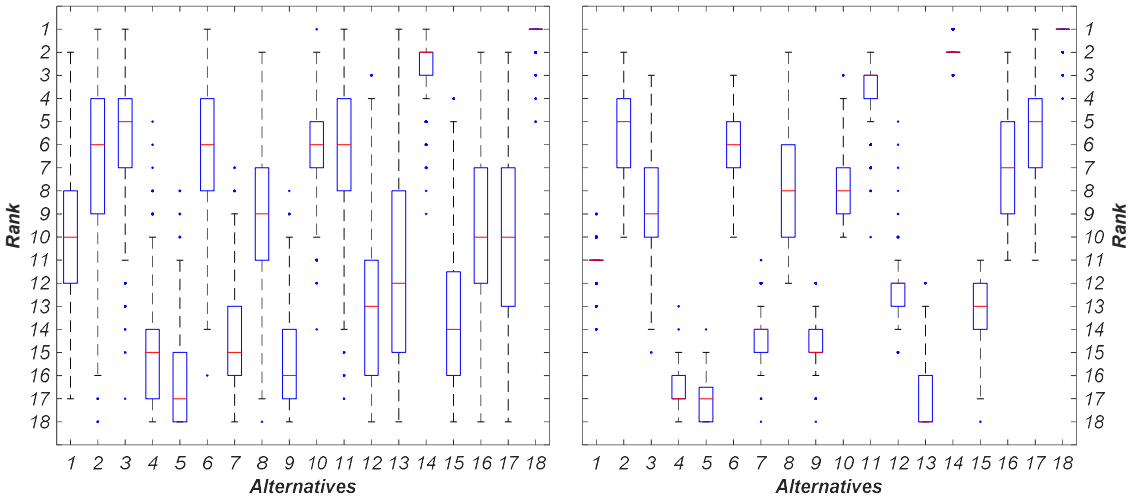

(a) Random weights *(b) Rank-order weights*

Figure 2.4. Ranking comparison for 5000 simulated weights. Red lines correspond to the median ranking; the box encloses middle 50% of the ranking distribution; dashed lines are 75% of the ranking distribution; and dots are the outliers

Solutions 18 and 14 appeared to be reliable solutions with relatively narrow ranking distribution. Solution 18 was top-ranked for 75-percent of the simulations; while for the rest of the simulations (25-percent) it was ranked in the top five. Solution 14 can be considered as the second-best solution ranking in the top three for 75-percent of the simulations. In a similar fashion, Solutions 5 and 9 were narrowly distributed in the low ranking. The ranking of the solutions 5, 9, 14, and 18 were distributed within relatively

narrow range, which means these solutions are less sensitive to the changes in the weights of the criteria.

On the other hand, most solutions, especially Solutions 2, 3, 8, 13, 16, and 17, were ranked in a wide range, which means they are highly sensitive to the changes in the weights of the criteria. To obtain more specific results, the selection of the weights needs to be somewhat constrained based on importance of the criteria.

2.7.1.2. Rank-Order Weights

When a criterion is obviously 'more important' than others but the exact weights are still legitimately questioned, *rank-order weights* may be used to analyze the stability of alternatives. The *rank-order weight* is the weight of a criterion randomly selected in accordance with the *rank-order* of the criteria based on its importance. For example, if criterion C_1 is more important than criterion C_2, a weight for C_1 may be any number smaller than the weight for C_2. In this study, the rank-order of the criteria based on the given opinion from the asset owners was adopted herein: '*Strength'* is the most important and followings are in order of '*Cost'*, '*Constraints'*, '*Constructability'*, '*Durability'*, and '*Ease of monitoring*'.

Figure 2.4(b) shows a comparative ranking of the solutions which was determined with the *rank-order weights*. The range of possible rankings for the solutions narrowed, as expected when the rank-order of the criteria was adopted.

The most critical criterion may be determined by changing the rank-order of the criteria and identifying the criterion that narrows down the distribution range the most.

However, it is more practical to use the deterministic method to find the critical criterion instead of using simulation approaches.

2.7.2. Deterministic Method

The deterministic method developed by Triantaphyllou and Sánchez [70] focuses on two major factors: (i) the most critical criterion (C_j); and (ii) the most critical measure (a_{ij}). Both can be determined by using a sensitivity coefficient (SC_k) of the criterion (C_k). The SC_k is the largest reciprocal of percent amount where the current values must change to switch ranking of alternatives.

2.7.2.1. The Most Critical Criterion

To determine the most critical criterion, the case of changes in the initial weights of the decision criteria was considered. The minimum change in the current weight, W_k, of a criterion, C_k, to reverse the ranking of alternatives A_i and A_j is denoted as δ_{kij}. In this study, the minimum changes in percent (relative), δ'_{kij}, are used and can be obtained as follows:

$$\delta'_{kij} = \delta_{kij} \times \frac{100}{W_k} = \frac{S_j - S_i}{a_{jk} - a_{ik}} \times \frac{100}{W_k}, \text{for any } 1 \le i < j \le M \text{ and } 1 \le k \le N \qquad (2.2)$$

δ'_{kij} may not be feasible when it is impossible to reverse the existing ranking of the alternatives A_i and A_j by making changes on the current weight of a criterion C_k. Therefore, for the value of δ'_{kij} to be feasible, $\delta_{kij} \le W_k$ should be satisfied. All possible δ'_{kij} values need to be calculated to determine the most critical criterion. Note that there are $N \times (M(M-1))/2$ such possible δ'_{kij} values [70]. In this study, eighteen alternatives, $M = 18$, are evaluated in six criteria, $N = 6$. Therefore, a total of 918 values of δ'_{kij} are

obtained. The entire process were programmed in MATLAB to iterate the process automatically.

The most critical criterion is defined in two alternative ways: (i) a criterion with the smallest change in the current data (score) causes a ranking change in any alternative referred as *percent-any critical criterion*; and (ii) a criterion with the smallest change in the current data causes a ranking change in the best (top) alternative referred as *percent-top critical criterion*. The *percent-any critical criterion* applies when one is interested in changes in the ranking of any alternatives, while the *percent-top critical criterion* can be adopted when one is only interested in changes in the best alternative. To find *percent-any* and *–top* critical criteria, the SC_k can be expressed by $SC_k = max\{1/|\delta'_{kij}|\}$. If δ'_{kij} is infeasible ($\delta_{kij} > W_k$), then $SC_k = 0$.

Figure 2.5 presents the sensitivity coefficients for each solution corresponding to each criterion. The *percent-any critical criterion* can be identified by the maximum SC_k value. The sensitivity coefficient for the considered six decision criteria are; $SC_1 = 0.21$, $SC_2 = 0.19$, $SC_3 = 0.04$, $SC_4 = 0.15$, $SC_5 = 0.16$, and $SC_6 = 0.06$. Therefore, the most sensitive criterion (or *percent-any critical criterion*) is C_1 (*Strength*), followed by C_2 (*Cost*), C_5 (*Durability*), C_6 (*Ease of monitoring*), C_4 (*Dimensional constraints*), and C_3 (*Constructability*). With changing the lowest percent (4.7 percent = $1/SC_1 = 1/0.21$) in *Strength* may change the rank orders of the alternatives.

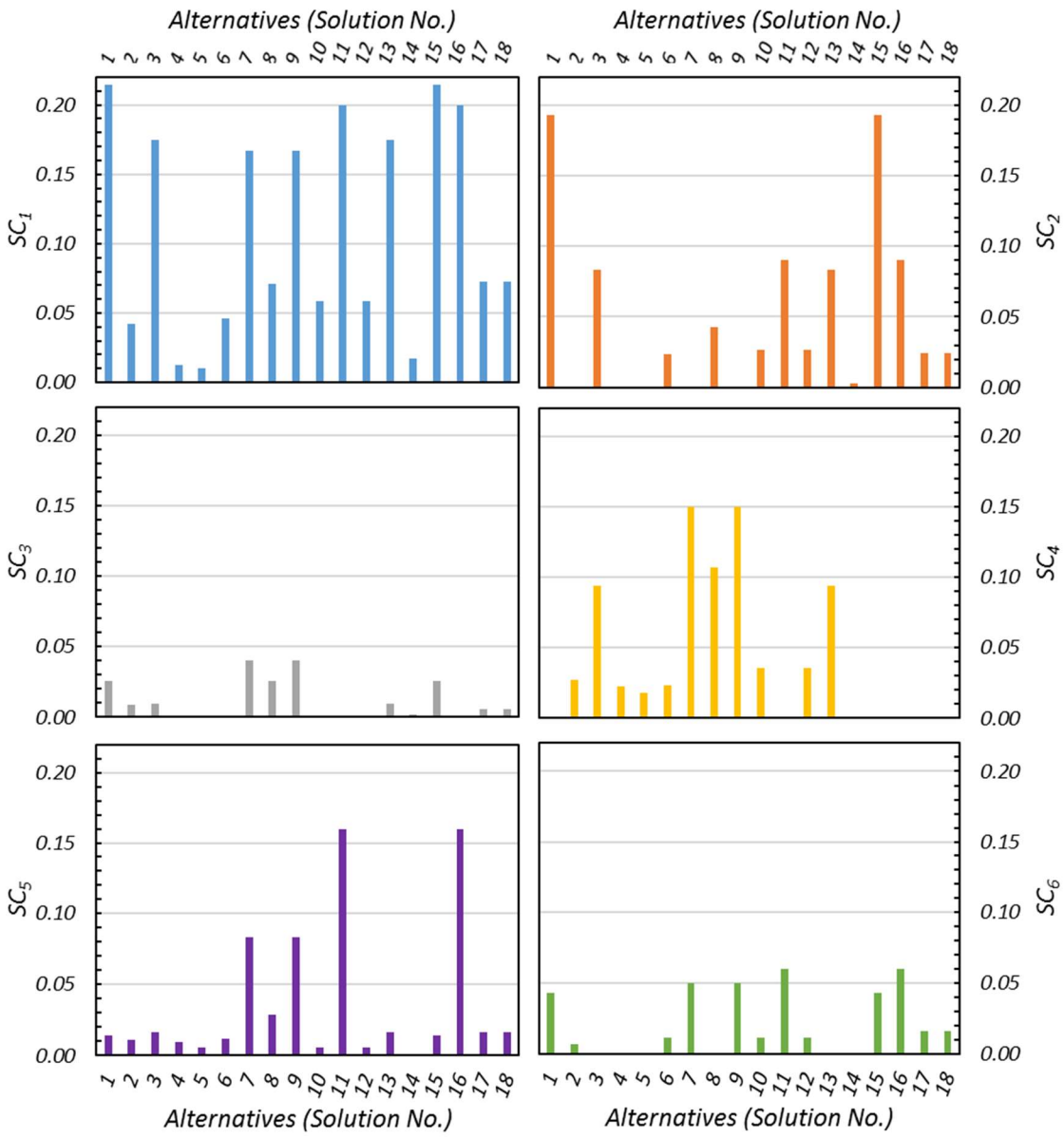

Figure 2.5. The largest sensitivity coefficient (SC_k) values for each solution corresponding to each criterion (C_k)

The *percent-top critical criterion* can be identified by investigating the largest SC value related to Solution 14 (top alternative). The SC values for Solution 14 are listed in Table 2.5. The largest sensitivity coefficient was 0.0171 corresponds to criterion C_1 (SC_1 = 0.0171) with the pair alternatives Solutions 14 and 18. That means, the minimum weight change to make Solution 14 not be the best is 58 percent (1/SC = 1/0.0171) reduction in C_1. Table 2.5 shows a lot of zeros. This indicates Solution 14 is highly dependent on (or less sensitive to) the weight of any criteria.

Table 2.5. All possible SC_k related to top ranked alternative, Solution 14

Pair of Alternatives	C_1	C_2	C_3	C_4	C_5	C_6
A1 & A14	0.0000	0.0000	0.0000	-0.0006	0.0000	0.0000
A2 & A14	0.0110	-0.0010	-0.0008	-0.0010	0.0000	0.0000
A3 & A14	0.0114	-0.0010	-0.0007	0.0000	0.0000	0.0000
A4 & A14	0.0000	0.0000	0.0000	0.0000	-0.0002	0.0000
A5 & A14	0.0000	0.0000	-0.0002	0.0000	0.0000	0.0000
A6 & A14	0.0107	0.0000	-0.0010	-0.0010	0.0000	0.0000
A7 & A14	0.0000	0.0000	-0.0003	0.0000	0.0000	0.0000
A8 & A14	0.0000	-0.0012	0.0000	0.0000	-0.0003	0.0000
A9 & A14	0.0000	0.0000	-0.0001	0.0000	0.0000	0.0000
A10 & A14	0.0000	0.0000	0.0000	-0.0009	0.0000	0.0000
A11 & A14	0.0101	0.0000	-0.0005	-0.0011	-0.0008	0.0000
A12 & A14	0.0000	0.0000	0.0000	0.0000	-0.0006	0.0000
A13 & A14	0.0000	0.0000	-0.0002	0.0000	-0.0005	-0.0004
A14 & A15	0.0000	0.0000	-0.0003	-0.0006	0.0000	0.0000
A14 & A16	0.0000	0.0000	-0.0005	-0.0011	0.0000	0.0000
A14 & A17	0.0000	0.0000	-0.0009	-0.0017	0.0000	0.0000
A14 & A18	**0.0171**	-0.0028	-0.0017	-0.0014	-0.0012	0.0000

$^{*}SC_k$ = 0.0 when $\delta_{kij} > W_k$; impossible to reverse the ranking by changing weights of the criterion C_k

2.7.2.2. The Most Critical Measure

Similar to determining the most critical criterion, the threshold value of τ_{kij}, which is the minimum change of score (or measure, a_{ik}) to change ranking between alternatives A_i and $A_{j,}$ can be calculated in relative terms as follows:

$$\tau'_{\mathrm{kij}} = \tau_{\mathrm{kij}} \times \frac{100}{a_{ik}} = \frac{S_j - S_{\mathrm{i}}}{W_k} \times \frac{100}{a_{ik}}, \text{for any } 1 \le i, j \le M \text{ and } 1 \le k \le N \qquad (2.3)$$

To have feasible values of τ'_{kij} should satisfy the condition of $\tau'_{\mathrm{kij}} \le 100$. With *M* alternatives, each a_{ik} is associated with a total of *(M-1)* such threshold values [70]. In this study, a total of 306 τ'_{kij} values are calculated for eighteen alternatives.

To determine the critical measure, *SC* values for each a_{ik} measure are expressed by $SC_k = max\{1/|\tau'_{\mathrm{kij}}|\}$. Figure 2.6 shows SC_k of each solution for all six criteria. The most critical measure is the score for Solution 17 in C_1 (*Strength*) criteria with the maximum *SC* value of $SC_1 = 2.70$. It means that if the score of Solution 17 for *Strength* criterion changes, the ranking of the solutions will be switched with the given weight factors.

2.8. Discussion

A simple and popular multi-criteria decision analysis tool, the *weighted sum model* (WSM), was used to evaluate and rank the retrofit solutions based on the six criteria. The weights provide the engineers the ability to control and represent the desired influence of each criterion. All eighteen retrofit solutions were rated based on the six considered criteria and the total scores were calculated by summing the weighted scores under each criterion.

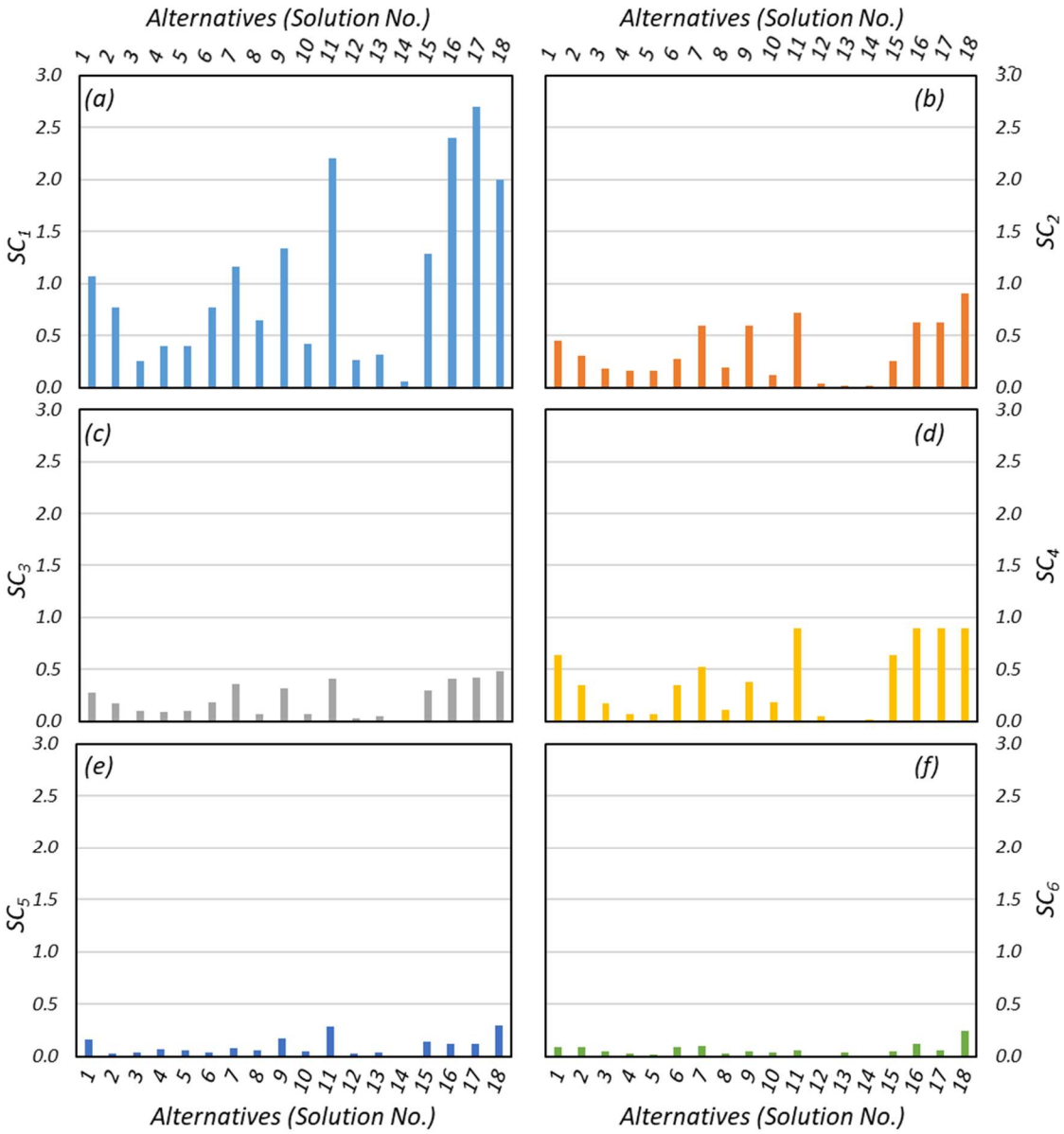

Figure 2.6. Sensitivity coefficient (SC_k) of each solution for six criteria

Table 2.6 lists total scores and rankings of the solutions with three different scenarios. First, eighteen alternative retrofit solutions were ranked based on their average unweighted total scores. This case represents the importance of criteria is the same; all criteria have the same weight factors. Based on the unweighted scores, the top five solutions are Solutions 18, 14, 6, 11, and 10.

Table 2.6. Total score and ranking changes for retrofit solutions with modified weight factors

Ranking	Unweighted		w/ Given Weight		w/ Modified Weight	
	Solution No.	Avg. Total Score	Solution No.	Total Score	Solution No.	Total Score
1	18	8.72	14	7.76	18	8.58
2	14	8.09	17	7.00	14	8.36
3	6	7.30	18	7.37	11	7.59
4	11	7.24	8	6.63	2	7.58
5	10	7.19	16	6.72	6	7.57
6	2	7.18	11	6.81	10	7.35
7	3	6.94	2	6.72	17	7.30
8	8	6.77	6	6.68	16	7.22
9	16	6.63	10	6.53	8	7.09
10	1	6.62	12	6.02	3	6.97
11	17	6.50	13	5.34	1	6.74
12	13	6.30	3	6.02	12	6.22
13	12	5.99	1	5.77	15	6.22
14	15	5.94	15	5.58	7	5.98
15	7	5.70	9	5.12	9	5.76
16	4	5.67	7	5.21	13	5.67
17	9	5.57	4	4.81	4	5.50
18	5	5.28	5	4.74	5	5.32

Second, using strength-driven approach, *Strength* criterion was emphasized by a 50 percent weight factor. In this case, the rank-order of criteria is followed: *strength, cost, clearance constraints, constructability, durability, and ease of monitoring*. With given weights on six criteria as listed in Table 2.3, top five solutions are determined as Solutions 14, 17, 18, 8, and 16. Among them, the rank of Solution 17 increased somewhat when compared to the first case. This is because the *Strength* score for Solution 17 is the most critical measure (see in Figure 2.6).

Finally, another set of weights was defined to evaluate robustness of solutions with the given rank-order of the criteria. W_1 was reduced from 0.5 to 0.25 (50 percent reduction which is the maximum change to keep rank-order of the criteria), and the difference is equally distributed to the other weight factors to maintain the sum of weight factors as unity: $W_1 = 0.25$, $W_2 = 0.20$, $W_3 = 0.15$, $W_4 = 0.20$, $W_5 = 0.10$, and $W_6 = 0.10$. The top five solutions with reevaluated scores are Solutions 18, 14, 11, 2 and 6. Although this case results in different top five solutions when comparing to the results with the second case, the most favorable nine solutions remained in the same regardless of the weights when the rank-order of criteria remains the same.

Solutions 14, 17, 18, 8, 16 and 3 were selected by Hurlebaus et al. [6] to investigate the effectiveness of the solutions. There is a high possibility of adopting these solutions for field applications since they remained consistently the top ranked candidates. Further experimental validation of these solutions is presented in Hurlebaus et al. [6].

2.9. Closing Remarks

Eighteen alternative retrofit solutions for existing inverted-T bent caps were evaluated using a *multi-criteria decision making* (MCDM) method to determine which solutions are most viable. The *weighted sum model* (WSM) was adopted with a given set of weight factors in terms of six criteria: (i) strength increase, (ii) total cost, (iii) constructability, (iv) dimensional and clearance constraints, (v) durability, and (vi) ease of monitoring. To verify the stability of the optimal solutions (alternatives), the sensitivity analyses were conducted using both simulation and deterministic approaches. Based on the analysis, the following conclusions are drawn:

1) The current objective, to rate and rank diversity of retrofit solutions to improve serviceability of inverted-T bent caps, was achieved in a robust fashion. Weighted sum model efficiently considered all six criteria while providing flexibility to consider different weight factors for each criterion depending on their importance.
2) Based on sensitivity analysis results, the most critical criteria and measure was '*Strength'* followed by '*Cost'*. The results represent that the weights for '*Strength*' and '*Cost'* criteria are highly contributed to the ranking of the alternative solutions, and thus, it should be carefully decided based on the condition of the bridges. With the given rank-order of the criteria, top half solutions are determined to be viable with any reasonably defendable combination of weights.
3) For this study, a load balancing PT solution (Solution 14), concrete infill with partial- and full-depth FRP wrap with waling solutions (Solutions 16 and 17),

enlarged bearing pad solution (Solution 18), and through-web post-installed PT threadbar with catcher channel (Solution 8) are deemed the most viable.

.

3. IMPROVING THE SERVICEABILITY AND STRENGTH OF EXISTING INVERTED-T BENT CAPS: SUPPLEMENTAL STEEL RETROFITTING

3.1. Section Summary

Undesirable cracking at the web-to-ledge interface is commonly observed in existing bridge piers with inverted-T bent caps. While such cracking is unexpected, it raises the question: do such cracked bent caps possess sufficient ultimate strength capacity with increasing volume of traffic? In this study, retrofit solutions were developed and experimentally investigated. The solutions were designed to provide supplemental ledge and hanger load paths by attaching additional steel components: through-web post-install post-tensioning (PT) threadbar with "catcher" channel and end-region stiffener. The test results demonstrated the retrofitted inverted-T bent caps remain in a good (operational) condition to levels above the service limit state. The solutions also successfully improved the maximum load carrying capacities by some 60 percent above specified ultimate load demands. These experimental observations were also compared to the calculated strength capacities, and the code-based strength capacities were determined to be overconservative. Repair and retrofit design recommendations were provided, including limitations, based on the experimental investigation.

3.2. Introduction

Bridges often benefit when the piers are constructed using inverted-T bent caps. The clearance beneath such bent caps is improved and the overall bridge elevation is lower, often meaning the approach earthworks require considerably less fill. Many such bridges

were built in Texas during the 1960s. Those bridges exhibit undesirable cracks at the web-to-ledge interface of the inverted-T bent caps, as shown in Figure 3.1(a). Such cracks on inverted-T bent caps may potentially decrease service life and/or are a possible indication of a structural deficiency. One major reason for the cracks is those bridges were built in the age of working stress design when there was a general lack of understating of inverted-T beam behavior. It is not until the work of Mirza and Furlong [14] a better understanding emerged. They investigated the serviceability behavior and failure mechanisms of inverted-T bent caps. They verified that the inverted-T beam bent caps have different structural behavior from conventional top-loaded beams. Mirza et al. [13] provided design criteria which became the basis of the current design codes for inverted-T beam ledges. The criteria require that the beam ledges should resist: (i) flexure, shear, and horizontal forces at the web-to-ledge interface; (ii) tension force in the supporting element; (iii) punching shear at points of loading; and (iv) bearing (seating) forces.

Figure 3.1(b) shows a simple strut-and-tie representation of load paths of an inverted-T bent cap and demonstrates hanger- and ledge-deficiencies. When the ledge tie (reinforcement) capacity (ϕT_f) is less than the load demand (V_u) the structure is ledge-deficient. Whereas, the hanger capacity (ϕT_h) is less than V_u, the structure is hanger-deficient.

(a) Cracks on two bent caps near Austin, Texas.(crack highlighted)

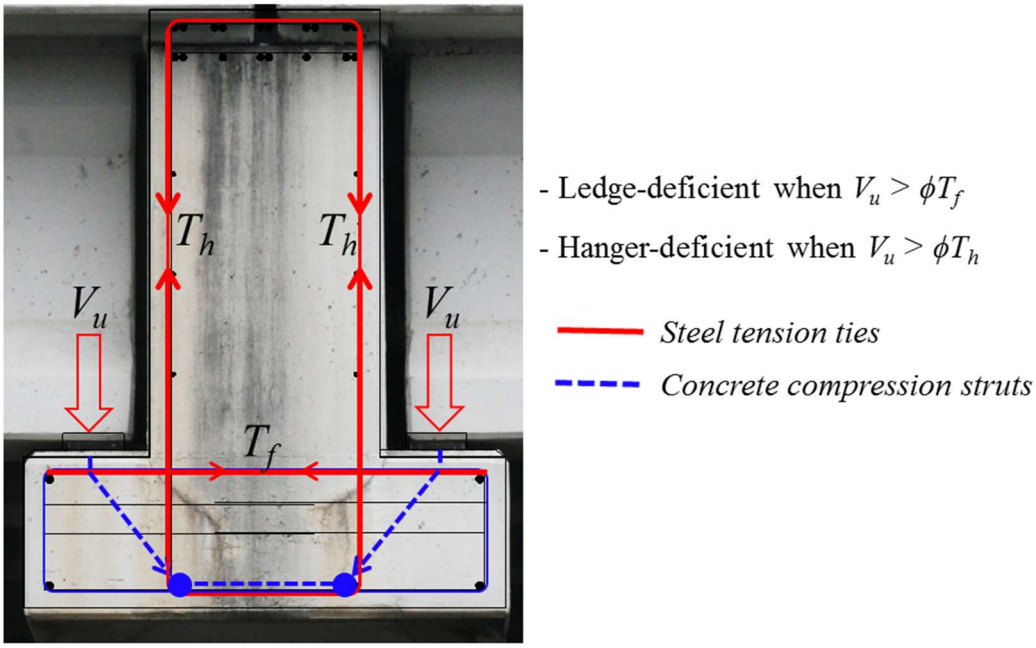

(b) Strut and tie representation of load path that define ledge and hanger deficiencies.

Figure 3.1. Typical cracks at web-ledge interface of in-service inverted-T bent caps.

Zhu et al. [17] investigated the serviceability of inverted-T bent caps. Based on experimental tests, the web-to-ledge interface crack widths were measured. From the results, crack control design provisions to check service limit for both interior and exterior portion of inverted−T bent caps were proposed.

The work described herein investigates methods to address and strengthen existing inverted-T bent caps constructed prior to the work Zhu et al. [17]. These in-service inverted-T bent caps often possess marginally deficient strength capacities when evaluated against current standards. Therefore, replacement or retrofitting of the damaged parts are needed. Retrofitting the structure may be an effective and economical solution as an alternative to replacement.

Since there is a diversity of inverted-T bent caps, which may need rehabilitation, Hurlebaus et al. [6] designed a total of eighteen potential solutions to improve serviceability and strength of in-service inverted-T bent caps. These solutions were broadly grouped as mechanical solutions, external post-tensioning solutions, and FRP solutions. Using generic conceptual designs, Hurlebaus et al. [6] evaluated the solutions based on six criteria: strength increase, total cost, constructability, durability/longevity, dimensional constraints, and ease of monitoring. The six most efficient solutions were adopted for further experimental validation. The selected solutions were tested at one-half scale to investigate their effectiveness.

In-service inverted-T bent caps have shown signs of distress through a series of disquietening cracks observed in the field (Figure 3.1). When evaluated against current standards, such inverted-T bent caps often possess marginal strength capacities. To

economically retrofit such deficient structures, alternative load paths are necessary. This paper presents and focuses on the solutions that providing supplement load paths: through-web post-installed post-tensioning (PT) threadbar with "catcher" channel and an end-region stiffener. This solution was highly ranked as they do not require special equipment and are easy to construct when compared with other viable solutions.

3.3. Design Concepts

To efficiently retrofit deficient in-service inverted-T bent caps showing signs of distress, alternative load paths are necessary. By installing additional steel components, the supplemental load paths are provided through the retrofit systems: (i) through-web PT threadbar plus channel; and (ii) end-region stiffener. Figure 3.2 presents the two basic concepts which provide alternative load paths.

Figure 3.2(a) shows the strut-and-tie model (SAT model) demonstrating the supplemental load path system for the retrofit solution using through-web post−installed PT threadbar connected to an external "catcher" channel. This retrofit solution is designed to provide an additional hanger capacity via PT threadbar, while the channel provides a supplement load path to resist ledge flexure. Therefore, in addition to the original load paths (blue SAT model), the PT threadbar performs as a hanger to transfer the girder loads into the web, and the channel catches the loads passing through the ledge (red SAT model).

Figure 3.2(b) shows the cross-sectional and elevation views of the through-web PT threadbar with catcher channel solution showing the combined SAT load paths. The threadbar is placed within the web and essentially anchored with a nut and thick plate washer. By prestressing the threadbar, this retrofit system actively resists a part of dead

load of the girder and restrains pre-existed cracks. At the bent cap soffit, a steel channel is placed in the transverse direction. If needed, the alignment of the threadbars can be staggered to avoid the longitudinal reinforcement in the bent cap. The solution is applicable to both straddle and cantilever bent caps.

Figure 3.2(c) demonstrates the SAT load paths for the end-region stiffener retrofit solution. The end‑region stiffener solution consists of a steel plate bond to and also anchored via bolts to the end-face. The anchored steel end-plate functions similarly to the internal hangers thereby providing a supplemental load path.

It should be noted that there is a class of inverted-T bent caps that exist on hammerhead (cantilever) piers where the ledge is tapered with increasing thickness toward the central support column. The end of the cantilever, where the ledge is the thinnest, is often the only vulnerable location. Therefore, this bonded and bolted steel end-plate solution alone may suffice in retrofitting the piers. Moreover, where access is available it can easily be installed from off the bridge thereby minimizing or negating lane closures.

3.4. Design Verification Check

In accordance with AASHTO [10] specification, the designed strength (or resistance, V_r) of a retrofitted system should be verified by

$$\phi V_r = \phi(V_n + V_{ret}) > V_u \tag{3.1}$$

in which V_n = nominal resistance of the beam ledge which is elaborated upon below; V_{ret} = strength increase due to the retrofit solution; $V_u = 1.25V_{\text{DL}} + 1.75V_{\text{LL+I}}$ = ultimate factored load demand calculated in accordance with AASHTO [10], where V_{DL}

= dead load and $V_{\mathrm{LL+IM}}$ = live load plus impact effects; and ϕ = resistance factor (in AASHTO [10], this is taken as $\phi = 0.9$).

The ledges of the inverted-T beams are supported primarily by the transverse reinforcement (hanger and ledge reinforcement). This reinforcement controls their respective hanger and ledge capacities. For capacity calculations, the yield strength of the reinforcement (f_y) is used in code-based design equations, which do not include the strain-hardening effect. If an excessively large crack occurs, as noted by Zhu et al. [17], any additional reserve capacity due to the strain-hardening effect may be activated. To account for the lower and upper limits, a strain-hardening scalar (λ) may be included to provide insight on expected performance as follows:

$$V_{\mathrm{n}} = A_{\mathrm{sh}}\, \lambda\, f_{\mathrm{y}}\, \frac{l_{\mathrm{h}}}{s} \tag{3.2}$$

in which A_{sh} = nominal area of the hanger reinforcement; l_h = tributary length of the hangers that participate in the failure mechanism; s = center-to-center reinforcement spacing; f_y = yield strength of hanger reinforcement; and λ = strain-hardening scalar which has a maximum of $\lambda = f_{su}/f_y$ where f_{su} = ultimate strength of the reinforcement. The ledge flexure capacity limits could also be obtained in a similar fashion.

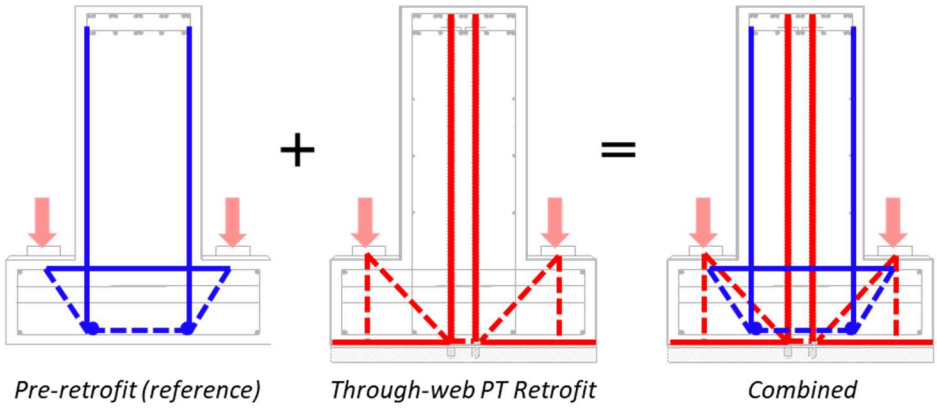

(a) Interior region sectional SAT model shows load paths without and with through-web post-installed PT threadbar connected to external "catcher" channels

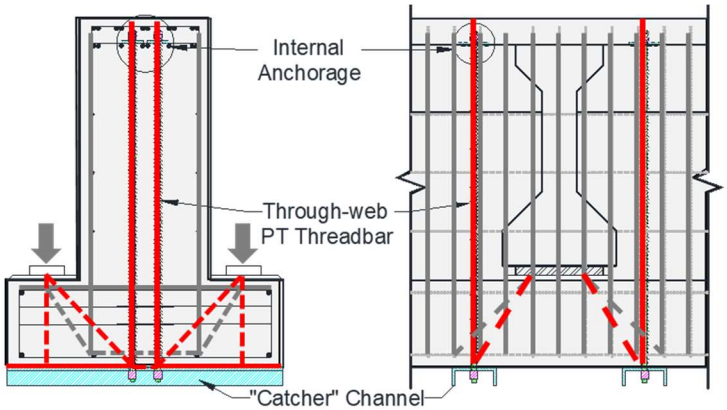

(b) Cross-section and elevation views show SAT load paths at an interior girder location

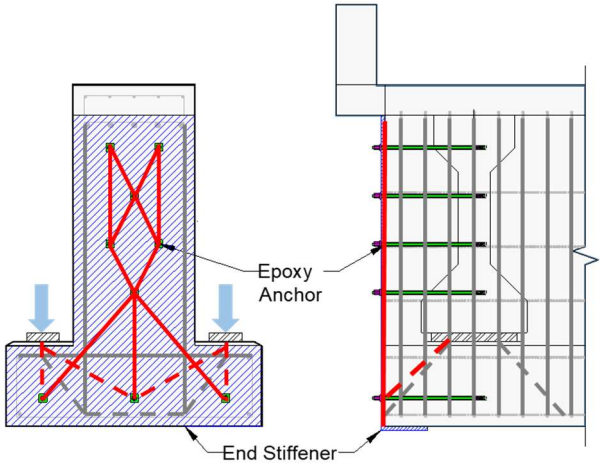

(c) End-region stiffener retrofit showing SAT load paths

Figure 3.2. Concepts for mechanical retrofit solutions providing additional load paths with simple SAT model

3.4.1. Through-Web Post-Installed PT Threadbar with "Catcher" Channel

For the through-web post-installed PT threadbar with "catcher" channel solution, the threadbar and channel should be considered as an independent supplemental load path system to check additional strength.

As a post-installed PT threadbar, it is recommended that a high-strength threadbar be adopted to enable some prestress effect to be applied during construction. An additional hanger strength provided by the threadbar may be obtained by

$$V_{ret} = A_{s\_PT} f_{y\_PT} \tag{3.3}$$

in which A_{s_PT} = nominal sectional area of a threadbar and f_{y_PT} = yield strength of the threadbar. To increase hanger capacity, threadbars need to be placed as close to the center of the girder location as practicable. Due to reinforcement congestion, if it is not possible to place the threadbars near the center of the web, then successive threadbars should be alternated on both sides of the web centerline.

To resist ledge flexure, the channels should place to bend about the minor axis; thus, a compactness check is required [71]. If the channel section defined as compact, then the full plastic capacity can be mobilized and a local buckling is not expected. The flexure capacity of the channel to resist ledge flexure can be from lesser of:

$$M_n = 1.6 S_y f_y \tag{3.4}$$

$$M_n = Z_y f_y \tag{3.5}$$

in which M_n = flexural capacity of steel channel; S_y = elastic modulus of the channel about the minor axis; and Z_y = plastic modulus of the channel about the minor axis.

3.4.2. End-Region Stiffener

For the end-region stiffener, the end plate needs to be designed based on the tensile strength of the plate to provide sufficient additional hanger capacity. The epoxy anchors, which are used to affix the plate on the end face, must provide sufficient shear or a combination of shear and tension (pullout) capacity. Anchors must be checked for minimum steel strength (tensile and shear), concrete breakout strength, bond strength (only for adhesive anchors), and concrete pryout strength based on ACI Committee 318 [72]. Generally, the shear strength of the anchors governs the anchor capacity. For construction, minimizing the number of anchors is recommended; while the number of anchors on the ledge should be a minimum of three and placed at the lower kern point of the ledge.

3.5. Experimental Test Program and Procedures

Based on laboratory constraints and time limitations, this study investigates the performance of six one-half scaled test specimens. The half-scaled prototype inverted-T bent cap, which consists of both straddle and cantilever parts, designed to represent both multi-column bent and hammerhead bent. A total fifteen individual experimental tests were conducted on four half-scale specimens, and text matrix is provided in Table 3.1.

To distinguish failure modes of the specimens, two types of specimens were designed in accordance with the sectional strength design method and referred as *hanger-deficient (HD)* and *ledge-deficient (LD)* specimen.

Table 3.1. Test matrix

Specimen	Test ID	Solution	Purpose of Solution	Scheme
Hanger Deficient	T1W1	None	HD Reference	
	T1I1	None	HD Reference	
	T1E1	2-PT threadbar	H, L, P	
	T2E1	End-region stiffener	H, L, P	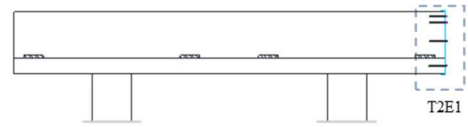
	T8W1	1-PT threadbar	H, L, P	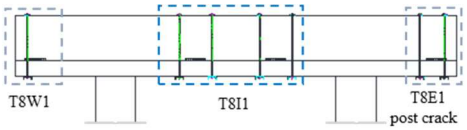
	T8I1	2-PT threadbar	H, L, P	
	T8E1	2-PT threadbar (Post-crack)	H ,L, P	
Ledge Deficient	T4W1	2-PT threadbar	H, L, P	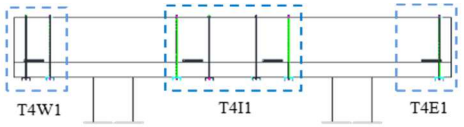
	T4I1	2-PT threadbar	H, L, P	
	T4E1	1-PT threadbar	H, L, P	
	T5E1	None	LD Reference	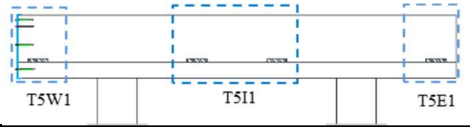
	T5I1	None	LD Reference	
	T5W1	End-region stiffener	H, L, P	
	T7W2	End-region stiffener (Post-crack)	H, L, P	
	T7E2	2-PT threadbar (Post-crack)	H, L, P	

H = Hanger, L = Ledge shear, and P = Punching shear

3.5.1. Experimental Test Setup

Figure 3.3 shows dimensions and reinforcing details of the experimental test specimens. The inverted-T beam specimen had a total length of 6706 mm and a height of 1016 mm. Each specimen was seated on two 610 mm square by 762 mm high columns, whose centers were 3658 mm apart (Figure 3.3 (a)). The two columns were seated on 914 mm square steel plates (Figure 3.3(b)). The inverted-T test specimen was vertically post-tensioned through threadbars to the laboratory strong floor via the columns (Figure 3.3 (a)).

Cross section details of the specimens are shown in Figure 3.3(c) and (d). To investigate the ability of the retrofit solutions to strengthen specific deficiencies, the test specimens were designed to provide two distinct characteristics by varying transverse reinforcement: *hanger-deficient* (*HD*) and *ledge-deficient* (*LD*) specimens.

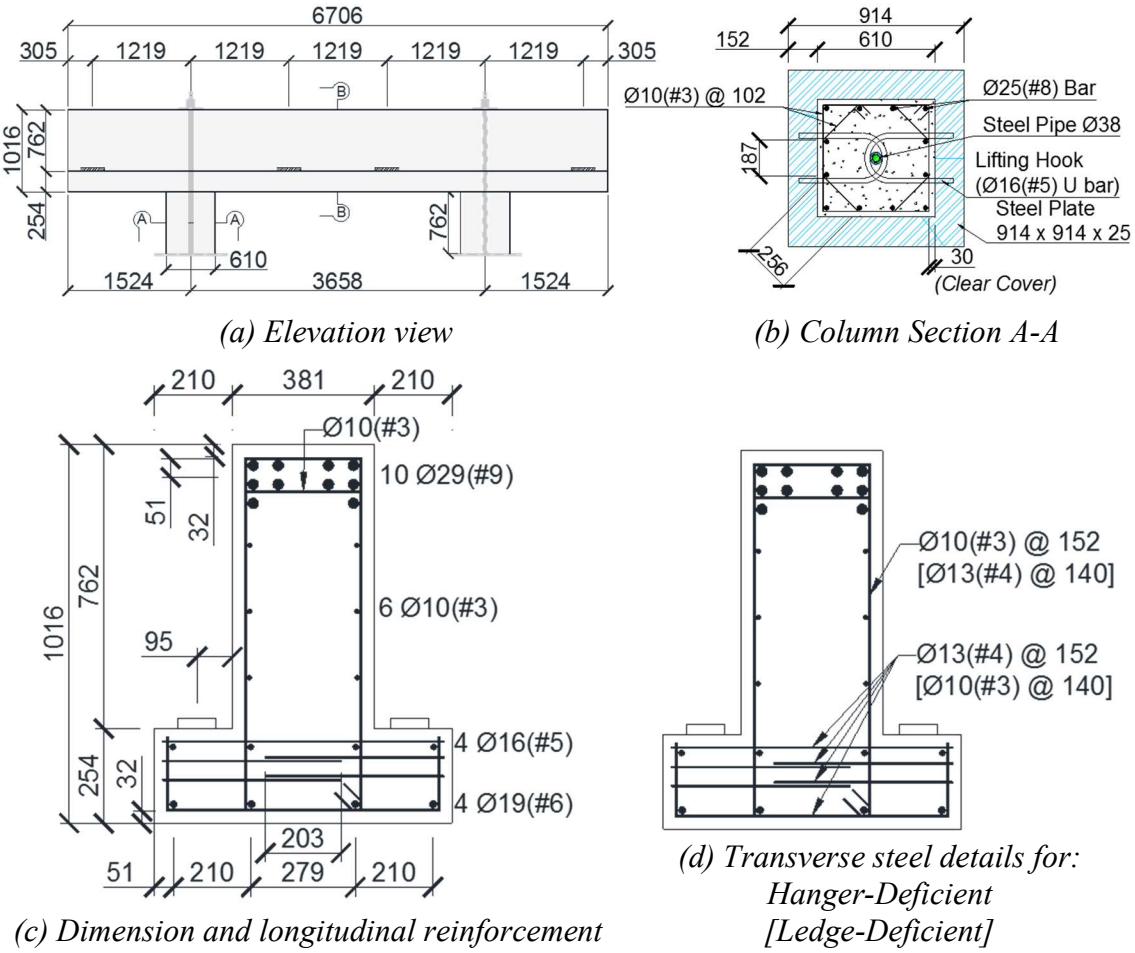

(a) Elevation view

(b) Column Section A-A

(c) Dimension and longitudinal reinforcement

(d) Transverse steel details for: Hanger-Deficient [Ledge-Deficient]

Figure 3.3. Geometric and reinforcement details of half-scale specimens (mm)

Figure 3.3 (d) illustrates the transverse reinforcement details for each specimen. For the *hanger-deficient* Specimens 1, 2, and 8, the hoopsets were spaced at 152 mm, whereas for the *ledge-deficient* Specimens 4, 5, and 7, the hoopsets were spaced at 140

mm. Table 3.2 and Table 3.4 list the measured concrete properties and tensile strength of the reinforcement.

The string pots were placed to obtain deflection profiles beneath each loading point. The load-deflection presented herein is providing the profiles at the loading point where deflected the most.

Table 3.2. Concrete compressive strength

Specimen Type*	Specimen No.	Retrofit	28-day strength (MPa)	Age at test day	Test day strength (MPa)
HD	1	N	23	175	30
	2	Y	23	248	27
LD	5	N	24	125	31
	7	Y	25	229	36

**HD = Hanger-deficient specimen and LD = Ledge-deficient specimen*

Table 3.3. Reinforcing rebar tensile strength

Bar Size	Yield Strength (MPa)	Ultimate Strength (MPa)
#3 (D10)	441	688
#4 (D13)	467	662
#5 (D16)	441	722
#6 (D19)	425	717
#9 (D29)	479	779

The experiments were conducted in such a way to determine the performance of (a) bent caps seated on two or more columns, referred to herein as "*interior*" tests; and (b) bent caps with cantilever overhangs referred to as "*exterior*" tests.

Figure 3.4 presents an overview of the experimental setups for the *interior* and *exterior* tests. *Interior* tests simulated two girder lines spaced at 1.2 m and centered on the specimen as shown in Figure 3.4(a). At each simulated girder line, a 600-kip hydraulic jack was used on the loading frame, which equally transferred the load to each ledge through hollow structural sections. Two loading frames were connected by 25 mm diameter threadbars to provide stability during testing. As shown in Figure 3.4(a), base plates were placed between the loading frames and the bearing pads to evenly distribute the load on each pad. Figure 3.4(b) depicts the general test setup for the *exterior* test region to simulate one girder line.

The specimen designation notation is as follows. For example, *T1W1*, where the first numeral is the specimen number, *W, E*, or *I* represent the tested region (the west, east, or interior regions, respectively), and the last numeral is the test order for that region.
The retrofit solutions were adopted from the solutions presented in Hurlebaus et al. [6]. Based on full-scale prototypes, appropriate adaptations were made to suit the one-half scale test specimens and laboratory constraints.

Figure 3.4(c) shows the details of the post-installed PT retrofit solution adopted for the experimental tests. The through-web post-installed PT threadbar with "catcher" channel solution has two major attributes: (i) the threadbars provide increased hanger capacity; and (ii) the channels provide increased ledge flexure capacity. To install the

retrofit solution, a 23 mm diameter hole was bored from the top side of the beam through to the bottom. A 19 mm diameter high strength threadbar (862 MPa ultimate strength) was fed through the holes and connected to the channel. The catcher channels were installed with rapid hardening grout between each channel and the inverted-T beam soffit. The threadbar was fastened and the nuts were torque-wrench tightened.

In Figure 3.4(d), details of stiffened end-region are given. For the end-region stiffener solution, a 9.5 mm thick inverted-T shape steel end-plate was adopted. To anchor the end-plate to the end face of the inverted-T beam, a total of eight horizontal holes (14.5 mm diameter and 254 mm long) were bored into the concrete and anchors were epoxied in place. Four hours later, the grout based mortar was placed between the end plate and specimen, and the anchors were wrench tightened.

3.5.2. Experimental Test Procedures

To investigate the effectiveness of the retrofit solutions, a total of fifteen experimental tests were conducted. These experiments included four reference tests, eight through-web post-installed PT threadbar tests, and three end-region stiffener tests. The experimental test results for *retrofitted* specimens are compared to those for the *reference* specimens.

During the tests to mark and investigate cracks, each test was temporarily paused at around the nominal dead load, the service limit state, and the ultimate load demand levels. Thus, the *interior* tests were paused at 120 kN, 220 kN, and 340 kN, and the *exterior* tests were paused at 100 kN, 200 kN, and 300 kN. Beyond these limits, loads were further increased to either the peak load (defining the capacity) or failure occurred.

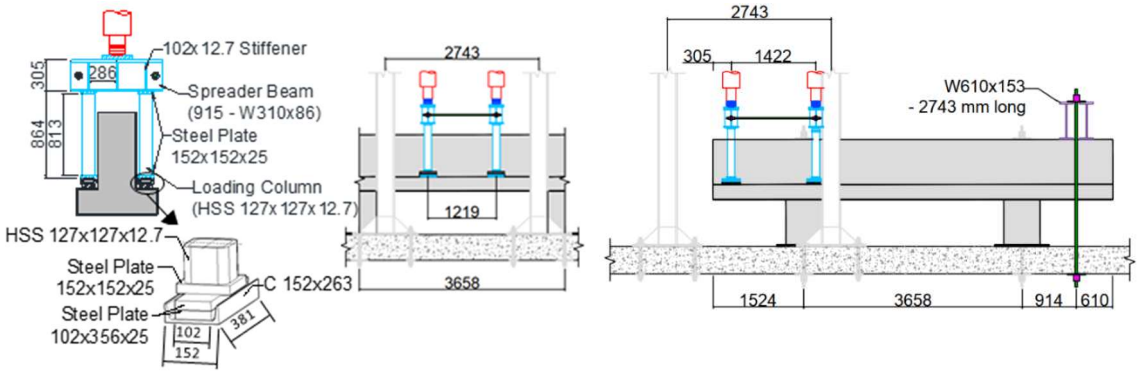

(a) Interior test setup *(b) Exterior test setup*

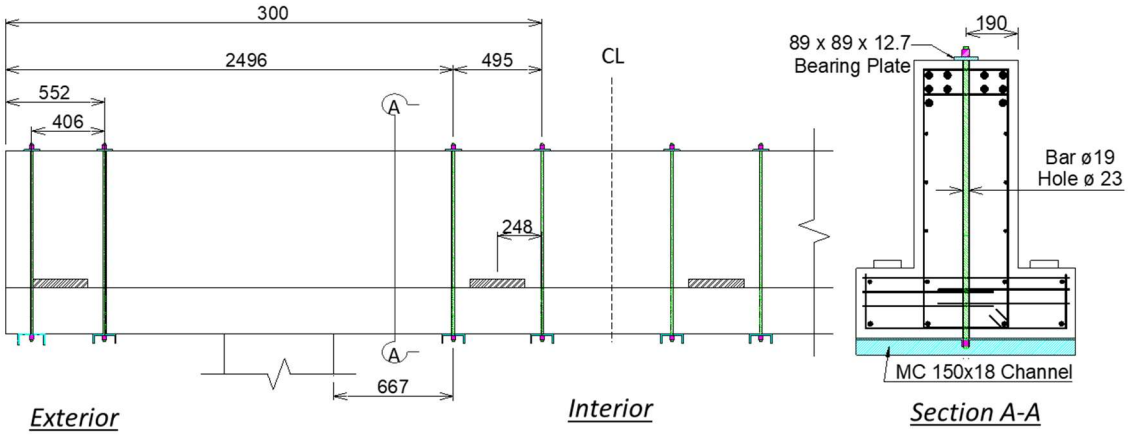

(c) Through-web post-installed PT threadbar with external "catcher" channel

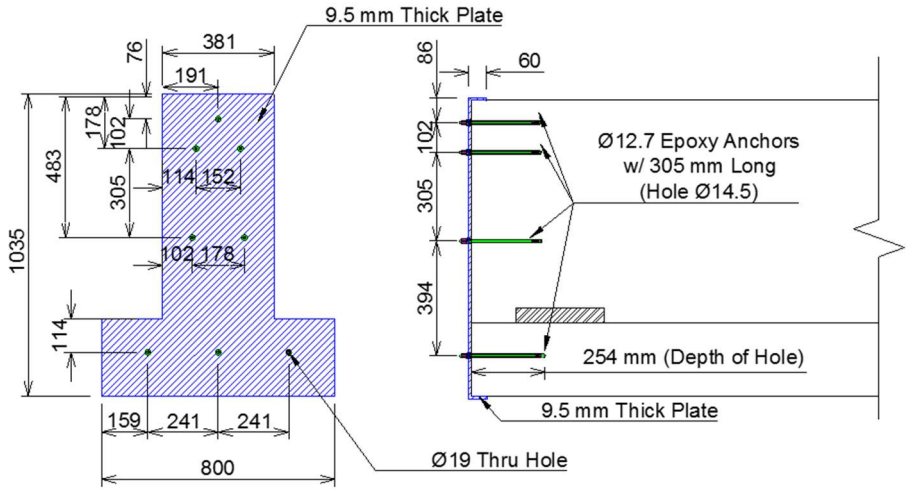

(d) End-region stiffener

Figure 3.4. Test setup for one-half scaled experimental test without and with retrofit solutions

3.6. Experimental Results for The Interior (Straddle) Region

Figure 3.5 shows the comparative experimental *interior* region test results; the left column is for the *hanger-deficient* specimen tests, and the right column is for the *ledge-deficient* specimen tests. For *interior* tests, the load on each simulated girder line was equally increased. A total of four *interior* tests were conducted including two *reference* tests and two *through-web PT threadbar retrofit* tests.

3.6.1. As-built (Pre-Retrofit)

The *hanger-deficient interior reference* test (*T1I1*) was conducted within the *interior* region of the *hanger-deficient Specimen 5*. Figure 3.5(a) shows the crack patterns (highlighted in blue) at the ultimate load demand (ULS/ϕ = 373 kN). The first cracks were observed at the web-to-ledge interface behind each bearing pad when nonlinear behavior commenced at 175 kN (see red diamond symbol in Figure 3.5(e)). The second hanger crack (as labeled in Figure 3.5(a)) was also formed prior to the service limit state (*SLS* = 223 kN). Between the serviceability (*SLS*) and ultimate (ULS/ϕ) limits, the web-shear cracks and flexural cracks formed and lengthened. At ULS/ϕ, the web-to-ledge interface and the web-shear cracks opened to 2.5 mm and 2.2 mm, respectively, as shown in Figure 3.5(a). The specimen reached its maximum load capacity at 401 kN.

For the *ledge-deficient* specimen, the *interior reference* test (*T5I1*) was performed within the *interior* region of the *Specimen 5*. Figure 3.5(b) shows a photograph taken at the ultimate limit state (ULS/ϕ) with the cracks highlighted. When nonlinear behavior initiated at 142 kN (see red diamond symbol in Figure 3.5(f)), first cracks were observed at the web-to-ledge interface behind each bearing pad.

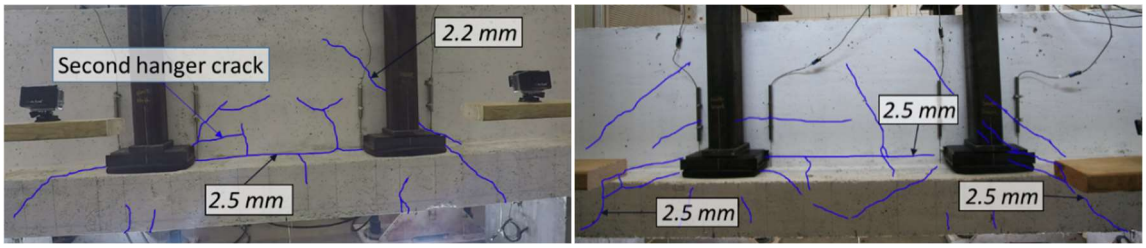

(a) Hanger-deficient reference (T1I1) *(b) Ledge-deficient reference (T5I1)*

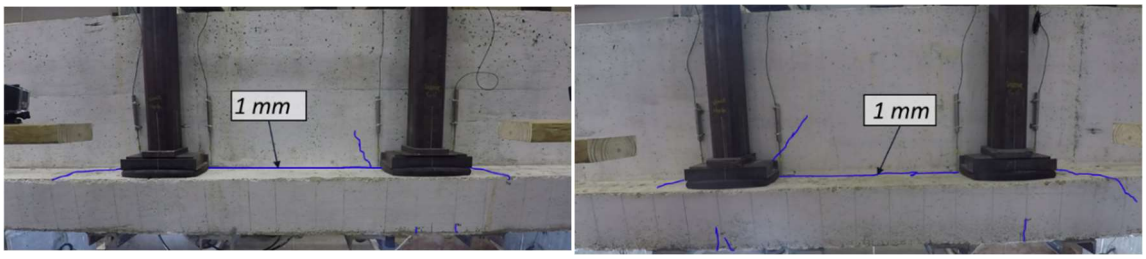

(c) Hanger-deficient 2-PT threadbar (T8I1) *(d) Ledge-deficient 2-PT threadbar (T4I1)*

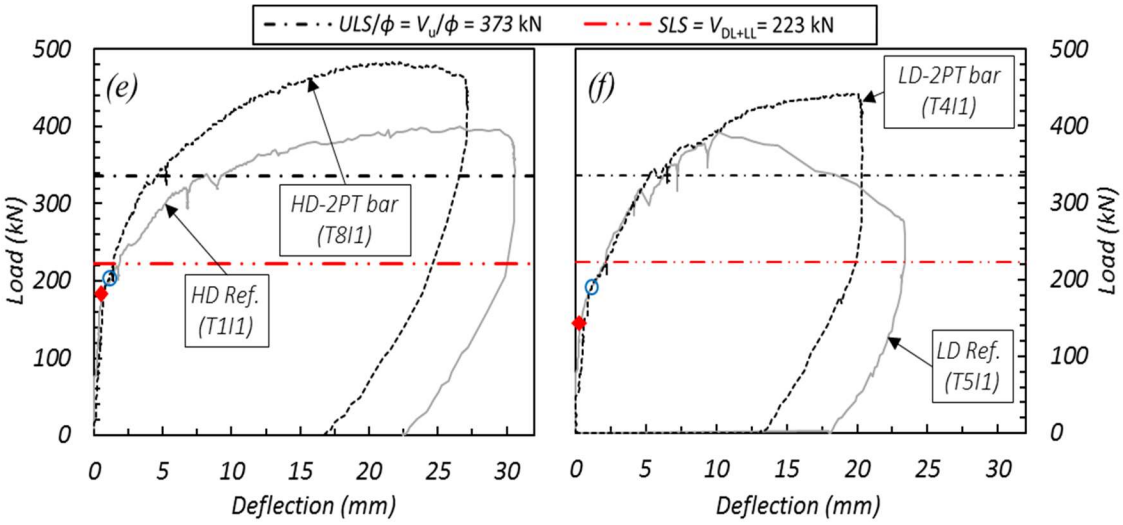

Note the diamond symbols indicate initial cracking point

(e) HD specimen load-deflection behavior *(f) LD specimen load-deflection behavior*

Figure 3.5. *Interior* region comparative test results without and with post-installed through-web PT threadbar with "catcher" channel. (a) to (d) photographs show crack condition at 373 kN (ULS/ϕ); (e) and (f) plots for the load-deflection behavior beneath the loading point.

A web-shear crack between the loading points and the flexural cracks at the specimen soffit was also observed before the load reached the *SLS*. As the load approached *ULS,* these cracks extended to the side of the ledge as shown in Figure 3.5(b). At *ULS*/ϕ, the width of the web-to-ledge interface and ledge cracks widened to 2.5 mm as depicted in Figure 3.5(b). The specimen reached its maximum load capacity at 378 kN.

3.6.2. Through-Web Post-Installed PT Threadbar with Catcher Channel Retrofit

For an *interior* location, threadbars with channels were used to form a supplemental hanger and catcher system. This through-web PT threadbar retrofit system was used on both *hanger-deficient* (*T8I1*) and *ledge-deficient* (*T4I1*) specimens.

Figure 3.5(c) shows the crack patterns on the *hanger-deficient interior through-web PT retrofit* specimen (*T8I1*) at the ultimate load demand (*ULS*/ϕ). For the *T8I1* test, the initial crack was found at the web-ledge interface behind each bearing pad shortly before the serviceability limit (*SLS*) was reached. The blue circled in Figure 3.5(e) shows this load (213 kN) which evidently was also the onset of nonlinear behavior. Between the serviceability (*SLS*) and ultimate (*ULS*/ϕ) limits, flexure cracks were detected on the bent cap soffit beneath the loading points. At *ULS*/ϕ, the web-to-ledge interface crack width grew to 1 mm. Beyond *ULS*/ϕ, a few new cracks formed throughout the specimen, but the existing crack widths rapidly increased. A peak load of 485 kN was observed at the displacement of 20 mm. The test was terminated and unloaded when a displacement of 27 mm was achieved.

Figure 3.5(d) presents a photograph where the cracks may be seen on the *ledge-deficient interior through-web PT retrofit* specimen (*T4I1*) at *ULS*/ϕ. The first cracks were

observed at the web-to-ledge interface at 188 kN where the nonlinear behavior commenced (see blue circle in Figure 3.5(f)). As the load approaching the *SLS*, flexural cracks were also formed on the bottom of the bent cap beneath the loading points. Between the *SLS* and *ULS/ϕ*, a shear crack on both sides of the web formed as shown in Figure 3.5(d). At the *ULS/ϕ*, the web-to-ledge interface crack opened to 1 mm. As the load increased beyond the *ULS/ϕ*, the cracks on the ledges grew significantly. The maximum load of 441 kN was observed when the displacement reached 20 mm. At this load, pyramid-shaped cone failures were clearly observable beneath each bearing pad.

3.7. Experimental Results for The Exterior (Cantilever) Region

For the *exterior* region tests, the jack on each loading frame applied a load equally up to the equivalent dead load, at which point the load over the column was held constant until the test terminated. Eleven *exterior* region tests were conducted on three *hanger-deficient* and three *ledge-deficient* specimens, which included two *reference* tests, six *through-web PT threadbar retrofit* tests, and three *end-region stiffener retrofit* tests.

3.7.1. As-built (Pre-Retrofit)

The *hanger-deficient exterior reference* test (*T1W1*) was conducted on an *exterior* region of Specimen 1. Figure 3.6(a) shows the observed cracks on the end face at the ultimate limit (*ULS/ϕ* = 312 kN). The first hanger cracks at the web-to-ledge interface, which extended to the end face, were observed at 144 kN. At this load, nonlinear behavior commenced as marked with red diamond symbol in Figure 3.6(i). Between the serviceability (*SLS* = 187 kN) and ultimate (*ULS/ϕ*) limits, the second hanger crack (see Figure 3.6(a)) formed at 200 kN. Following the second hanger crack, strain-hardening of

the hanger reinforcement initiated as depicted in Figure 3.6(i). The third hanger cracks also formed on the end face at this stage, see Figure 3.6(a). Before the load achieved the ultimate limit (ULS/ϕ), the specimen failed in hanger yielding at 294 kN; shortly thereafter the third hanger crack commenced. At the maximum load of 294 kN, the hanger crack at the web-to-ledge interface opened to 15 mm wide.

Figure 3.6(b) shows the crack patterns at the ultimate limit (ULS/ϕ) for the ledge-deficient exterior reference test (T5E1). The test conducted on an exterior region of the ledge-deficient Specimen 5. The initial crack formed at the web-to-ledge interface behind the bearing pads before reaching the SLS. The red diamond symbol in Figure 3.6(j) depicts the load at 141 kN which was also at the onset of nonlinear behavior. The crack from each ledge propagated along with the interface to the end face at between serviceability limit (SLS) and the maximum load of 294 kN. Just prior to the failure, a horizontal crack on the end face through the web formed near the neutral axis of the bent cap (Figure 3.6(b)). The ledge-deficient reference exterior specimen (T5E1) failed at 294 kN, about 5 percent less than the predicted ultimate limit (ULS/ϕ). At failure, the web-to-ledge interface crack widened to 2.5 mm.

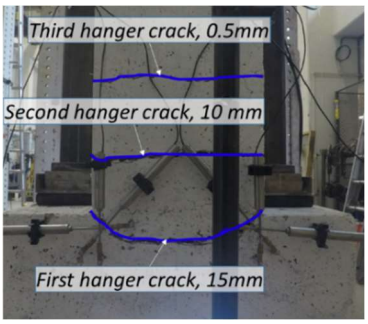

(a) Hanger-Deficient (HD) reference (T1W1)

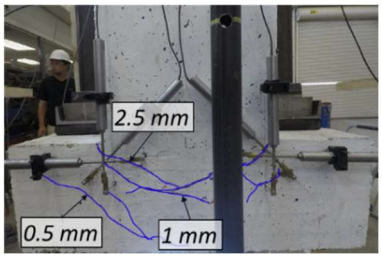

(b) Ledge-Deficient (LD) reference (T5E1)

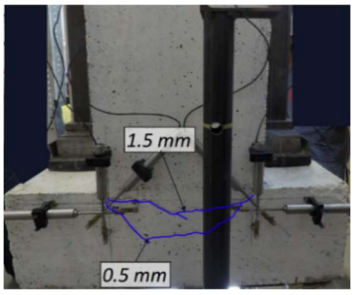

(c) HD-1PT threadbar (T8W1)

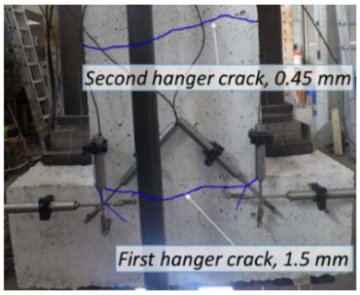

(d) HD-2PT threadbar (T1E1)

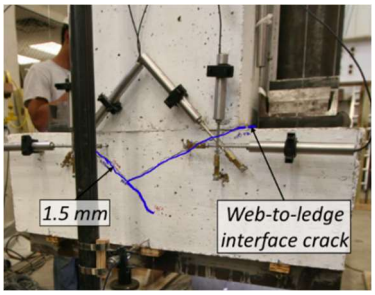

(e) HD-2PT threadbar repair (T8E1)

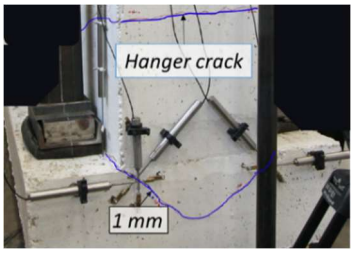

(f) LD-1PT threadbar (T4E1)

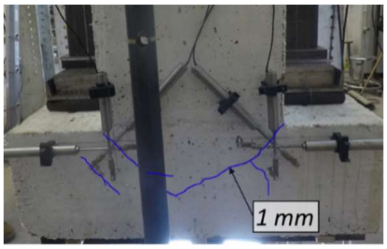

(g) LD-2PT threadbar(T4W1)

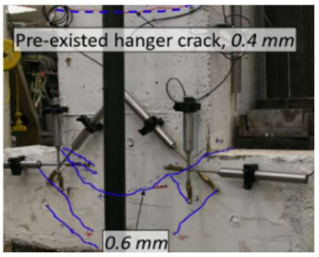

(h) LD 2PT threadbar repair (T7E2)

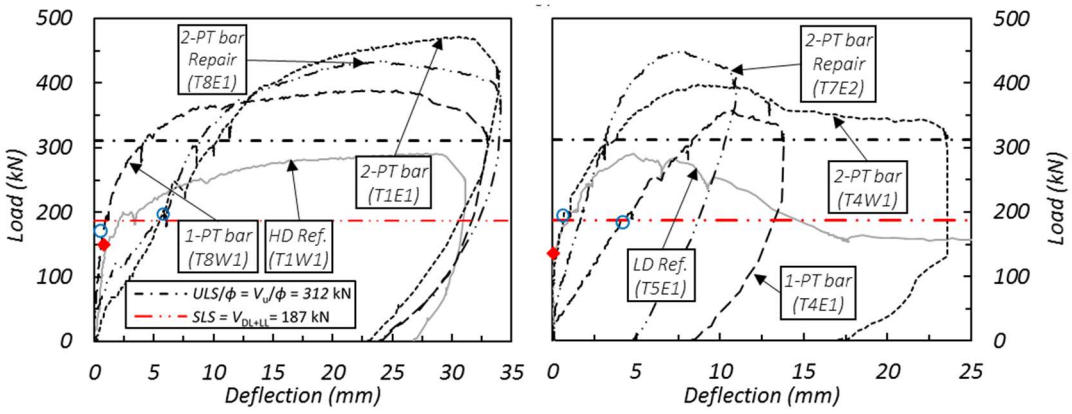

(i) HD specimen load-deflection curve *(j) LD specimen load-deflection curve*

Figure 3.6. Comparative test results without and with post-installed through-web PT threadbar with "catcher" channel. Photographs were taken at ultimate limit state.

3.7.2. Through-Web Post-Installed PT Threadbar with Catcher Channel

For the *retrofit* (or *repair*) tests, the *through-web PT threadbar retrofit* solution was installed under three conditions;

1) *PT bar* used one threadbar with a catcher channel only at the exterior side of the loading point (T8W1 and T4E1),
2) *PT bar* used two threadbars with catcher channels, one at each side of the loading point (T1E1 and T4W1), and
3) *PT bar repair* used two threadbars with catcher channels after specimen cracked (after *SLS*) to evaluate the retrofit system on the already damaged bent cap (T8E1 and T7E2).

Each condition was applied to both *hanger-deficient* (*T8W1, T1E1*, and *T8E1*) and *ledge-deficient* specimens (*T4W1, T4E1*, and *T7E2*).

The *T8W1* test was conducted on the *exterior* region of the *hanger-deficient* Specimen 8 which used a single threadbar with channel. Figure 3.6(c) shows the crack condition on the end face at the ultimate load demand (*ULS/ϕ).* The web-to-ledge interface cracks formed first at 168 kN. At this load, the nonlinear behavior commenced as marked with blue circle on the dashed line in Figure 3.6(i). *A*s the load approached the serviceability limit (*SLS*), the cracks extended to the end face. Several top flexural cracks (arising from negative moments) were observed between the serviceability (*SLS*) and ultimate (*ULS/ϕ*) limit states. At the end face, 1.5 mm and 0.5 mm hanger cracks formed at *ULS/ϕ* (see Figure 3.6(c)). Shortly thereafter another hanger crack formed near the neutral axis of the bent cap; the specimen reached its maximum capacity of 391 kN.

Figure 3.6(d) shows the cracks on the end face of the tested *exterior* region of the *hanger-deficient* Specimen 1 (*T1E1*) at the ultimate limit (*ULS/ϕ*). For the *T1E1* test, two threadbars with catcher channels were used. Prior to the service limit (*SLS*), no cracks were observed at the tested region. On reaching *SLS*, hairline cracks appeared at the web-to-ledge interface behind the bearing pads as depicted by the blue circle on the dotted line in Figure 3.6(i). Subsequently, the crack propagated to the end face and formed the first hanger crack (see Figure 3.6(d)) at 250 kN. Shortly after the initial hanger crack formed, a second hanger crack also formed. Following the formation of these hanger cracks, the applied load dropped slightly as shown in the dotted line of Figure 3.6(i). At *ULS/ϕ*, the first and second hanger cracks widened to 0.45 mm and 1.5 mm, respectively. Beyond *ULS/ϕ*, rapid crack opening and extension were observed. Following the maximum load (472 kN), the hangers yielded and the load dropped, refer to Figure 3.6(i).

Figure 3.6(e) shows a photograph taken at the ultimate limit (*ULS/ϕ*) to present a crack condition at the end face of the *repaired hanger-deficient exterior* specimen (*T8E1*). The *T8E1* test was conducted on the untested *exterior* region of the *hanger-deficient* Specimen 8. Before applying any load at the test region, two threadbars with catcher channels were installed but not fastened. The loads were then applied up to the equivalent service load (*SLS*) to simulate the demands of in-service bridges. Under the serviceability limit (*SLS*), cracks were observed at the web-to-ledge interface behind the bearing pads as shown in Figure 3.6(e*)*.

After marking cracks, the repair was initiated. The threadbars were wrench-tightened and the previously formed cracks closed as a result of the repair. On further

loading, new cracks were not observed and the existing cracks remained essentially closed. Between the serviceability (*SLS*) and ultimate (*ULS/ϕ)* limits, the web-to-ledge interface cracks extended and formed a 1.5 mm V-shape crack at the end face as depicted in Figure 3.6(e). New cracks on the web and ledges were also formed. Beyond *ULS/ϕ*, the existing cracks grew significantly. At 334 kN, a hanger crack formed on the end face slightly above the aforementioned V-shape crack. The hanger crack opened up to 5.5 mm at the maximum load of 436 kN. At this load, the specimen failed. The test was terminated and unloaded when a displacement of 34 mm was achieved.

The *ledge-deficient exterior* region test (*T4E1*) using a single threadbar with a catcher channel was conducted at the *exterior* region of the *ledge-deficient* Specimen 4. Figure 3.6(f) shows the crack condition at the end face at the ultimate limit (*ULS/ϕ*); this 1 mm crack did not indicate impending failure. Prior to this, the initial cracks formed at the web-to-ledge interface behind a bearing pad and propagated to the end face shortly after the load reached the serviceability limit (*SLS*). Between *SLS* and *ULS/ϕ,* the cracks at the reentrant corner formed a 1 mm V-shape at the end face as shown in Figure 3.6(f). Negative moment (top) flexure cracks and shear cracks were also observed. Subsequently, a horizontal hanger crack (see Figure 3.6(f)) formed at the end face at 254 kN. Beyond *ULS/ϕ*, the cracks grew significantly along with the formation of new cracks; however, the width of the hanger crack remained constant. At the maximum capacity of 356 kN, pyramid-shaped cone failures were observed beneath each bearing pad.

Figure 3.6(g) shows the crack condition at the end *face* for the *T4W1* test at the ultimate limit (*ULS/ϕ*). The test was conducted on the *ledge-deficient exterior* region of

Specimen 4, which was retrofitted with two threadbars plus catcher channels (*T4W1*). For the *T4W1* test, the initial cracks formed at the web-ledge interface behind the bearing pads at 200 kN as marked with blue circle on the dotted line in Figure 3.6(j). As the load increased, the cracks propagated to the reentrant corner at the end face along with the web-to-ledge interface. Between the serviceability (*SLS*) and ultimate (*ULS/ϕ*) limit states, the two reentrant corner cracks extended and formed a 1 mm V-shape crack at the end face (see Figure 3.6(g)). Beyond *ULS/ϕ*, significant extension of existing cracks and new crack formation, such as a hanger crack at the end face and diagonal cracks on the ledges, were observed. The specimen reached its maximum capacity of 400 kN. At this load, the ledge reinforcement yielded and the load dropped gradually.

Figure 3.6(h) presents a photograph taken at the ultimate limit state (*ULS/*ϕ) to show the crack condition after the *repair* of the *ledge-deficient* specimen with two threadbars plus channels (T7E2). First, the load was applied until cracks initiated. Then, after the cracks were marked, the specimen was completely unloaded.

Without any applied load, the repair was implemented. The threadbars plus channels were installed and wrench-tightened; the previously formed cracks closed as a result of this repair. On the further loading, slight opening of the existing cracks and a new crack formation at the end face was observed. Between the serviceability (*SLS*) and ultimate (*ULS/ϕ*) limit states, several new cracks formed along the entire test region, including a 0.6 mm parabolic-shaped crack at the end face as shown in Figure 3.6(h). At *ULS/ϕ*, the pre-existed hanger crack (see Figure 3.6(h)) opened to 0.4 mm. As nonlinear behavior commenced at 400 kN, a pyramid-shaped cone failure formed beneath the

bearing pads (see the dashed line in Figure 3.6(j)). Following the pyramid cone crack initiation, the specimen reached its maximum capacity of 449 kN.

3.7.3. End-Region Stiffener

For the end-region stiffener *retrofit* (or *repair*) tests, an end plate was installed at the end face of the specimen. For the *hanger-deficient* specimen, only a *retrofit* test (*T2E1*) was conducted while both *retrofit* and *repair* tests (*T5W1* and *T7E2*) were conducted on the *ledge-deficient* specimens. Figure 3.7 and 2.7 show comparative test results for both the *hanger-* and *ledge-deficient* specimens. Crack maps and the photographs show the crack condition at the end of the test.

Figure 3.7(b) shows a crack condition at the end of the *hanger-deficient exterior retrofit* test (*T2E1*). The *T2E1* test was conducted at an *exterior* region of the *hanger-deficient* Specimen 2. Within the serviceability limit (*SLS*), no cracks were observed. The first cracks were observed at the specimen soffit (see Figure 3.7(b)) at 244 kN (marked by the blue circle in Figure 3.7(c)). Following crack initiation, a web-to-ledge interface crack formed behind the bearing pads. As the load approaching the ultimate limit (*ULS/ϕ*), significant web shear cracks were observed as well as other new cracks over the entire test region. Beyond the *ULS/ϕ, d*iagonal side ledge cracks, which propagated from the exterior side of the bearing pad to the end face as shown in Figure 3.7(b), were observed. At the maximum load of 347 kN, the specimen failed and the load dropped due to the excessive compressive load at the bottom corner concrete as depicted in Figure 3.7(b). The end plate was bent near the neutral axis of the plate at the end of the test.

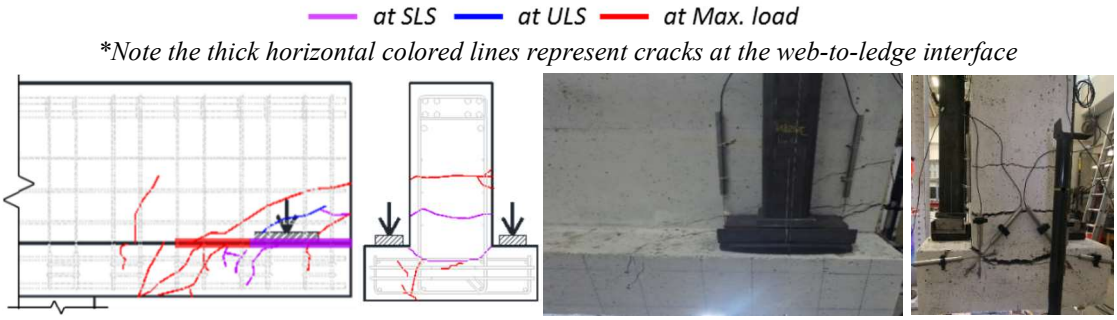

**Note the thick horizontal colored lines represent cracks at the web-to-ledge interface*

(a) HD reference (pre-retrofit) specimen (T1W1) showing cracked condition

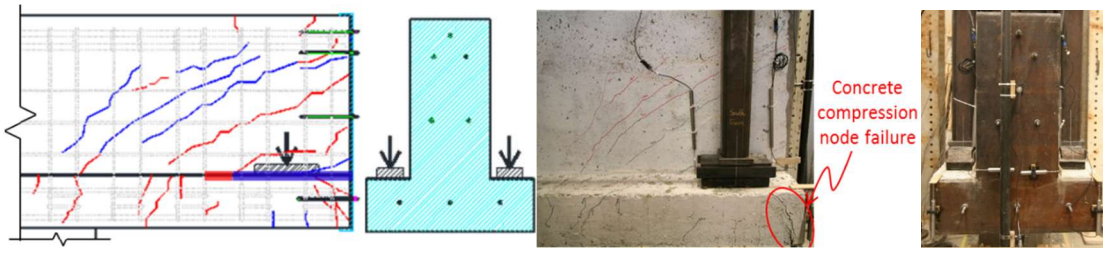

(b) Retrofitted specimen (T2E1) showing end-region with photo at the end of test

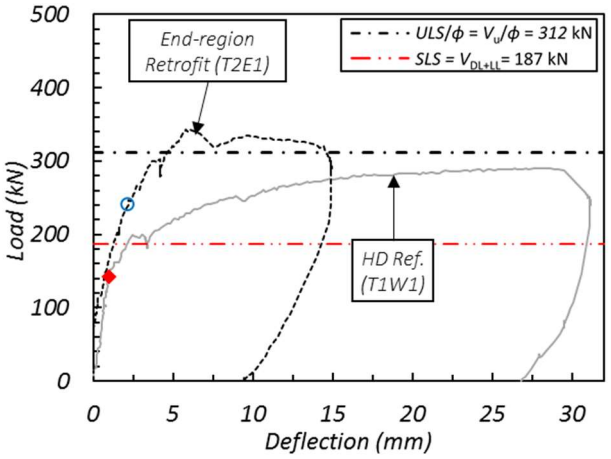

(c) Load-deflection behavior under loading point

Figure 3.7. *Hanger-deficient* exterior comparative test results without and with the end−region stiffener. (a) and (b) show crack condition at the maximum load; (c) for the load-deflection behavior beneath the loading point

Figure 3.8(b) shows the test result for the *ledge-deficient exterior retrofit* test (*T5W1*). The *T5W1* test was an *exterior retrofit test* conducted on the *ledge-deficient* Specimen 5. The initial cracks formed at the web-to-ledge interface behind the bearing pads as shown in Figure 3.8(b). The blue circle in Figure 3.8(d) indicates this load (176 kN) which is slightly below the serviceability limit (*SLS*). Between *SLS* and *ULS/ϕ* limit states, diagonal ledge cracks were observed near the bottom corner of the ledge side face (see Figure 3.8(b)). Beyond the ultimate limit (*ULS/ϕ)*, the cracks within the grout bed between the end plate and the bent cap were observed at 356 kips. The specimen reached its maximum capacity at a load of 383 kN where the bottom lip of the end plate opened due to the excessive concrete compression as depicted in Figure 3.8(b).

Figure 3.8(c) shows the test result for the *repaired ledge-deficient* specimen (*T7W2*). The *T7W2* test was conducted on the *pre-cracked ledge-deficient Specimen 7.* Prior to installing the end-plate, a load was applied to initiate cracks at the test region. After marking cracks, the specimen was completely unloaded.

The repair was implemented without any applied load. The end plate was installed and the anchor bolts were wrench-tightened. On further loading, opening of the previously formed cracks and formation of the new cracks were observed at the serviceability limit (*SLS*). On reaching the ultimate limit (*ULS/ϕ)*, ledge cracks and negative moment flexure cracks formed. Following the *ULS/ϕ,* opening at the tip of the end plate initiated at 343 kN. At the maximum load of 392 kN, more cracks were observed on both sides of the web and ledge. With the excessive concrete compression at the bottom corner of the specimen, the pyramid-cone crack failure was observed beneath the bearing pads.

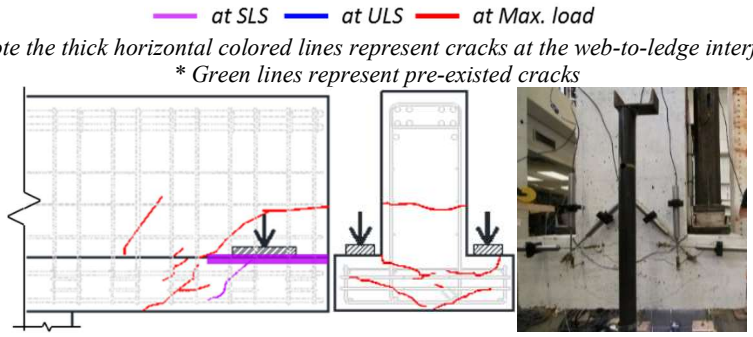

(a) LD reference (Pre-retrofit) specimen (T5E1) showing side elevation and end views of cracked condition with photo at end of test.

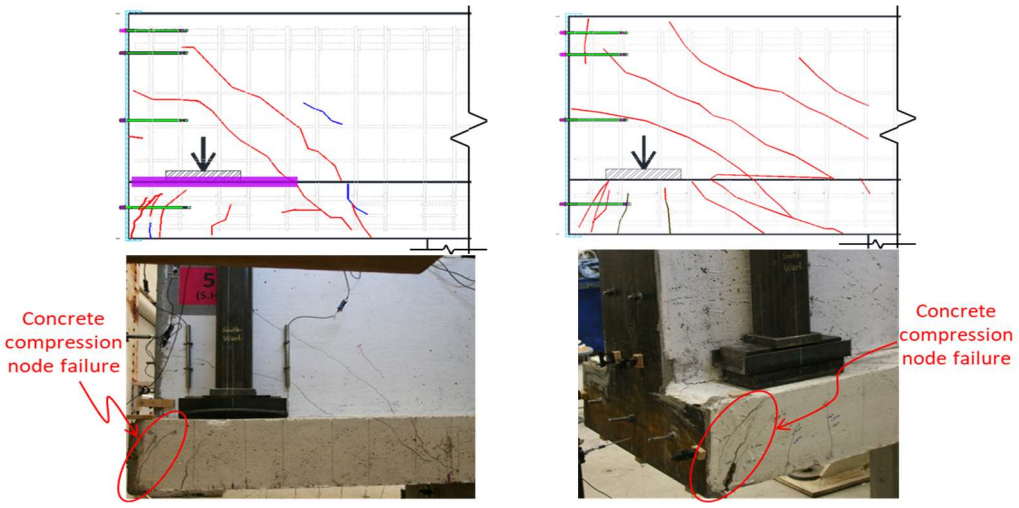

(b) Retrofitted specimen (T5W1) *(c) Repaired specimen (T7W2) after cracking*

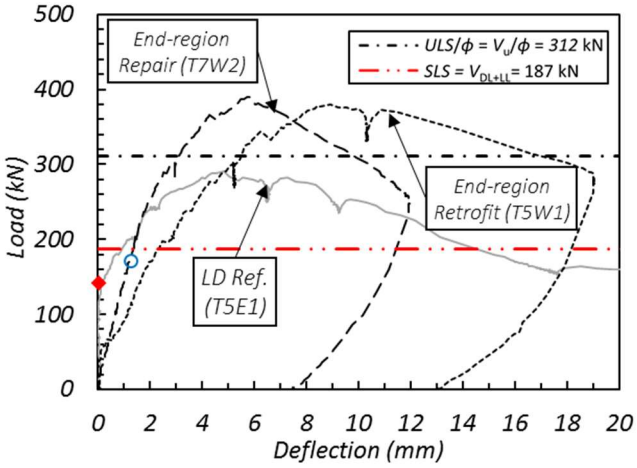

(d) Load-deflection behavior under loading point

Figure 3.8. *Ledge-deficient* exterior comparative test results without and with end-region stiffener. (a), (b), and (c) show crack condition at the maximum load; (d) shows for the load-deflection behavior beneath the loading point

3.8. Analysis of Experimental Results

This section evaluates the effectiveness of the retrofit systems based on the experimental observations. The capacity of the specimens, as designed, is calculated and compared to the test results. Table 3.4 to 2.4 list comparative test results and provide observed and estimated design capacities for the *through-web PT threadbar with catcher channel retrofit* specimens.

Similar to observations of cracked prototype inverted-T bent caps in the field (Figure 3.1), the *reference* test specimens experienced severe cracks prior to reaching the serviceability limit state (*SLS*). On the other hand, only hairline cracks formed on the *retrofitted* specimens within the *SLS*. Although the *through-web PT threadbar with catcher channel* solution allowed cracking within service limit state ($SLS = V_{DL+LL}$), the initial cracking load increased by at least 15 percent compared to the *reference* specimen (see *relative serviceability* rows in Table 3.4 to 2.4). On the *repaired* specimens, such pre-existing cracks closed up and remained as hairline cracks only.

For the ultimate limit state strength condition, the *reference* test specimens failed with the cracks in excess of 2.5 mm at a load near the predicted ultimate limit (ULS/ϕ). The *retrofit* solution increased ultimate strength of the specimens by 41 and 32 percent of the *hanger* and *ledge* capacity, respectively; and the enhanced strength exceeded ULS/ϕ. These results are provided as a *relative strength* in Table 3.4 to 2.4. The vertically prestressed threadbar (plus transverse channel) within the web of the inverted-T section effectively improved performance of both the straddle (interior) and the cantilever (exterior) specimens.

The specimen capacities were calculated in accordance with the sectional stress method specified in AASHTO [10]. These results are given in Table 3.4 to 2.4, along with ratios of observed to code-based strength. Results demonstrate that the code-based approach, which assumed the failure associated with the yield strength of the reinforcement, provides quite conservative strength estimates. The predicted strengths remain some 41 percent and 26 percent conservative (on average) for the *hanger* and *ledge-flexure* capacity, respectively.

For a more practical estimation, if the tributary length is modified to account for all reinforcement that participates in the failure mechanism (as observed in the tests), a more realistic outcome is obtained. Figure 3.9 depicts AASHTO [10] distribution length and the modified tributary length at both *interior* and *exterior* regions for *hanger* and *ledge-flexural* strengths. As depicted in Figure 3.9(a), AASHTO [10] hanger distribution length is determined from the center-to-center spacing between the load points, *S*, or distance from the exterior load point to the end face, *c*. The estimated capacities using the modified tributary width listed in the *limit analysis* rows of Table 3.4 to 2.4. The conservativeness is lowered to an average of 15 and 8 percent for *hanger*- and *ledge-deficient* specimen, respectively. The high values for the *hanger-deficient* specimens are attributed to significant strain-hardening that occurs in the hanger reinforcement. The strain hardening scalars, λ, are listed in the tables and it is clear the experiment outcome lies between the lower bound (initial yield) condition and the upper bound (hoop fracture) condition.

Table 3.4. *Interior* region test results and estimated strength without and with through-web post-installed PT threadbar with "catcher" channel

		Specimen Type[1]	HD Int.		LD Int.	
		Test ID	***T1I1***	**T8I1**	***T5I1***	**T4I1**
		Condition	*Ref.*	2-PT bar	*Ref.*	2-PT bar
Serviceability	**Service Limit State (*SLS, kN*)**		223 kN			
	Observed	Cracking. Load (kN)	*175*	213	*142*	188
		Relative Serviceability[2]	*1.0*	1.22	*1.0*	1.32
Ultimate Strength	**Ultimate Limit State Demand (*ULS, kN*)**		373 kN			
	Observed	Max. Load (kN)	*401*	485	*378*	441
		Relative Strength[3]	*1.0*	1.21	*1.0*	1.17
		Controlling mode	*Hanger*	Hanger	*LF[4]*	LF & P
	Code-based (AASHTO)	Code-based (kN)	*251*	407	*328*	388
		Ratio	*1.59*	1.19	*1.15*	1.14
	Limit Analysis[5]	Lower bound (kN)	*313*	469	*378*	435
		$\lambda^{\dagger}$	*1.28*	1.03	*1*	1.01
		Upper bound (kN)	*489*	531	*582*	636

[1] *HD = Hanger-deficient, LD = Ledge-deficient*
[2] *Relative serviceability= retrofitted cracking load/reference cracking load*
[3] *Relative strength = retrofitted maximum load / reference maximum load*
[4] *LF = Ledge-flexure, P = punching shear*
[5] *Limit analysis adopted modified tributary length to calculate lower and upper bound (see* Figure 3.9*)*
† *λ = maximum load/lower bound*

Table 3.5. *Hanger-Deficient Exterior* region test results and estimated strength without and with through‑web pot‑installed PT threadbar with "catcher" channel

		Test ID	*T1W1*	T8W1	T1E1	T8E1
		Condition	*Ref.*	1-PT bar	2-PT bar	2-PT bar Repair[1]
Serviceability	**Service Limit State (*SLS, kN*)**		187			
	Observed	Cracking. Load (kN)	*144*	165	190	-
		Relative Serviceability[2]	*1.0*	1.15	1.32	-
Ultimate Strength	**Ultimate Limit State Demand (*ULS/ϕ, kN*)**		312			
	Observed	Max. Load (kN)	*294*	391	472	436
		Relative Strength[3]	*1.0*	1.33	1.61	1.48
		Controlling mode	*Hanger*	Hanger	Hanger	Hanger
	Code-based (AASHTO)	Code-based (kN)	*188*	266	344	344
		Ratio	*1.56*	1.47	1.37	1.27
	Limit Analysis[4]	Lower bound (kN)	*251*	329	407	407
		λ†	*1.17*	1.19	1.16	1.07
		Upper bound (kN)	*391*	469	547	547

[1] *Repair = repaired of a specimen that was cracked under simulated service conditions and then repaired*
[2] *Relative serviceability= retrofitted cracking load/reference cracking load*
[3] *Relative strength = retrofitted maximum load / reference maximum load*
[4] *Limit analysis used modified tributary width to calculate lower and upper bound (see* Figure 3.9*)*
† *λ = maximum load/lower bound*

Table 3.6. *Ledge-Deficient Exterior* region test results and estimated strength without and with through‑web pot‑installed PT threadbar with "catcher" channel

		Test ID	*T5E1*	T4E1	T4W1	T7E2
		Condition	*Ref.*	1-PT bar	2-PT bar	2-PT bar Repair[1]
Serviceability	**Service Limit State (*SLS, kN*)**		187			
	Observed	Cracking. Load (kN)	*141*	190	200	-
		Relative Serviceability[2]	*1.0*	1.35	1.42	-
Ultimate Strength	**Ultimate Limit State Demand (*ULS/ϕ, kN*)**		312			
	Observed	Max. Load (kN)	*294*	356	400	449
		Relative Strength[3]	*1.0*	1.21	1.36	1.53
		Controlling mode	*LF*	LF & P[4]	LF & P	LF & P
	Code-based (AASHTO)	Strength Capacity (kN)	*213*	268	331	340
		Ratio	*1.38*	1.33	1.21	1.32
	Limit Analysis[5]	Lower bound (kN)	*271*	330	392	356
		λ†	*1.08*	1.08	1.02	1.26
		Upper bound (kN)	*417*	473	534	540

[1] *Repair = repaired of a specimen that was cracked under simulated service conditions and then repaired*
[2] *Relative serviceability= retrofitted cracking load/reference cracking load*
[3] *Relative strength = retrofitted maximum load / reference maximum load*
[4] *LF = Ledge-flexure, P = punching shear*
[5] *Limit analysis used modified tributary width to calculate lower and upper bound (see* Figure 3.9*)*
† *λ = maximum load/lower bound*

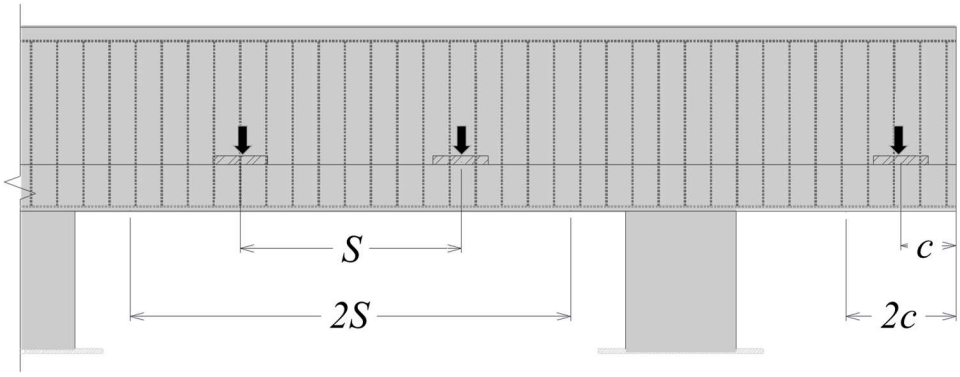

(a) AASHTO (2017) specified hanger distribution widths

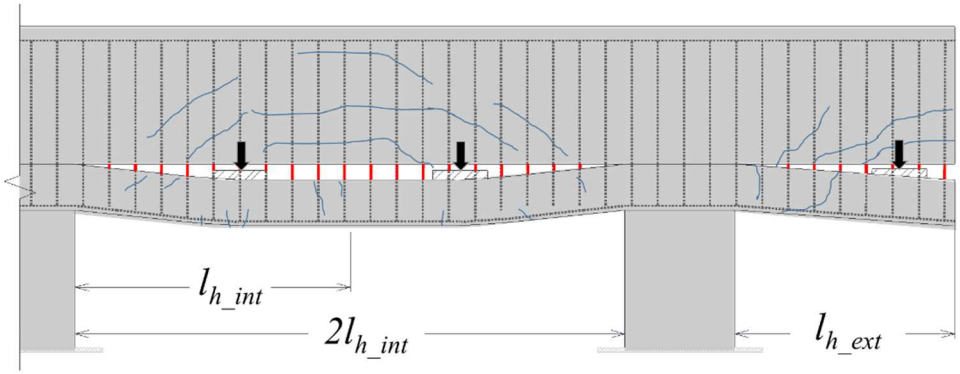

(b) Modified hanger tributary lengths based on the experimental observation

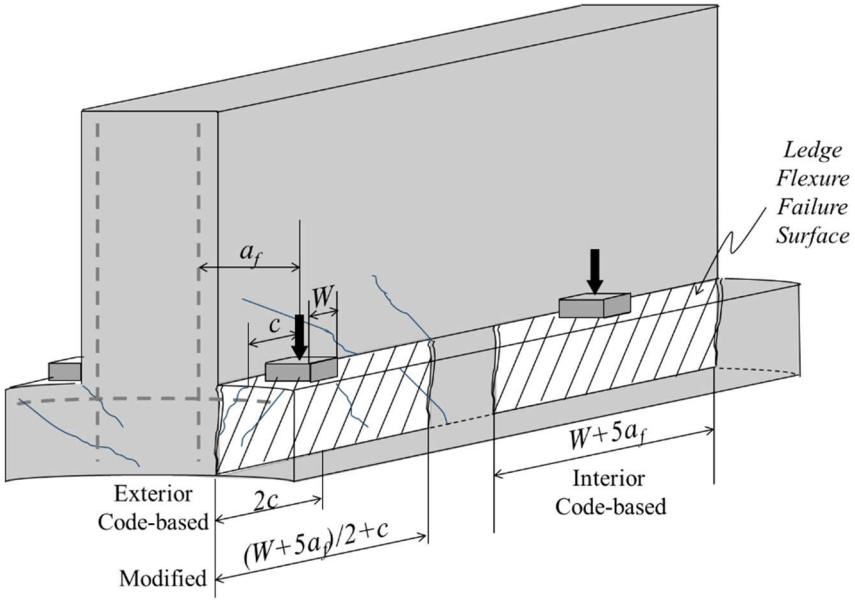

(c) AASHTO [10] and modified ledge flexure tributary lengths

Figure 3.9. Reinforcement tributary length for ledge flexure and hanger

Table 3.7 lists comparative test results for the specimens without and with the *end-region stiffener retrofit* solution. With the *relative serviceability* of 1.69 and 1.27 for both *hanger*- and *ledge-deficient* specimens, the externally attached steel end-plate successfully delayed crack initiation and kept the specimen in good condition within the *SLS*.

Although the *retrofit* and *repair* specimens failed due to excessive compressive stress at the bottom corner of the specimens as depicted in Figure 3.7 and Figure 3.8, the strength capacities of the specimens increased by 18 and 32 percent for the *hanger*- and *ledge-deficient* specimens, respectively. The improved strength capacity exceeds the ULS/ϕ.

To avoid the concrete compression node failure, a rational modification is proposed as shown in Figure 3.10. In the initial design, the corner node size was evidently too small, as seen in Figure 3.10(a). This led to excessive compressive stress at the bottom corner and thereby premature failure. To improve this situation, it is proposed that the bottom lip of the endplate should be extended to accommodate a large nodal dimension as depicted in Figure 3.10(b).

It is also recommended that the embedded depth of the ledge anchors be extended beyond the potential damage region by a length h_e in Figure 3.10(b). To provide additional stiffness to the plate, the use of triangular edge stiffeners is also recommended as shown in Figure 3.10(c).

Table 3.7. Summary of comparative test results without and with end-region stiffener

		Specimen Type	HD Ext.		LD Ext.		
		Test ID	***T1W1***	**T2E1**	***T5E1***	**T5W1**	**T7W2**
		Condition	*Ref.*	End-region	*Ref.*	End-region	End-region Repair[1]
Serviceability	**Service Limit State (*SLS, kN*)**		187				
	Observed	Cracking. Load (kN)	*144*	244	*138*	176	-
		Relative Serviceability[2]	*1.0*	1.69	*1.0*	1.27	-
Ultimate Strength	**Ultimate Limit State Demand (*ULS/ϕ, kN*)**		312				
	Observed	Max. Load (kN)	*294*	347	*294*	383	391
		Relative Strength[3]	*1.0*	1.18	*1.0*	1.3	1.33
		Controlling mode	*Hanger*	Strut-tie	*LF*[4]	Strut-tie	LF & P
	Code-based (AASHTO)	Strength Capacity (kN)	*188*	265	*213*	227	242
		Ratio	*1.56*	1.31	*1.38*	1.69	1.62
	Limit Analysis[5]	Lower bound (kN)	*251*	328	*271*	283	298
		λ†	*1.17*	1.06	*1.08*	1.35	1.31
		Upper bound (kN)	*391*	468	*417*	427	444

[1] Repair = repaired of a specimen that was cracked under simulated service conditions and then repaired
[2] Relative serviceability= retrofitted cracking load/reference cracking load
[3] Relative strength = retrofitted maximum load/reference maximum load
[4] LF = Ledge-flexure, P = punching shear
[5] Limit analysis used modified tributary width to calculate lower and upper bound (see Figure 3.9*)*
† λ = maximum load/lower bound

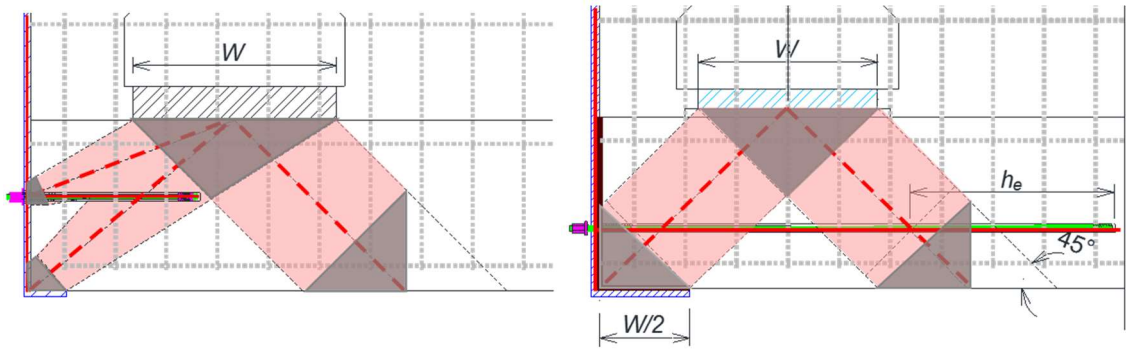

(a) Compression nodes for initial end-region stiffener design

(b) Rational compression nodes to prevent concrete compression node failure

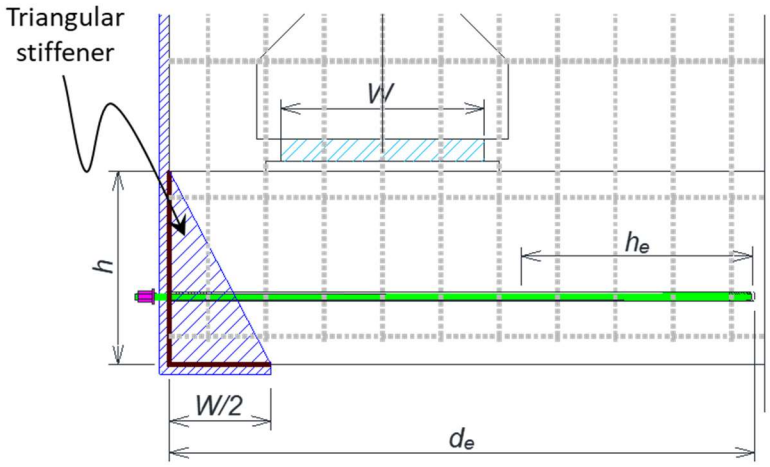

(c) Recommended design modification for end-region stiffener with triangular stiffener

Figure 3.10. Rationale using strut-and-tie modeling for ledge with end-region stiffener retrofit. Note h_e = bar anchorage beyond node.

3.9. Closing Remarks

This research has developed retrofit solutions by attaching additional steel components to in-service inverted-T bent caps that may be capacity deficient and cracked. Based on the experimental investigation presented herein, the following conclusions are drawn:

1) To economically retrofit such deficient structures, alternative load paths are necessary. The method investigated herein is to provide supplemental hanger and ledge capacity via bolts drilled through the web of the inverted-T section and connected to a catcher channel. The end region of a cantilever inverted-T bent cap beam is also often deficient and this can be retrofitted by bonding and bolting a steel end-plate system.
2) Experiments, conducted as proof-of-concept tests, demonstrated that both serviceability and the ultimate limit state conditions may be markedly improved by providing supplemental load paths.
3) For both the straddle (interior) and cantilever (exterior) parts of the inverted-T specimens, the through-web post-installed PT threadbar with catcher channel solution successfully postponed and reduced cracking. That is, the retrofitted specimens remained in a serviceable condition below the *serviceability* limit and without significant cracking until the *ultimate* limit was approached.
4) The end-region stiffener solution also successfully delayed cracking and provided additional strength to the cantilever (exterior) part of the inverted-T bent cap specimens. With the proposed rational modification, this solution may be the most

efficient approach for end-region capacity deficient or cracked cantilever inverted-T bent caps.

5) The code-based strength capacities are quite conservative when compared to the experimental test results. To obtain more accurate, but still conservative, strength capacity estimates for design, it is recommended to conduct limit analysis using a modified tributary width proposed as shown in Figure 3.9.

4. CAPACITY IMPROVEMENTS FOR EXISTING INVERTED-T BENT CAPS USING LOAD BALANCING EXTERNAL POST-TENSIONING

4.1. Section Summary

Inverted-T bent caps have been widely used to provide increased clearance beneath bridges. Bridges with inverted-T bent caps often experience a prevalence of cracking at the web-to-ledge interface. To prevent these cracks, ledges require sufficient capacity to enable the transfer of applied loads from the girder seats to the pier column. This experimental investigation developed a retrofit solution which uses externally installed post-tensioned strands to balance dead loads thereby improving the capacity of the in-service inverted-T bent caps. Based on experimental results, the solution successfully improved the load carrying capacity of the bents and restrained existing cracks. The cracking load estimation was investigated to evaluate serviceability of the inverted-T bent caps without and with the PT retrofit. Ultimate strength predictions calculated using code-specified sectional methods and limit analysis were compared and contrasted with the experimental observations to evaluate their accuracy in estimating the observed ultimate strength. Based on the experimental observations and analytical comparisons; design, repair, and retrofit recommendations were provided, including their limitations.

4.2. Introduction

Existing bridges some of which may be rather old and built to historic specifications are often found to be substandard in their strength capacity when judged by contemporary standards. Some bridges, which are not particularly old, may also show some signs of distress. This distress may arise due to a lack of knowledge of the expected structural

performance at the time of design. Rather than replacing such deficient structures, retrofitting the deficient parts of the structure, by adding capacity to meet modern expectations both in terms of serviceability and strength, is often a more expedient approach.

Inverted-T bent caps have been extensively used to reduce the overall height of a bridge as well as to improve the available clearance beneath the bridge girders. Many bridges with inverted-T bent caps fall into both of the above categories; they are somewhat old, and the cap beams often show disquietening cracks at the web-to-ledge interface, as shown in Figure 3.1(a). Zhu et al. [17] and Zhu and Hsu [16] also noted the prevalence of such cracking and suggested a crack control design method.

Mirza and Furlong [7, 14] investigated the behavior of inverted-T beams. They found that inverted-T beams may fail due to local mechanisms such as hanger failure, punching shear failure, and ledge failure. Compared to flexural and shear failures that may be commonly found in rectangular or standard-T beams, hanger, ledge, and punching of inverted-T beams require special consideration. In accordance with current codes, five additional nominal capacities must be checked for sufficiency: (i) web-to-ledge interface shear; (ii) ledge flexure and horizontal force; (iii) punching shear; (iv) hanger reinforcement; and (v) bearing (seating) capacity.

For existing structures with deficient concrete beams, there are various strengthening methods, including addition of structural material using steel or reinforced fiber polymer (FRP) jackets, bonded steel plates [35]. Among them, external post-

tensioning (PT) method has been increasingly used because they are applicable to a wide range of structure [28].

Aravinthan and Suntharavadivel [25] investigated the effectiveness of an external PT technique for a rectangular bent cap. The authors conducted experimental tests to investigate an external PT retrofit on the rectangular cantilever and straddle bent caps. The test results demonstrated that the bent caps were successfully strengthened with the conventional external PT after repairing cracks by epoxy injection.

Minimal research attention has been found in the literature in investigating strengthening techniques for inverted-T beams. Most of previous studies on inverted-T beams focused on their design and evaluation [7, 9, 14, 16, 17], while research on retrofitting inverted-T beams concentrated on the methods utilizing FRPs [6, 12, 19].

In this study, an external post-tensioning technique is utilized as a solution to improve serviceability and extend service life of existing inverted-T bent caps because of its practical advantages including low cost, minimal disruption to traffic, easier construction and compaction, wide range applicability, and ease of monitoring and maintenance [73]. The external PT solution for inverted-T bent caps is designed to balance off dead load, and thus, strengthen the entire inverted-T bent cap at once. PT installation can be rapid and mostly non-invasive. The external load-balancing post-tensioning (PT) solution is experimentally investigated to validate its effectiveness.

Since there is a diversity of inverted-T bent caps, Hurlebaus et al. [6] also presented a series design concepts for eighteen alternative strengthening solutions (FRP, mechanical, and external PT solutions).

4.3. External Load Balancing Post-Tensioning Solution

Figure 4.1 presents a load-balancing design philosophy for the retrofitting of single- and double-column bridge bents. Proposed as the basis for the retrofit design, the load-balancing concept uses external PT and thereby tends to cancel much of the self-weight moments and shears. The inclined PT profile similar to the bending moment diagram for the unretrofitted bent is intended to counteract dead load moments with an eccentricity, e_0, and to balance the reaction of the fascia girders at the anchored ends. Figure 4.1(a) shows shear force and bending moment diagrams for a pre-retrofit prototype single-column (cantilever) bent, where tension is on the top of the bent. After retrofitting the bent with PT as shown in Figure 4.1(b), the dead load moments and shears are balanced; this results in a decrease in the overall maximum shears and moments under service.

The double-column bent (Figure 4.1(c) and (d)) has both cantilever and interior parts. To cancel the dead load between columns, the PT strands need to be placed beneath the interior girders and transfer the loads to the adjacent column. At harp points in the PT profile, transverse forces are introduced to balance gravity force arising from the girder seats.

Figure 4.2 presents a stress block concept as a complementary view to the load balancing design philosophy. Figure 4.2(a) shows the applied strain profile that results in cracked concrete stresses on the upper surface prior to retrofitting at a critical cracked section (in this case, exterior girder location).

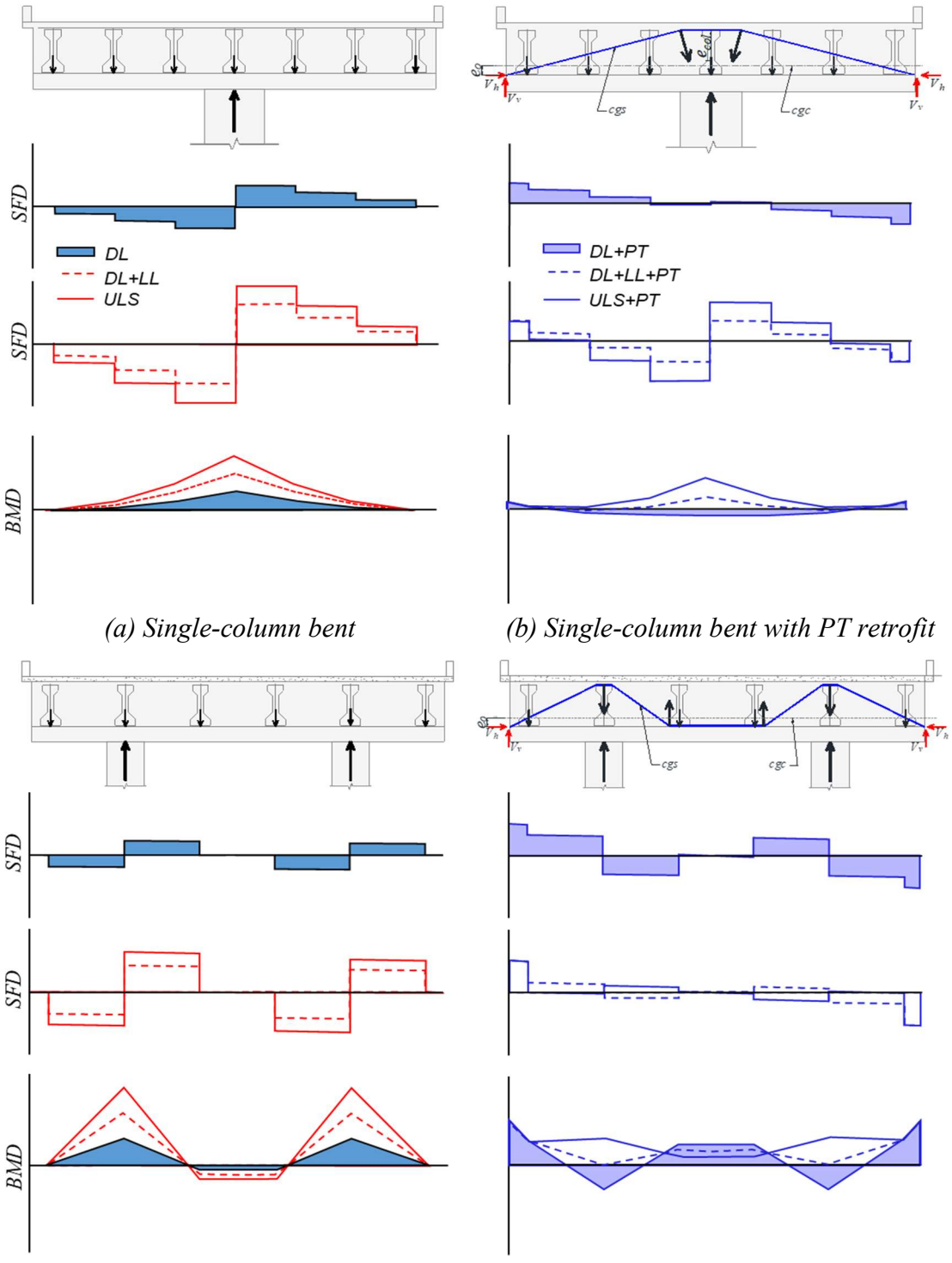

(a) Single-column bent *(b) Single-column bent with PT retrofit*

(c) Double-column bent *(d) Double-column bent with PT retrofit*

Figure 4.1. Load balancing concept for a post-tensioned retrofit solution

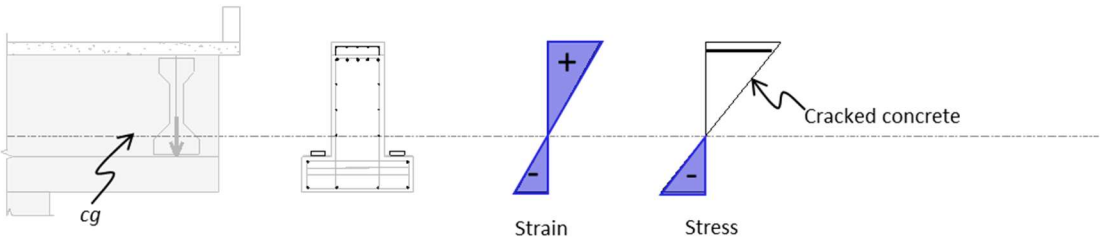

(a) Strain and stress prior to retrofit under service loads

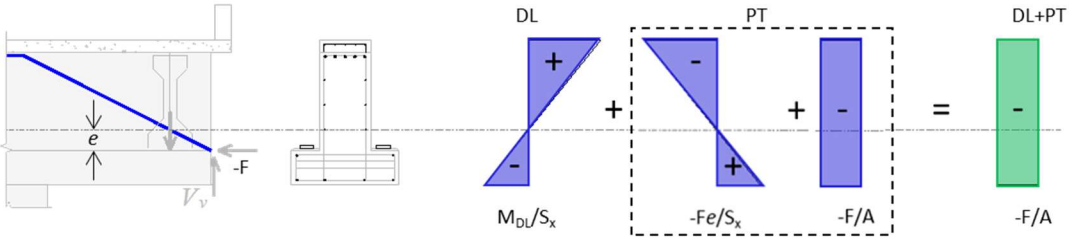

(b) Balancing the dead loads to give uniform stress (-F/A)
(Note existing flexure cracks should close)

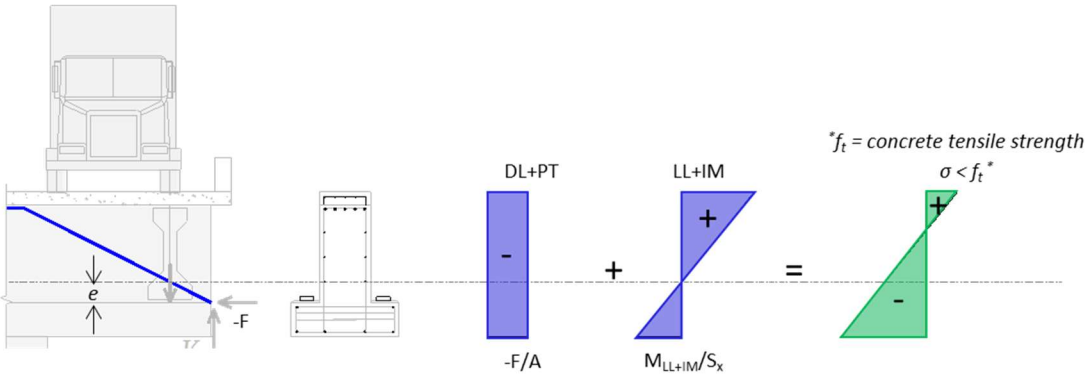

(c) Stresses at service limit state after PT retrofit showing serviceability design objective

Figure 4.2. The post-tensioned retrofit design concept based on stress blocks in the service range.

Figure 4.2(b) illustrates that if the dead loads can be balanced (as well as practicable with prestress), then no moments or shears exist when no traffic is on the structure; in essence, the bent cap remains in a state of uniform axial stress (-F/A). Figure 4.2(c) shows that when live load (and impact) are applied under service conditions, uncracked bending behavior is possible–thus no cracking should be observed under working load (service) conditions. Naturally, ultimate strength conditions must still be verified as acceptable.

4.3.1. Design Concept

Figure 4.3 presents the PT design concepts and associated load paths for external load balancing prestress applied to typical prototype single- and double-column bent caps. The PT profiles must be designed such that the points provide deviations which form gradual angular changes that satisfy minimum bend radii to avoid kinks. Lightly reinforced concrete saddles are therefore placed near column locations to ensure a viable load path for the PT strands.

Figure 4.3(a) shows the basic design concept of the single-column bent where tension is on the top of the bent cap. The load balancing PT is anchored at the ends and draped over concrete saddle blocks with an inclination angle, $\tan^{-1}(h/L)$, to provide sufficient upward force to balance the girder self-weight reactions. The reaction forces to the PT are directly transferred to the columns via the reinforced concrete saddle blocks.

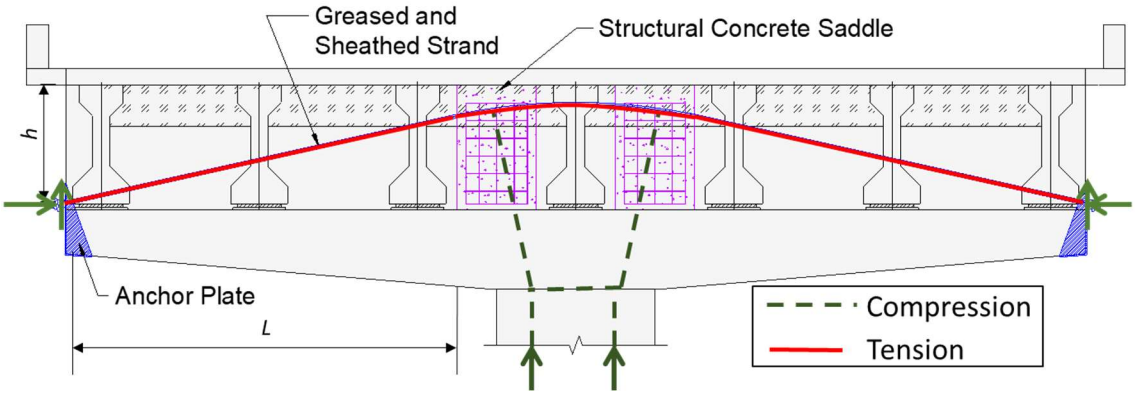

(a) Single-column bent with external PT retrofit

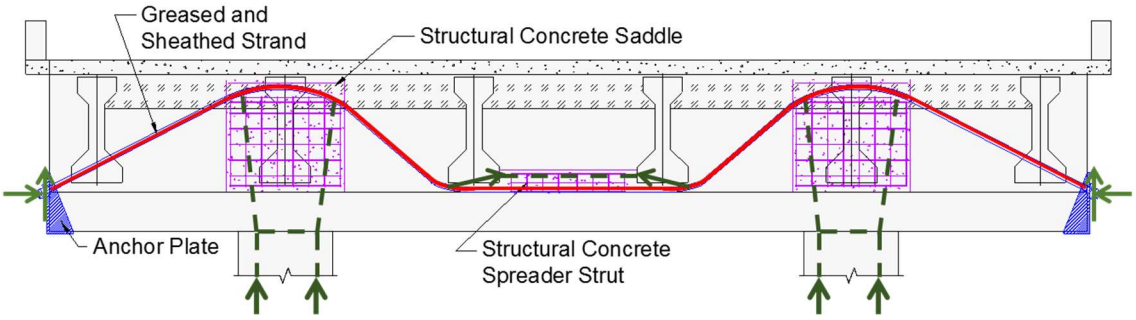

(b) Double-column bent with external PT retrofit

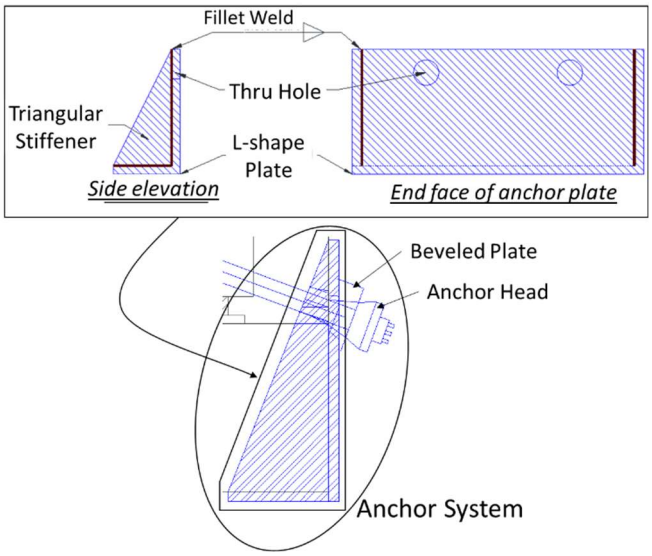

(c) Details of End Region Anchor System

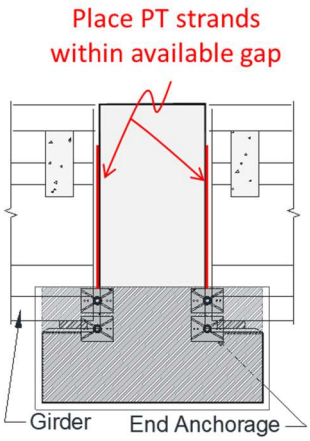

(d) Side view of end face

Figure 4.3. Design Concept and Load Path of Load Balancing PT Technique.

Figure 4.3(b) likewise presents the PT solution for the double-column bent. While similar to the single-column bent application, the cantilever portion of the double column bent requires a steeper inclination angle. The short distance between saddle blocks may create challenges for achieving an effective inclination angle to keep the strand bend radius within acceptable limits. In the region between the two columns, the PT strands are placed beneath the girders with a concrete spreader strut to resist compression between the girders.

After the PT strands are placed over the concrete saddle blocks and/or beneath the concrete spreader strut, the strands must be anchored with an appropriate anchorage system at the beam ends. Figure 4.3(c) shows one such detail that may be used to anchor the PT strands without causing distress to the concrete bent cap.

Figure 4.3(d) presents an end view of the PT anchorage system. It is generally necessary to fit all hardware (unbonded sheathed and greased strand) within the confines of the restricted space between the girder end and web of the inverted-T bent cap. In some cases, the girders may be too close (or even touching) to the web of the inverted-T bent cap. In such cases an additional effort is necessary to drill about 1.0 in. diameter hole to pass the PT strands through.

4.3.2. Design Verification Checks

Following the load-balancing design of the prestress system, it is necessary to conduct serviceability and ultimate strength checks.

Within the service limit state, the inverted-T bent cap, ideally, should remain uncracked to provide enduring service. The cracking load for the inverted-T beams may

be estimated as the lesser of the load for the beam flexure/shear crack or for the web-to-ledge interface crack (hanger or ledge crack). AASHTO LRFD *Bridge Design Specification* [10] provides hanger design provisions for the service limit state conservatively using one-half of the yield strength of the hanger reinforcement. To determine the web-to-ledge interface cracking load (V_{cr}) more accurately, the crack control method for the inverted-T bent caps proposed by Zhu and Hsu [16] was adopted herein. To meet serviceability conditions, the cracking load should be greater than the service limit state load in accordance with AASHTO [10]: $V_{\mathrm{cr}} > V_{\mathrm{SLS}} = V_{\mathrm{DL}} + V_{\mathrm{LL+I}}$.

For the beam flexure cracking, the concrete modulus of rupture, $f_t = 0.5\sqrt{f_c'}$, was used to calculate the cracking load. Any prestressing force for resisting the flexure cracking load should be considered as depicted in Figure 4.2.

For the crack control method, the web-to-ledge interface crack width for a full-size inverted-T bent cap limits to a "critical crack width": 0.15 mm and 0.33 mm for *end face of exterior* and *vicinity of applied load* regions, respectively, where the concrete stiffness reduces rapidly and the stresses in the reinforcement increase [16]. The method takes the stiffness of a steel tie with concrete cover as

$$EA = E_s A_S + E_c A_c \tag{4.1}$$

in which E_s = tensile modulus of elasticity of steel = 200 GPa; E_c = tensile modulus of elasticity of concrete = $155\sqrt{f_c'}$ MPa (Zhu et al., 2003); A_c = concrete area surrounding a steel reinforcement = $\pi(clear\ cover + 0.5d_b)^2$; and A_s = nominal area of the steel

reinforcement. For any prestressing force, the vertical component of the force, V_p, should be added to the calculated web-to-ledge interface cracking load.

For the ultimate strength condition, the factored sectional resistance (ϕV_r) of an inverted-T bent cap must be greater than the factored ultimate load demand. When determining factored resistance, it should include the vertical component of the prestressing force, if any, in addition to existing strength. To satisfy the ultimate strength in accordance with AASHTO [10]:

$$\phi V_r = \phi\left(V_n + V_p\right) > V_u \tag{4.2}$$

in which V_p = vertical component of the prestressing force in the direction of applied force; ϕ = resistance factor as specified in AASHTO [10], ϕ = 0.9; V_r= sectional resistance; and V_n = nominal resistance of the beam ledge which is elaborated upon below. Rearranging, Eq. (4.2) can be expressed as

$$\frac{V_u}{\phi} - V_n \leq V_p \tag{4.3}$$

in which $V_u = 1.25V_{\mathrm{DL}} + 1.75V_{\mathrm{LL+IM}}$ = ultimate factored load demand calculated in accordance with AASHTO [10], where V_{DL} = dead load and $V_{\mathrm{LL+I}}$ = live load plus impact effects.

Code-based design equations for capacity calculations are conservatively based on the yield strength of the reinforcement (f_y); the strain-hardening effect remains as additional reserve capacity. If the concrete is severely cracked, as often observed in certain existing inverted-T bent caps, some of this reserve capacity may have been consumed.

Therefore to calculate the upper limit state, a strain-hardening scalar (λ) was accounted in Eq. (3.2)

The applied prestressing force should satisfy the strength limit inequality provided in Eq. (4.3) with its vertical component (V_p). With load-balancing, the ideal range of enhanced capacity provided by the PT (V_p) is expected to be such that $1.0V_{\mathrm{DL}} \leq V_p < 1.25V_{\mathrm{DL}}/\phi$. The strand layout along with the angle is designed based on the girder and column locations since reinforced concrete saddles need to be cast near each column.

4.4. Experimental Program

Since the large full-scale prototype inverted-T bent cap dimensions are physically not possible to fit with given laboratory constraints, reduced-scale test specimens were necessary. A prototype inverted-T bent cap, which consists of both straddle and cantilever parts, designed to represent both multi-column bent and hammer head bent. Seven individual experimental tests were conducted on four half-scale specimens.

To emphasize hanger and ledge deficiencies, two types of specimens were designed in accordance with the sectional strength design method, and referred as *hanger-deficient (HD)* and *ledge-deficient (LD)* specimen.

4.4.1. Test Specimens

Figure 3.3 shows geometric and reinforcement details for both *hanger-deficient* (*HD*) and *ledge-deficient* (*LD*) specimens. Figure 3.3(a) provides an elevation view of a general test specimen seated on two columns. The total length of the inverted-T beam specimen is 6706 mm, the overall height is 1016 mm, and the bent caps were centered on two 610 mm

square columns. Each column had a 762 mm height and placed with their centers 3658 mm apart. Figure 3.3(b) depicts details of a column placed on a 914 mm square steel plate. Steel base plates were used to provide a flat-bottom surface connection to the laboratory strong-floor. A 38 mm diameter steel pipe was placed along the vertical axis of the column and welded to the steel base plate to allow a high strength threadbar tie-down to clamp the specimen and column to the laboratory strong-floor. Strong columns were designed to ensure minimal damage; a concrete with 28-day compressive strength of 70 MPa was used thereby enabling reuse of the columns for all tests.

To investigate the ability of the designed retrofit solution to strengthen specific deficiencies, the *hanger-deficient* and the *ledge-deficient* specimens were designed and constructed. Both specimen types had the same cross-sectional dimensions and longitudinal reinforcement layout as shown in Figure 3.3(c). The ledge height and width of the specimens were 254 mm and 210 mm, respectively, with a web width of 381 mm.

A total of four specimens (two *hanger-deficient* and two *ledge-deficient* specimens) were constructed to conduct experimental tests to evaluate the performance of the load balancing PT technique. Specimens 1 and 2 were cast on the same day, while Specimens 5 and 7 were cast at a later date. Ready-mix concrete with a target compressive strength of 25 MPa was used, and slump tests were conducted prior to each concrete pour. Only a modest concrete strength was used, reflective of field cast mixes of the 1960's. It is also considered important to keep the concrete on the weak side to avoid false-positive test results. Three standard 100 mm x 200 mm cylinders per each concrete cast were tested at 28-days and on the day of testing. Table 3.2(a) lists the measured concrete properties.

Figure 3.3(d) shows transverse reinforcement details that controlled sectional failure mode. Grade 60 reinforcement was used with the measured material properties given in Table 3.2(b). The *hanger-deficient* specimens (Specimens 1 and 2) have D10 (#3) a hanger reinforcement and D13 (#4) ledge reinforcement with an average spacing of 152 mm to achieve hanger failure mechanism for the un-retrofitted specimen. The *ledge-deficient* specimens (Specimens 5 and 7) have D13 (#4) hanger reinforcement and D10 (#3) ledge reinforcement with an average spacing of 140 mm to have ledge flexure failure. Note herein #3 rebar (3/8-inch) is approximately 10 mm, hence D10 notation is used.

4.4.2. Test Setup

Figure 4.4 shows the test setup for both *exterior* and *interior* regions without and with PT retrofit. At each simulated girder line, a 600-kip hydraulic jack was used to apply loads that were equally transferred to each ledge as shown in Figure 4.4(a). Two layers of 25 mm thick 100 mm x 355 mm steel plates and a 380 mm long 150 mm deep x 16 kg/m (C 6 x 10.5) channel were stacked up between the bottom of the loading frame and the bearing pad to evenly distribute the load to the bearing pad. Figure 4.4(a) depicts the *exterior* region test setup that simulate one girder line loading. The loads increased at each jack equally up to the total equivalent dead load, at which point the load over the column was held constant. The load applied at 305 mm from the end face increased until the end of the test. Figure 4.4(b) shows *interior* region tests and the loading frame setups. *Interior* tests simulated two girder lines spaced at 1219 mm, centered on the specimen, centered on the specimen, and the loads are equally applied on each girder line until the tests were terminated.

String pots were used to obtain the vertical deflection beneath the bent cap at each loading point. Load-deflection curves at each loading point may be obtained from each test, and a curve for the loading point with the largest deflection is reported herein.

4.4.3. Installation of External Load Balancing Post-Tensioning

To load the *exterior* and *interior* regions separately, two different PT configurations were used, as shown in Figure 4.4(c) and (d). Greased 15 mm (0.6 in.) Grade 270 low-relaxation strands (f_{pu} = 1860MPa) were used for all PT retrofit tests. The strands were anchored in a similar fashion as shown in Figure 4.3(c) and 6. The anchor plates (and/or channel) were installed using a rapid hardening grout and mechanical anchors. For ease of construction and testing, detachable steel deviator plates were adopted instead of the concrete infill blocks depicted in Figure 4.3.

Figure 4.4(c) illustrates component details for the PT retrofit at the *exterior* region. A post-installed PT strand supported by a deviator plate was used on each side of the inverted-T web and had a 24-degree inclination angle. The deviator plates consisted of a saddle plate and a supporting plate. Each deviator plate was attached to the web with four mechanical anchors (16 mm diameter and 140 mm embedded depth).

As shown in Figure 4.4(d), for the *interior* tests, a steel deviator plate was placed beneath the loading frame and bearing pads without an anchorage for each ledge. Two strands were placed on each side of the web. The strands were individually placed in each notch of the plate: one strand passing in front of the load points and the other behind (strand configuration in Figure 4.4(d)). With the plates, the average inclination angles of

two strands were 14 degrees. To anchor the PT strands, identical anchor plates were installed at the top of both ends of the inverted-T bent cap specimen.

The prestressing force in each strand was designed to have 168 kN and 176 kN for *exterior* and *interior* tests, respectively, after immediate losses. This provided an uplift force (V_p) of 68 kN and 85 kN for the ex*terior* and *interior* portions, respectively. Each strand, before losses, was stressed to 200 kN. For interior tests with PT retrofit, a simulated girder dead load force of 100 kN was applied on each base plate at each loading point prior to applying prestress.

4.5. Test Results

Table 4.1 shows the list of conducted tests and a summary of test results; a total of seven tests, including three reference tests, were conducted to evaluate the performance of the external load balancing PT solution. For the *interior* region test, the solution was applied and evaluated only on a *hanger-deficient* specimen as a representative, since the solution designed to strengthen the entire sectional capacity by uplifting girders.

The loading for each test was temporarily paused for a short time to mark and investigate cracking patterns at around dead load, the service limit state, and the ultimate load levels for each test. The *interior* test was paused at 120 kN, 220 kN, and 340 kN, and each *exterior* test was paused at 100 kN, 200 kN, and 300 kN. Loads were increased to failure for the reference tests following ultimate loads. Experiments with PT strands were terminated prior to failure to avoid potential damage to instrumentation and other experimental hardware.

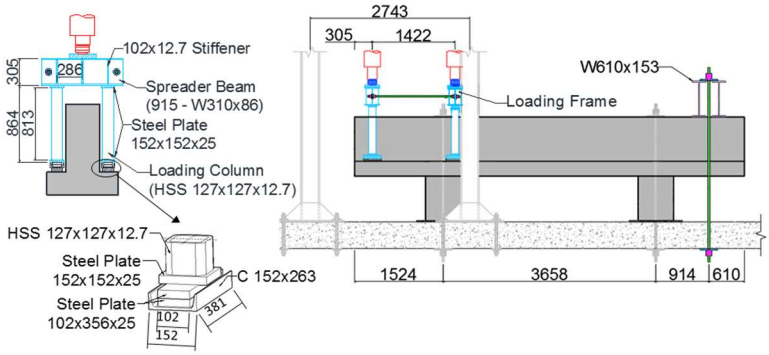

(a) Reference exterior test setup

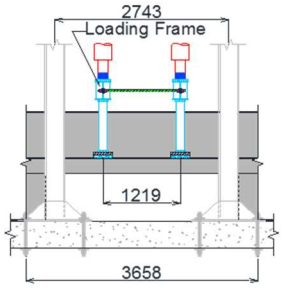

(b) Reference interior test setup

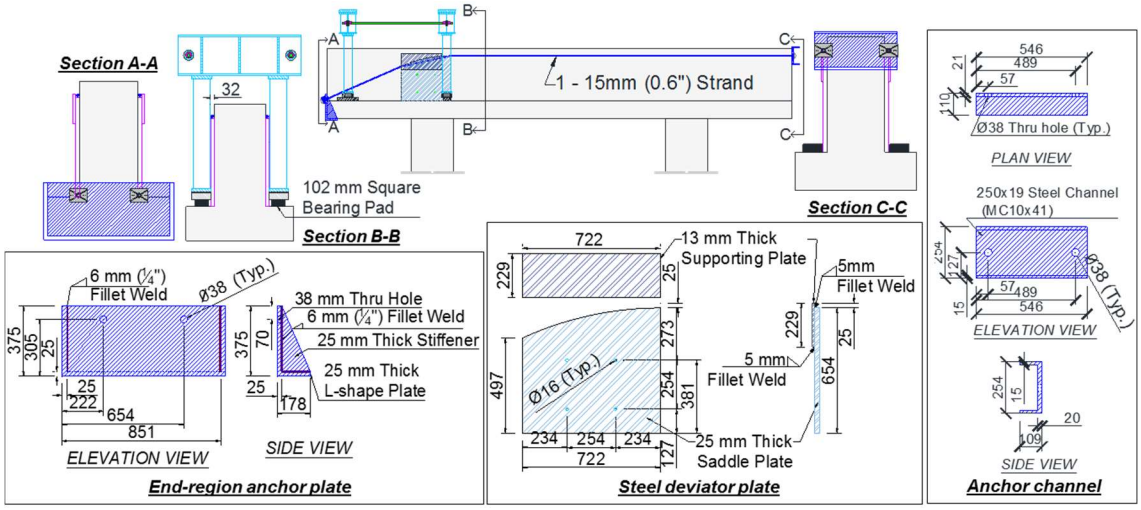

(c) PT installation for exterior test setup

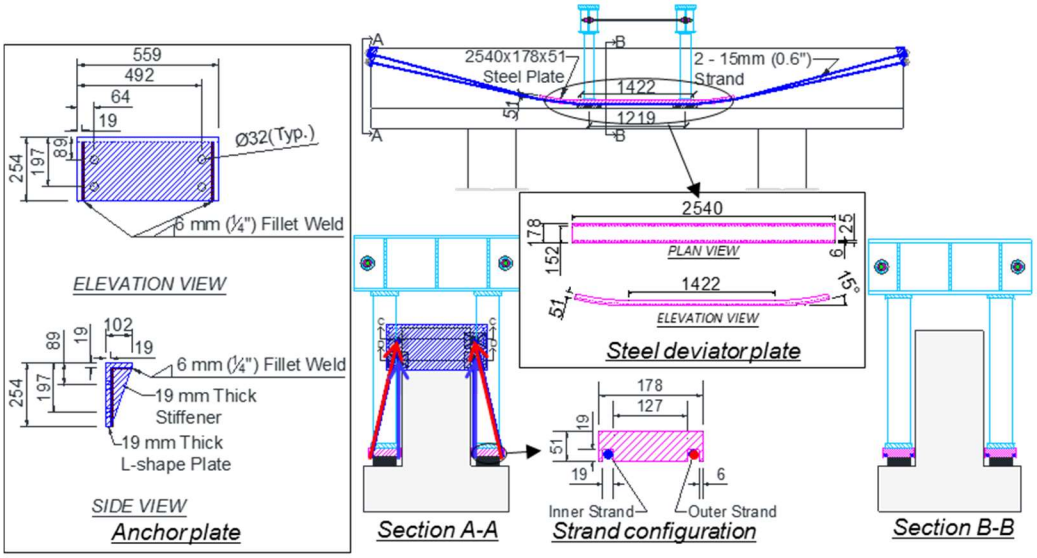

(d) PT installation for interior test setup

Figure 4.4. Component details for load-balancing PT experiments (mm)

4.5.1. Exterior (Cantilever) Specimen

Figure 4.5 shows the experimental test setups and the test results for the *exterior* regions where tension is on the top of the beam. A total of five *exterior* tests were conducted: two on the *hanger-deficient* specimens and three on the *ledge-deficient* specimens. On both the *hanger-* and the *ledge-deficient* specimens, one *reference* and one PT *retrofit* tests were conducted. An additional repair test (PT *repair*) was conducted on the *ledge-deficient* specimen to investigate the effectiveness of the PT retrofit for the existing cracked bent caps. Figure 4.5 shows test setups for (a) without and (b) with the PT retrofit.

For the hanger-deficient exterior case, reference tests (T1W1) were conducted on an overhang region of Specimen 1. Figure 4.5(c) show the observed cracks for hanger-deficient exterior reference specimen at the end of the test. The first crack, which was a hanger crack at the web-to-ledge interface, was observed at around 144 kN, at which point nonlinear behavior commenced as shown in Figure 4.5(g) (see red diamond on the grey solid line). Note that the cracking load was reached and nonlinear behavior was initiated prior to service limit state load level. After the applied load reached the service limit state of SLS = V_{DL+LL} = 187 kN (red horizontal dashed double dot line in Figure 4.5(g)), the second hanger crack occurred (see Figure 4.5(c)) at around 200 kN. Following the second hanger crack, strain-hardening of the hanger reinforcement commenced (see Figure 4.5(g)). Shortly after the third hanger crack commenced, the specimen failed at 294 kN; lower than the factored-up demand of ULS/ϕ = V_u/ϕ = 312 kN (black horizontal dashed dot line in Figure 4.5(g)). At the maximum load, the hanger crack at the web-to-ledge interface opened up to 15 mm wide.

Table 4.1. Summary of test results

Specimen ID[1]	Test ID[2]	Condition	Cracking Load V_{cr}^{test} (kN)	Relative Serviceability[3]	Failure Load, V_{max}^{test} (kN)	Relative Strength[4]
HD Ext.	T1W1	*Ref.*	*144*	*1.0*	*294*	*1.0*
	T2W1	Retrofit	246	1.71	366*[6]	1.24
LD Ext.	T5E1	*Ref.*	*141*	*1.0*	*294*	*1.0*
	T7W1	Retrofit	226	1.60	365*	1.24
	T7E1	Repair[5]	-	-	445*	1.52
HD Int.	T1I1	*Ref.*	*180*	*1.0*	*401*	*1.0*
	T2I1	Retrofit	318	1.77	467*	1.16

1. HD = hanger-deficient and LD = ledge-deficient

2. Test ID includes test information; first number = specimen number, last number = number of test on the location, and second letter = test location on the specimen (W = west, E = east, and I = interior)

3. Relative serviceability = retrofitted cracking.load / reference cracking.load

4. Relative strength = retrofitted max.load / reference max.load

5. Repaired after cracking; cracking load is not specified

*6. * = Test termination load (specimens with external PT did not reach limit).*

(a) Exterior test setup *(b) Retrofitted exterior girder location setup*

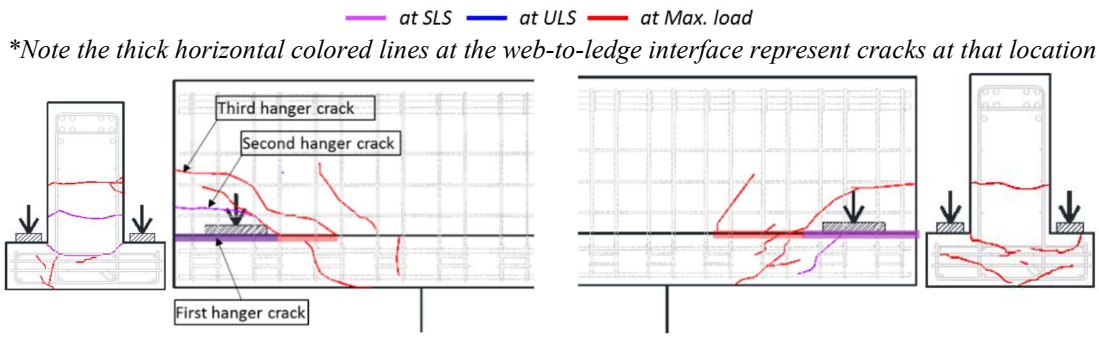

**Note the thick horizontal colored lines at the web-to-ledge interface represent cracks at that location*

(c) HD reference (T1W1) observed crack maps *(d) LD reference(T5E1) observed crack maps*

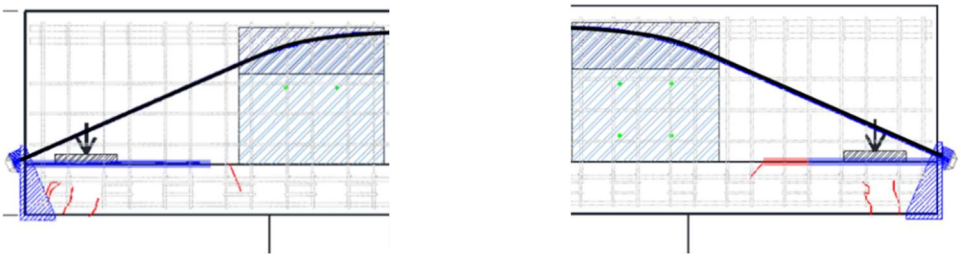

(e) PT retrofitted HD exterior crack map (T2W1) *(f) PT retrofitted LD exterior crack map (T7W1)*

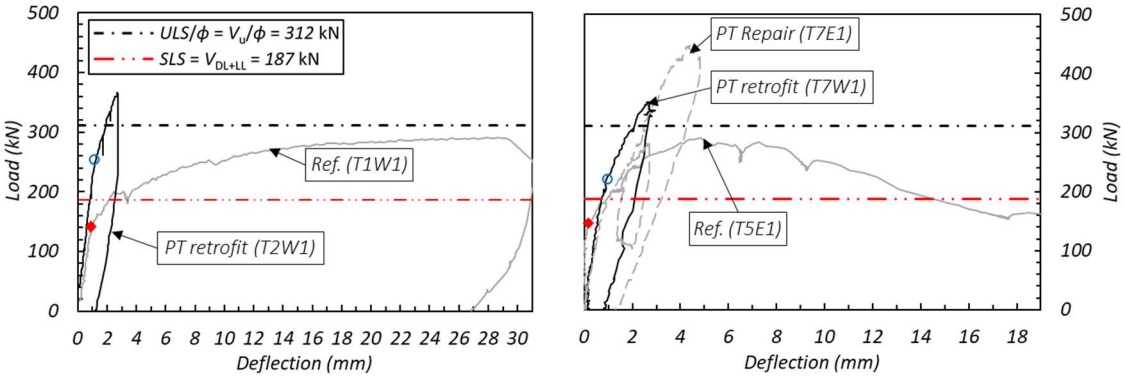

(g) HD exterior test load deflection behavior *(h) LD exterior test load-deflection behavior*

Figure 4.5. Experimental test results for *exterior* specimens where tension is on the top of the beam; (a) and (b) experimental test setup; (c), (d), (e), and (f) observed crack maps; and (g) and (h) load-deflection behavior with cracking load (♦ for *reference* ○ for *retrofit*).

For *hanger-deficient* exterior *PT retrofit* test (T2W1), an overhang region of hanger-deficient Specimen 2 was used; the observed cracks are mapped in Figure 4.5(e). At around 250 kN (greater than SLS = 187 kN), the first hanger crack at the web-to-ledge interface and hairline cracks in transverse direction at the bottom of the specimen were observed, as shown in Figure 4.5(e). At this load, nonlinear behavior commenced (black solid line in Figure 4.5(g)). When compared to the reference test, major cracks were observed for the reference specimen (Figure 4.5(c)) but no crack was found on the PT retrofit specimen (Figure 4.5(e)) within service limit state. Based on the observations and the load-deflection behaviors, the cracking load was increased by 60% *(*Table 4.1*)*. The test was terminated at 366 kN, approximately 20% higher than ULS/ϕ = 312 kN, at which point the width of the web-to-ledge interface crack was 1 mm; significantly smaller than that of the similar crack on the reference specimen (15 mm). *T*he PT retrofit specimen was also able to carry the load beyond the factored-up demand ULS/ϕ, while the reference specimen failed prior to achieving this. It is clearly evident the external PT solution successfully improved both serviceability and the hanger capacity of the exterior region of the inverted-T bent cap.

For the ledge-deficient exterior case, the experiments focused on the effectiveness of the external PT under different specimen conditions. A reference test was conducted on an exterior region of ledge-deficient Specimen 5, and both PT retrofit tests (retrofit the virgin uncracked specimen: T7W1, and PT repair: T7E1 that was pre-cracked under simulated serviced load conditions and then repaired) were conducted respectively on each

overhang end of ledge-deficient Specimen 7. Figure 4.5(d), (f), and (h) (right column) show the ledge-deficient specimens test results.

The initial crack on the ledge-deficient reference specimen formed at the web-to-ledge interface behind the bearing pad as shown in Figure 4.5(d) at around 141 kN, where the nonlinear behavior commenced (see red diamond symbol on grey solid line in Figure 4.5(h)) before reaching SLS = *187 kN*. The crack from each ledge propagated along the interface to the end face at between SLS and the maximum load. Several diagonal shear cracks formed on the web at around 260 kN; a stiffness change is observed from grey solid line in Figure 4.5(h). At around maximum load of 294 kN, a horizontal crack on the end face through the web commenced near the neutral axis of the bent cap (Figure 4.5(d)). The ledge-deficient reference exterior specimen (T5E1) failed at 294 kN, about 5 percent less than ULS/ϕ = 312 kN. At the failure, the maximum crack width of the web-to-ledge interface was 2.5 mm.

For the PT retrofit test (T7W1), the prestress (200 kN per strand) was applied prior to any load application. The first visible cracks were observed at the web-to-ledge interface behind the bearing pad after passing SLS (blue diamond symbol on black solid line in Figure 4.5(h)). This cracking load is 60 percent higher than that for the reference specimen (see relative serviceability column in Table 4.1). As the load increased, the cracks extended through the web-to-ledge interface toward the column. At around ULS/ϕ, hairline cracks formed on the bottom surface in the transverse direction under the bearing pad. To avoid potential damage to the specimen, the test was terminated at 365 kN (somewhat 20 percent higher than V_u/ϕ). At that load, cracks were observed on the side

of the ledge which propagated from the web-to-ledge interface (Figure 4.5(h)). The maximum widths of the web-to-ledge interface and ledge cracks were 0.25 mm and 0.1 mm, respectively.

For PT repair test (T7E1), before installing PT solution, the load was increased up to 280 kN (the observed damage level) with a short pause at SLS to pre-crack the specimen. When web shear cracks with the maximum width of 0.5 mm were observed at 280 kN, the force was reduced to the equivalent dead load (100 kN). Unlike the reference test, only hairline cracks at the web-to-ledge interface were observed at this load, possibly as a result of increased capacity provided by the preinstalled anchor plate. At the equivalent dead load, the load balancing PT was installed and prestressed. By post-tensioning, the cracks were restrained, and the applied force was increased because the vertical component of the PT force counteracts the applied load (black solid line in Figure 4.5(h)). After repairing the specimen, the load increased to the test termination load of 445 kN, and the existing cracks extended and few new cracks formed. Note that the test was terminated for the repaired specimen at the load somewhat 40 percent higher than V_u/ϕ, and it resulted higher value of the relative strength compared to the retrofitted specimen (see relative strength column in Table 4.1). The maximum width of the crack on the ledges increased to 0.25 mm while that of the web shear crack to 0.3 mm; smaller than the original (pre-repair) crack width.

Based on these tests (T7E1, T7W1), the external PT technique successfully improved serviceability of the inverted-T beams by delaying cracks with 70 percent

increase in cracking load and by restraining existing cracks. The load carrying capacity of the inverted-T beams with PT solution was also improved by more than 25 percent.

After repairing the specimen with PT, the load-deflection behavior of the specimen follows that of the PT retrofitted specimen and remained essentially linear as shown in Figure 4.5(h). It was demonstrated that the external PT solution serves as both on effective retrofit or repair.

4.5.2. Interior (Straddle) Specimen where Tension is at the Bottom of the Beam

Figure 4.6 presents the test setups and the experimental results for the *hanger-deficient interior region* tests. The photograph in Figure 4.6(a) provides a view of the *interior reference* test (T1I1) setup with two hydraulic jacks. Prior to achieving *SLS* = 223 kN, several cracks were observed. First observed were hanger cracks at the web-to-ledge interface (see Figure 4.6(c)). These cracks formed when nonlinear behavior commenced at 175 kN (see red diamond symbol on grey solid line in Figure 4.6(e)). The cracks propagated between the two load points as the force increased. The second hanger crack as labeled in see Figure 4.6(c) formed on the web between two load points. Between the *SLS* and *ULS/ϕ* , web shear and flexural cracks formed and extended to the side face of the ledges. Beyond the *ULS/ϕ*, additional web shear cracks propagated from the outside of the bearing pads. The specimen failed in hanger yielding with the maximum observed load of 401 kN. At this load, the web-to-ledge interface crack (the first hanger crack) and the top hanger crack (Figure 4.6(c)) opened to 5 mm and 2.5 mm wide, respectively.

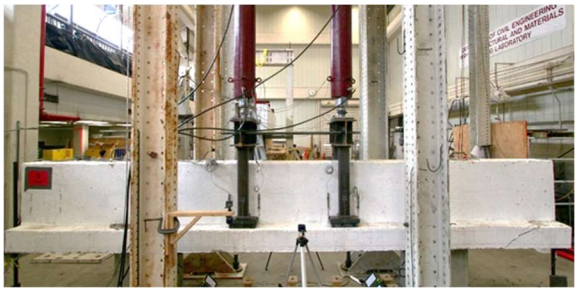

(a) Interior test setup

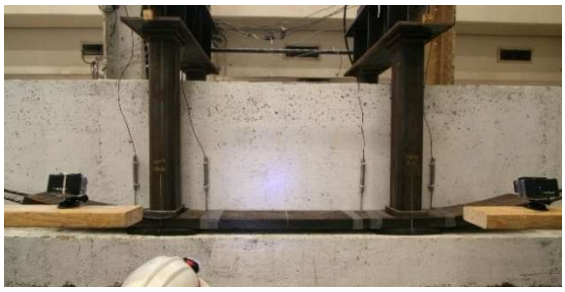

(b) Interior retrofit showing spreader strut

**Note the thick horizontal colored lines at the web-to-ledge interface represent cracks at that location*

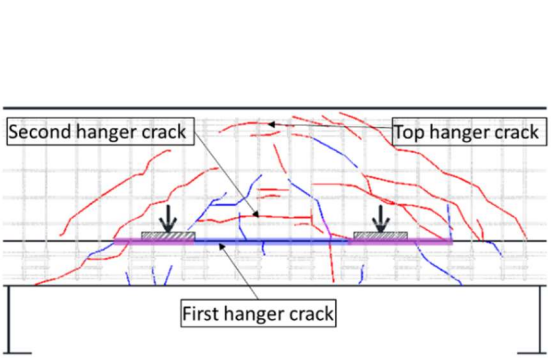

(c) HD interior reference (T1I1)

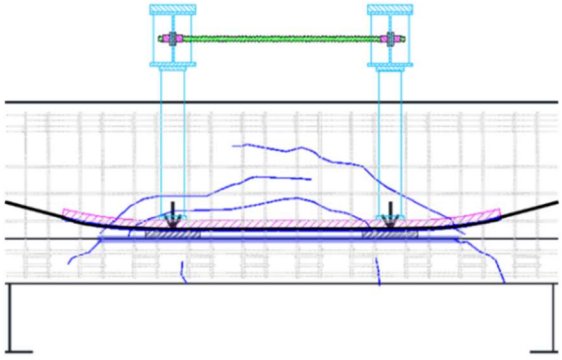

(d) HD interior retrofit (T2I1)

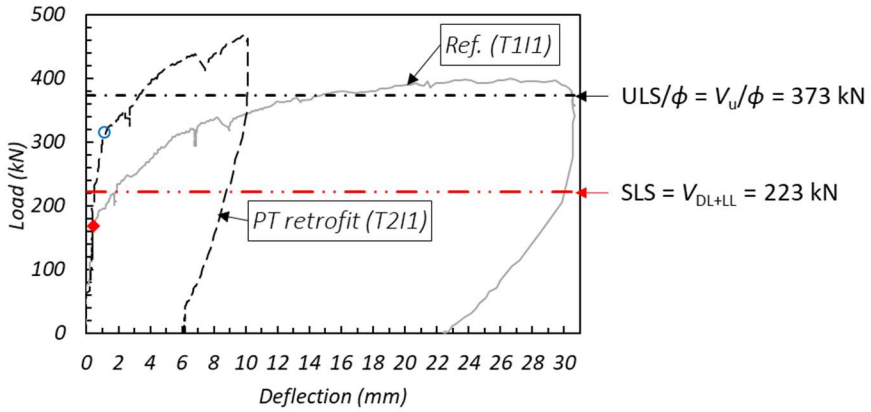

(e) HD interior load-deflection behavior

Figure 4.6. Experimental test results for *interior* specimens where tension is at the bottom of the beam; (a) and (b) experimental test setup; (c) and (d) observed crack maps; and (e) load-deflection behavior with cracking point (♦ for *reference* ○ for *retrofit*)

No damage was observed for the *PT retrofit hanger-deficient interior* Specimen 2 interior test (T2I1) up to 320 kN, at which point initial cracks formed at the web-to-ledge interface behind each bearing pad, and the behavior of the specimen become non-linear (black solid line in Figure 4.6(e)). This cracking load is 77 percent higher than the load for the *reference* specimen (see relative serviceability column in Table 4.1). As the load increased, the cracks propagated through mid-span between the two bearing pads and connected, as shown in Figure 4.6(d). Some flexure cracks on the bottom surface under the loading points and hanger cracks on the web were also observed. Beyond ULS/ϕ, no new cracks developed until the test termination load of test at 467 kN. Note the experiment was terminated before failure to avoid damage to instrumentation and the test setup.

4.6. Discussion

Based on the experimental test results, it was demonstrated that applying the PT to either retrofit or repair had two beneficial aspects: (i) remarkably delayed initial cracking and (ii) the number of cracks observed considerably reduced.

The conditions within the service limit state ($SLS = V_{\mathrm{DL+LL}}$) were experimentally checked to analyze the effectiveness of the retrofit solution. Cracking on the *reference* specimens was first observed before the load achieving the *SLS*; where undesirable nonlinear load-deflection behavior commenced. On the other hand, the first crack on the *PT retrofit* specimens was observed near ULS/ϕ; the load-deflection behavior remained linear beyond the *SLS*. The cracking load following the PT retrofit increased on average by 68 percent. That is, the overall specimen integrity remained in good condition (no cracks) for *PT retrofit* whereas the *reference* (unretrofitted) specimen experienced major

cracking. Especially for the *interior* region, the *PT retrofitted* specimen remained without any cracks up to a load that 40 percent higher than the *SLS*; the *PT* solution improved the entire sectional capacity of the bent cap. As the primary intention of the load balancing PT retrofit is to negate the potential for cracking under service load conditions, then it is to be expected only under severe overload conditions will occur cracking.

The experimental "as-built" capacity, V_{max}^{test}, would appear to be sufficient (or nearly sufficient) when compared to the factored-up demand $ULS/\phi = V_u/\phi$; thus, it can be said that $\phi V_{max}^{test} > V_u$, especially for the interior (straddle) tests. However, these experimental results include the effects of strain-hardening in the steel; it must be emphasized that this aspect is conservatively ignored, by design. Therefore, to analyze the adequacy of the PT retrofit one should judge the sufficiency of the enhanced strength, and whether this exceeds V_u/ϕ. It is also desirable to experimentally check the condition of the specimens at V_u/ϕ. For *exterior* and *interior reference* cases, the specimens failed with severe cracks over 2.5 mm wide shortly before and after the load achieved V_u/ϕ, respectively. The PT *retrofit* specimens remained in operational condition well beyond *SLS*; the prestress effectively delayed significant cracking until near *ULS*.

4.7. Comparative Analysis

Table 4.2 lists the comparative analysis results within the service limit condition and ultimate limit state for both the *reference* and *PT retrofit* specimens. The measured material properties were used for the service and strength capacity estimations. By comparing predicted service and strength limits to the experimental results, the accuracy of the analysis can be assessed.

4.7.1. Cracking Load Estimation for Establishing Serviceability Limits

To evaluate serviceability, the code-based calculation [10] and a crack control method proposed by Zhu and Hsu [16] were adopted herein. The serviceability rows of Table 4.2 compare the observed and the estimated values for both *exterior* and *interior* regions under service load conditions.

The code-based equation accounts one-half of the yield strength of the hanger reinforcement within the single hanger tributary length $W+3a_v$, where W = width of a bearing pad, a_v = distance from the loading point to the web surface. When compared to the experimental test results, the code-based nominal shear resistance for the serviceability limit state found to be quite conservative, with an average ratio of V_{cr}^{test}/V_{n_SLS} = 1.84. For the crack control approach, Zhu and Hsu [16] have suggested that a modified critical crack width should be adopted for reduced scale inverted-T beams based on the principle of similitude. Since the specimens tested herein were one-half scale, the critical crack widths of 0.08 m and 0.17 mm were adopted for *end face of exterior* and *vicinity of applied load* region cracking estimates (V_{cr}). Using these results, the estimated cracking loads for all specimens are conservative, with an average ratio of V_{cr}^{test}/V_{cr} = 1.19. It is demonstrated that the crack control approach is applicable to conservatively estimate cracking load for inverted-T bent caps and are reasonable to evaluate the serviceability limits for in-service inverted-T bent caps without and with PT retrofit.

Table 4.2. Comparative Analysis for Service and Strength limits

			Specimen*					
			HD Ext.		LD Ext.		HD Int.	
			T1W1** *Ref.*	T2W1 PT	T5E1 *Ref.*	T7W1 PT	T1I1 *Ref.*	T2I1 PT
Service Limit State	Observed	1 Cracking load, V_{cr}^{test}	*144*	246	*141*	226	*180*	313
	Code-based (AASHTO)	2 Code-based, V_{n_SLS}	*67*	135	*125*	193	*67*	152
		3 V_{cr}^{test}/V_{n_SLS}	*2.15*	1.85	*1.13*	1.17	*2.69*	2.06
	Crack Control (Zhu and Hsu, 2005)	4 Estimated, V_{cr}	*114*	180	*133*	205	*167*	252
		5 V_{cr}^{test}/V_{cr}	*1.26*	1.37	*1.06*	1.10	*1.08*	1.24
Ultimate Strength	Observed	6 Failure Mode	*Hanger*	-	*Ledge Flexure*	-	*Hanger*	-
		7 Failure Load, V_{max}^{test}	*294*	366†	*294*	365†	*401*	467†
	Code-based (AASHTO)	8 Controlling Mode	*Hanger*	-	*Ledge Flexure*	-	*Hanger*	-
		9 Sectional Method, V_n	*188*	256	*213*	283	*251*	337
		10 V_{max}^{test}/V_n	*1.56*	1.48	*1.38*	1.29	*1.59*	1.38
	Limit Analysis***	11 Lower Bound, V_{ny} (f_y = 441 MPa)	*251*	319	*271*	339	*313*	399
		12 $\lambda^{\dagger\dagger} = V_{max}^{test}/V_{ny}$	*1.17*	1.18	*1.08*	1.08	*1.28*	1.17
		13 Upper Bound, V_{nu} (f_{su} = 688 MPa)	*391*	459	*417*	485	*489*	574

* *HD = hanger-deficient and LD = ledge-deficient*

** *Test ID includes test information; first number = specimen number, last number = number of test on the location, and second letter = test location on the specimen (W = west, E = east, and I = interior)*

*** *Limit Analysis used modified tributary width as proposed in Figure 3.9*

† *Test termination load (specimens with external PT did not reach limit).*

†† *λ = Strain-hardening scalar, 1.0 <λ < $\lambda_{max} = f_{su}/f_y$= 1.56*

4.7.2. Capacity Estimations at the Ultimate Limit State (ULS)

To evaluate the estimated capacity for the *ULS*, the specimen capacities were calculated and compared to experimental observations. The ultimate limit state rows of Table 4.2 provides observed and estimated capacities for both *reference* and PT *retrofit* specimens.

The specimen capacities were first calculated in accordance with the sectional stress method specified in AASHTO [10]. The ratio of the observed to code-based strength demonstrated that the code-based approach, which assumed the failure associated with the yield strength of the reinforcement, provides significantly conservative strength estimates.

For a more practical estimation, the modified tributary length at both *interior* and *exterior* regions for *hanger* and *ledge-flexural* strengths are adopted herein as shown in Figure 3.9. As shown in Row 10 of Table 4.2, the code-based predictions are rather conservative – 45 percent on average. This is attributed to the fact that not all hangers participating in the failure mechanism were accounted for. This could not account entire hangers that contributed to the failure mechanism. The modified tributary length is shown in Figure 3.9(b), which is extended to the face of the column to account all hanging reinforcement. For ledge-flexure as depicted in Figure 3.9(c), the rational modification for the tributary length was also proposed for the *exterior* region.

The modifications produce more accurate strength prediction results as listed in Rows 11 and 12 of Table 4.2. The predicted strengths remain conservative 8 percent and 20 percent on average for ledge-flexure and hanger capacity, respectively. The high values for hangers are attributed to strain-hardening that occurs in the hanger reinforcement. Upper bound capacities at hanger fracture are listed in Row 13 of Table 4.2. It is clear the

experiment outcome lies between the lower bound (initial yield) condition and the upper bound (hoop fracture) condition.

4.8. Closing Remarks

This research has developed an external prestress retrofit solution for in-service inverted-T bent caps that may be capacity deficient and cracked. Based on the concept development, experimental investigation, and analysis presented herein, the following conclusions are drawn:

1) By balancing the dead load reactions at or nearby the girder seats using PT, both serviceability and the ultimate limit state conditions can be improved.
2) For both the cantilever and straddle parts of the inverted-T specimens, the PT *retrofit* solution successfully postponed cracking and failure. That is, the retrofitted specimens remained in a serviceable condition beyond *SLS* and without significant cracking until *ULS* was approached.
3) By repairing the specimen using external PT solution, pre-existing cracks were successfully restrained, and the ultimate strength was improved to provide similar performance obtained for the uncracked specimen that was retrofitted. Thus, both retrofit and repair of deficient inverted-T bent caps using external PT are a simple and effective means to extend the service life.
4) Based on the experimental analysis, it is demonstrated that the code-based serviceability and ultimate strength capacity predictions are somewhat conservative. For the serviceability limit, the crack control approach proposed by Zhu and Hsu [16] is applicable to conservatively estimate the serviceability limit

of inverted-T bent caps without and with the PT retrofit. To predict more practical ultimate strength capacity, it is recommended to adopt the modified tributary width as proposed in Figure 3.9, and conduct a limit analysis.

5. IMPROVING SERVICEABILITY OF CONCRETE RAILROAD TIES USING PRESTRESSED AFRP STRANDS

5.1. Section Summary

Prestressing with steel strands has been a key aspect in providing the required strength and durability for railroad ties (sleepers) needed to resist the loads on heavy haul lines in many countries. In spite of their improved durability in contrast to timber ties, a major flaw seen with concrete ties is deterioration due to the environmental or fatigue loading. Another issue found in concrete ties, not found in timber, is the electrical conductivity. The objective of this research is to design and to evaluate a class of concrete railroad ties utilizing aramid fiber reinforced polymer (AFRP) strand as the prestressing material. AFRP prestressed ties are constructed and tested for serviceability and strength following the guidelines provided by the American Railway Engineering and Maintenance-of-way Association (AREMA). Results demonstrated that AFRP strands are a potential substitute for steel strands. Some detail improvements may be necessary to mitigate cracking, this could be achieved by using smaller diameter strands.

5.2. Introduction

Following the advent of prestressed concrete, many railroad companies introduced prestressed concrete cross ties (sleepers) where the prestress effect was applied through high strength cold-drawn wires. Due to the scarcity of timber, the first application of prestressed concrete ties was on railways in the Great Britain during World War II. In the United States, common usage of prestressed concrete ties began in 1966 [36]. Nowadays,

the widespread use of prestressed concrete railroad ties is largely because of their superior strength, durability, and increased mass which leads to improved alignment stability. Nevertheless, there remain some issues where desirable improvements may be possible to enable concrete ties to reach their full potential [49, 74].

With the worldwide increase in heavy haul lines, there is a need for track systems capable of handling the increased demands imposed, particularly on the railroad ties. Based on the study of Ferdous and Manalo [43], the most common cause of failure of concrete railroad ties is rail seat deterioration. This occurs when a tie experiences a high axle-loads coupled with moisture beneath the rail seats. If the rail seat is damaged, there may a rail-to-rail electrical short leading to a fault within the signaling system. In addition to seat abrasion, another potential failure mode is the corrosion of the prestressing steel within the tie, leading to a loss of prestress and hence the overall strength of the tie. Van Dyk et al. [40] surveyed issues pertaining to prestressed concrete railroad ties among the several U.S. railroad companies. The survey results indicated that concrete cracks near the rail seats and at the center of ties remain an ongoing critical issue affecting tie performance. Consequently, this may lead to corrosion and thereby a loss of prestress and hence the overall strength of the tie [44, 45]. Accordingly, AREMA [37] sets forth stringent minimum standards for strength with the aim to avoid service cracks.

Research has been conducted to improve durability and overall performance of concrete ties so that the total maintenance cost may be lowered. Mindess et al. [47] investigated the ability of fiber reinforced concrete to increase the impact resistance of the tie. Fiber reinforced concrete ties can withstand larger peak loads and absorb more energy

before failure occurs than ordinary prestressed concrete ties. As a result, the use of fiber reinforced concrete has been found to increase the toughness and durability of concrete ties.

Recently, Zeitouni et al. [49] investigated the use of the high strength reduced modulus (HSRM) prestressed concrete railroad ties to overcome premature cracking near the central region of the tie. The authors conducted the four points bending tests and 3-D finite element analysis to investigate the performance of the HSRM ties. The HSRM ties delayed the initiation of tensile cracks with better stress distribution and decreased width and length of the cracks. However, there has been no indication of electrical conductivity and corrosion resistance improvement.

False signaling in the railroad system may become more prevalent than expected if the wet concrete becomes a partial conductor, or the prestressing strands become a high electrical conductor [46]. A standard railway signaling system uses a direct current (DC) circuit to indicate the presence of trains within a track block. Problems arise when deterioration exists in the fastening system or insulator pads, which are designed to electrically isolate the two rails from the steel shoulders anchored into the prestressed concrete. The key issue is that the shoulders are cast into the prestressed concrete ties and often touch or are in direct contact with the steel prestressing strands forming a potential circuit if rail-to-tie insulation breaks down. When shorts within a track block exists, it can be difficult in identifying the offending ties.

Tie failure due to corrosion of the steel reinforcing in the concrete ties is another major issue, particularly in coasted environs. To eliminate or mitigate the corrosion issue

in concrete structures, research on fiber reinforced polymer (FRP) started during the mid-twentieth century to replace steel in corrosion-prone concrete structures. Currently, FRP bars have been adopted in major infrastructure projects as an alternative considering their noncorrosive, high strength to weight proportion, and fatigue properties [51]. However, due to the substantial differences in the physical and mechanical properties between FRP and conventional steel, the use of FRP bars remains a significant challenge for engineers [29].

Gar et al. [75, 76] investigated aramid fiber reinforced polymer (AFRP) strands in an AASHTO I-girder Type I prestressed concrete girder and compared test results with conventional prestressed steel strands; they demonstrated that pretensioned AFRP met both serviceability and strength requirements. They also found that at failure, their AFRP prestressed girder deflections were somewhat less than the deflection of the companion steel prestressed girder. This was because the AFRP system sustained higher strains under service conditions whereas the steel based system yielded earlier. However, their research did not review the corrosion resistance of the AFRP girder in comparison to the prestressed steel girder and how it may affect serviceability.

The purpose of this research is to investigate the potential for a new class of concrete railroad tie that completely replaces the steel prestressing strands with non-corrosive and non-conductive strands. The use of FRP materials is therefore attractive with glass (GFRP), carbon (CFRP), and aramid (AFRP) as being possibilities. GFRP was ruled out due to its low stiffness. Although CFRP has superior stiffness compared to other alternatives including steel, it has been ruled out because the carbon is a capable

conductor, like steel. AFRP has both adequate insulating and stiffness characteristics and has been adopted for this investigation. These objectives may have the potential to benefit the railroad industry through increased safety and reliability of the track over its service lifespan, largely due to the enhancement in durability and serviceability expected from the use of AFRP.

In this study, concrete ties prestressed with AFRP strands are assessed in terms of standard AREMA [37] design and performance specifications. The results of three tests are reported, which consider vertical load and fatigue effects as well as ultimate strength tests.

5.3. Prestressed Concrete Tie Design Requirement

The basis of the present comparative design and performance investigation is a prestressed concrete tie used on heavy haul US railroad as shown in Figure 5.1. Based on the AREMA [37] manual, there are geometrical and strength requirements to design a prestressed concrete tie. These requirements were used to design the alternative prestress selection with AFRP strands.

Embedded shoulders used to fasten the flat-bottom rails to the tie are one of the major items that require consideration in the tie design and strand placement. The shoulders used for the prototype investigated herein were one of the commercial shoulders widely used within the U.S. railroad industry. The clear distance between the shoulders was 171 mm and imbedded 89 mm into the concrete.

There are different parts of a concrete tie that are involved in its design for limit states, including the location of the critical sections, the amount of loss experienced in

prestressing, and materials used for the concrete. AREMA has accounted for various loading and support conditions in the prescriptive minimum positive and negative moments located at the critical sections for the rail seat and tie center [52, 53]. For concrete railroad ties, the critical sections are at the rail seat section (Section A-A in Figure 5.1) under positive moment and at the center of the tie (Section B-B in Figure 5.1) under negative moment [37]. These are the factored design flexures (design moments) that occur when the wheels of a train are directly above the tie. The design moments were used to determine the most efficient layout of the AFRP strands at transfer and service limit state.

The design moments can be calculated based on AREMA [37] Ch. 30 Section 4.4.1.2 with the annual tonnage, average speed, and tie spacing. The factored design positive bending moment is given by

$$M = BVT \tag{5.1}$$

in which M = the factored design positive bending moment at the center of the rail seat; B = unfactored bending moment with a tie length and spacing specified in AREMA [37]; V and T = the speed and tonnage factors, respectively, specified in AREMA [37]. In this study, the design factors adopted are as follows: 600 mm tie spacing; 75 annual MGT (million gross tons); and 100 km/h speed.

(a) Side elevation

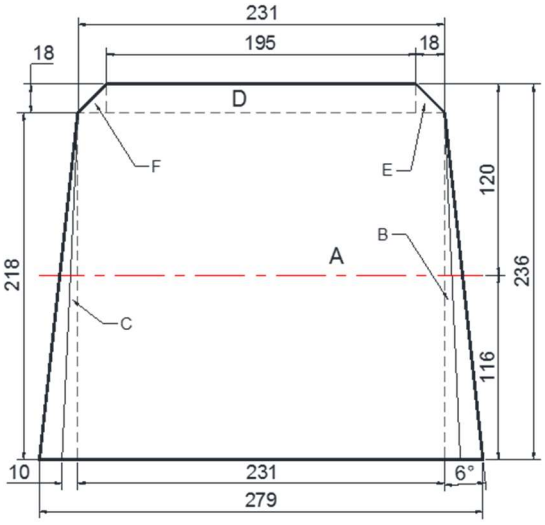

(b) Section A-A (Rail seat)

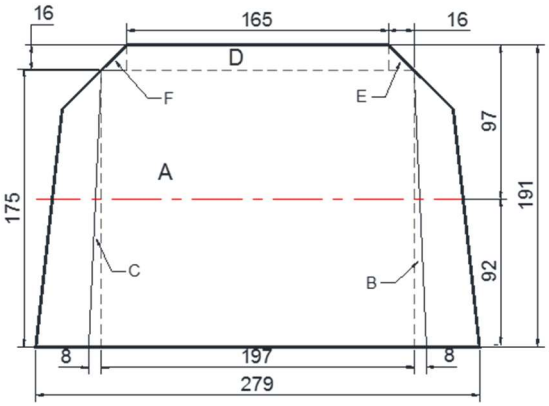

(c) Section B-B (Center)

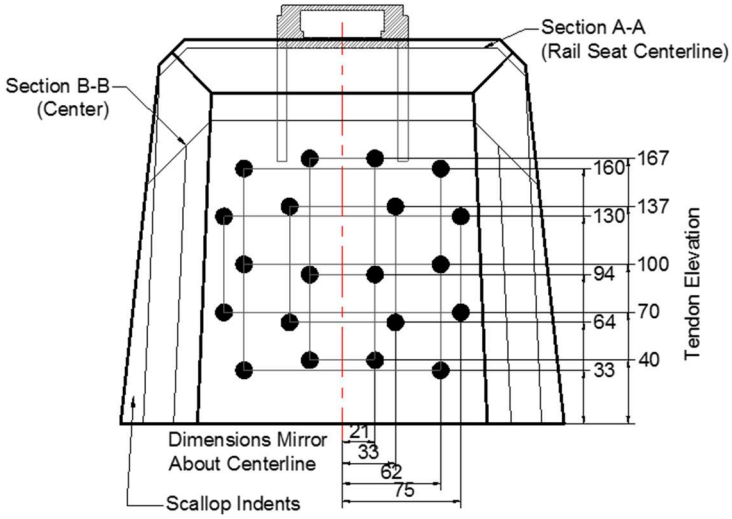

(d) Prestressing steel layout (20 - 5.32mm wires with 48 MPa concrete)

Figure 5.1 A prestressed concrete tie used on heavy haul US railroad: (a) side elevation; (b) rail seat and (c) center cross sections; and (d) combined section showing the location of prestressing wires (mm)

Factored design rail seat negative, the tie center negative, and tie center positive bending moments can be calculated from the factored design positive bending moment, M, using Table 5.1. The calculated design moments, M_{cal}, based on AREMA [37] are listed in Table 5.2.

To design the concrete tie, stresses at both the top and bottom of the tie for each of the four moments exist and need to be checked under service stresses with the design moment externally applied. As the rail seat under positive moment is the most critical to the tie, the primary limiting factor was tension at the bottom of the rail seat under positive moment. The other area of concern was the top of the center under tension stress with negative moment.

Table 5.1 Factors for Bending Moment Calculations

Tie Length	Rail Seat Negative	Center Negative	Center Positive
2.360 m (7'-9")	0.72M	1.13M	0.61M
2.440 m (8'-0")	0.64M	0.92M	0.56M
2.520 m (8'-3")	0.58M	0.77M	0.51M
2.590 m (8'-6")	0.53M	0.67M	0.47M
2.740 m (9'-0")	0.46M	0.57M	0.40M

Table 5.2 Calculated Design Moment

Position and Direction	M_{cal} (kNm)
Rail seat +	+ 34
Rail seat -	- 18
Center -	- 23
Center +	+ 15

The tendon layouts are generally limited by anchorage and stressing requirements. AREMA [37] specifications limit the center-to-center spacing of the AFRP strands to a minimum of 8 mm, while a minimum of 50 mm spacing between the strands was needed to fit the 148 mm diameter anchor.

In this study, Arapree aramid fiber reinforced polymer (AFRP) strands with 10 mm diameter and concrete with three different strengths (48 MPa, 55 MPa, and 62 MPa) were considered for the new concrete tie design. Based on the study of Gar et al. [61], 1400 MPa was adopted as the tensile strength of the AFRP strands.

A systematic search for an appropriate layout was necessary to efficiently use the AFRP strands while maintaining spacing and stress requirements [77]. Determining how many strands are needed per row and their location is an iterative process between finding appropriate spacing for a simple layout, calculating the centroid, and checking transfer and service stresses. Design options for the tie were developed by increasing numbers of AFRP strands. After several iterations, three layouts were found (shown in Figure 5.2) with the desire to have the AFRP centered between the neutral axes of the rail seat and center sections. These layouts are based around a staggered grid idea to ease the prestressing and maintain symmetry about the vertical axis of the cross-section. Figure 5.2 shows the design options, and a final design was selected for construction and testing among the options.

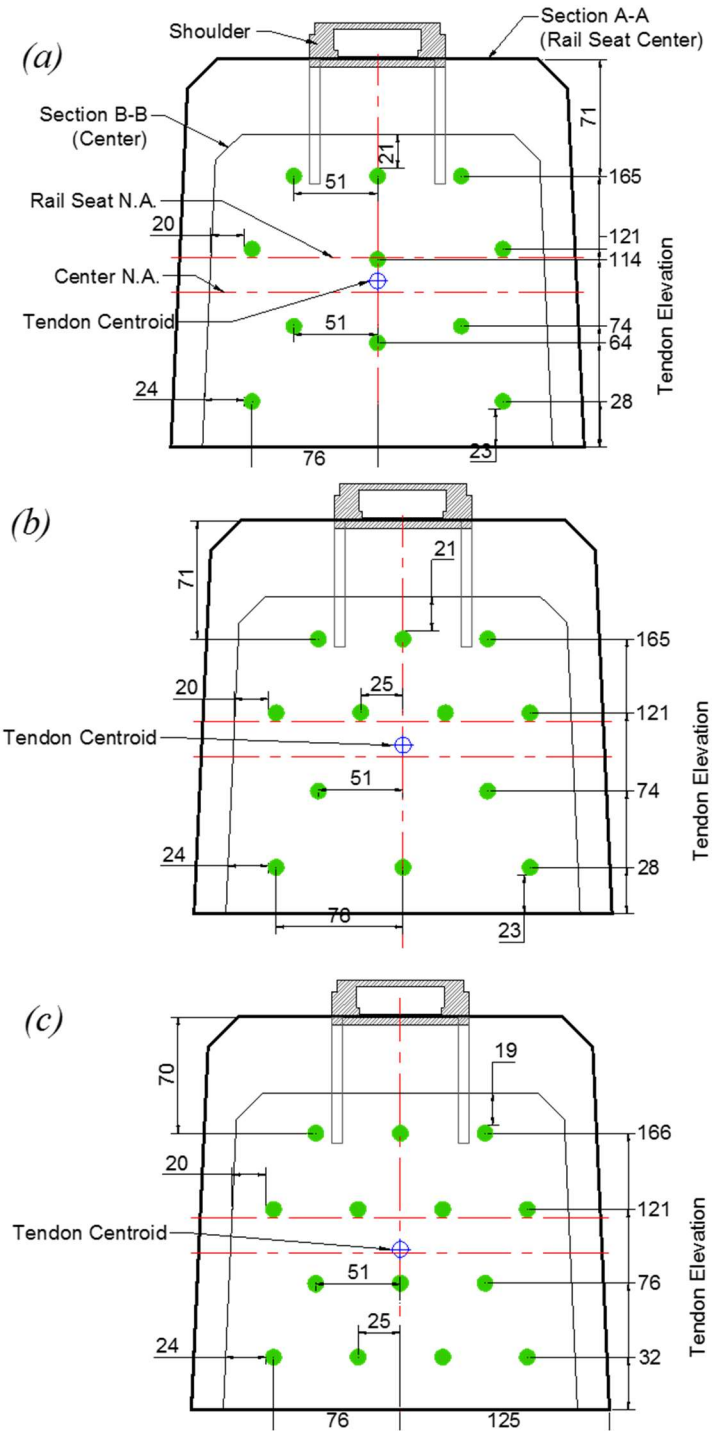

Figure 5.2 Design options showing results increasing numbers of strands for (a) 11 strands for 62 MPa concrete; (b) 12 strands for 48 MPa concrete; and (c) 14 strands with 55 MPa concrete (this layout was adopted for the experimental tests)

A final design was adopted, which utilized 55 MPa strength concrete and 49 kN of initial prestress per strand. This layout has a set of 14 strands in a staggered style as shown in Figure 5.2(c). Given the cover and strengthening clearance restraints at the smallest section at the center, it was found that 14 was the maximum number of strands that could be packed into the space available.

The transfer and service stresses were calculated to check the strength of the tie to meet the stress requirements set in ACI 318 [78] and PCI [79]. Four positions under service load were considered based on the design moments, M_{cal}.

Even though the new anchor can allow up to 60% of the bar capacity (64.8 kN) to be applied to the prestress, Gar et al. [61] recommended not to use initial prestressing of 60% of ultimate capacity. Therefore, a lower initial prestress (from 49 kN force or 45% of the aramid strand capacity) was used in this study, and this load was used as the transfer load in the design checks. With the assumption of 25% loss, 37 kN was the service load to which the design was based.

5.4. Comparative analysis of behavior: AFRP Strands vs. Steel Wires

Based on transformed cracked section calculation analysis and bilinear moment-deflection relationships [79], moment-curvature plots were created and used to expect the behavior of the prestressed concrete tie with AFRP strands under vertical load and to compare to that of a conventional tie with steel wires. The cracking moment is defined by:

$$M_{cr} = f_t S_{x,bot} + \frac{F S_{x,bot}}{A} \pm Fe \tag{5.2}$$

in which $S_{x,bot}$ = the section modulus of the cross-section at the tension face of the concrete tie; F = total initial prestressed force; A = area of tie cross-section; and e = eccentricity defined as the distance from the centroid of the strands to the centroid of the section; and f_t = tensile strength of concrete given by $f_t = 0.5\sqrt{f'_{c\,MPa}}$ where f'_c = specified concrete compressive strength.

Using Eq. (5.2), the cracking curvature may be found from

$$\emptyset_{cr} = \frac{M_{cr}}{E_c I_g} \tag{5.3}$$

in which I_g = second moment of area at the section under consideration; and E_c = concrete modulus, where $E_c = 4700\sqrt{f'_{c\,\mathrm{MPa}}}$.

Figure 5.3 shows the theoretical moment-curvature plots for both the new tie with AFRP strands and the conventional tie with steel wires at critical sections. Prior to the occurrence of cracking, the behavior of the ties with AFPR at each sectional region follows a similar trend to that of the conventional ties counterpart. Following cracking, the post-cracked stiffness of the ties with AFRP is slightly less than conventional steel ties due to the somewhat lower stiffness of AFRP. Nevertheless, this post-cracking behavior eventually leads to a relatively ductile failure when compared to conventional ties with steel prestressing.

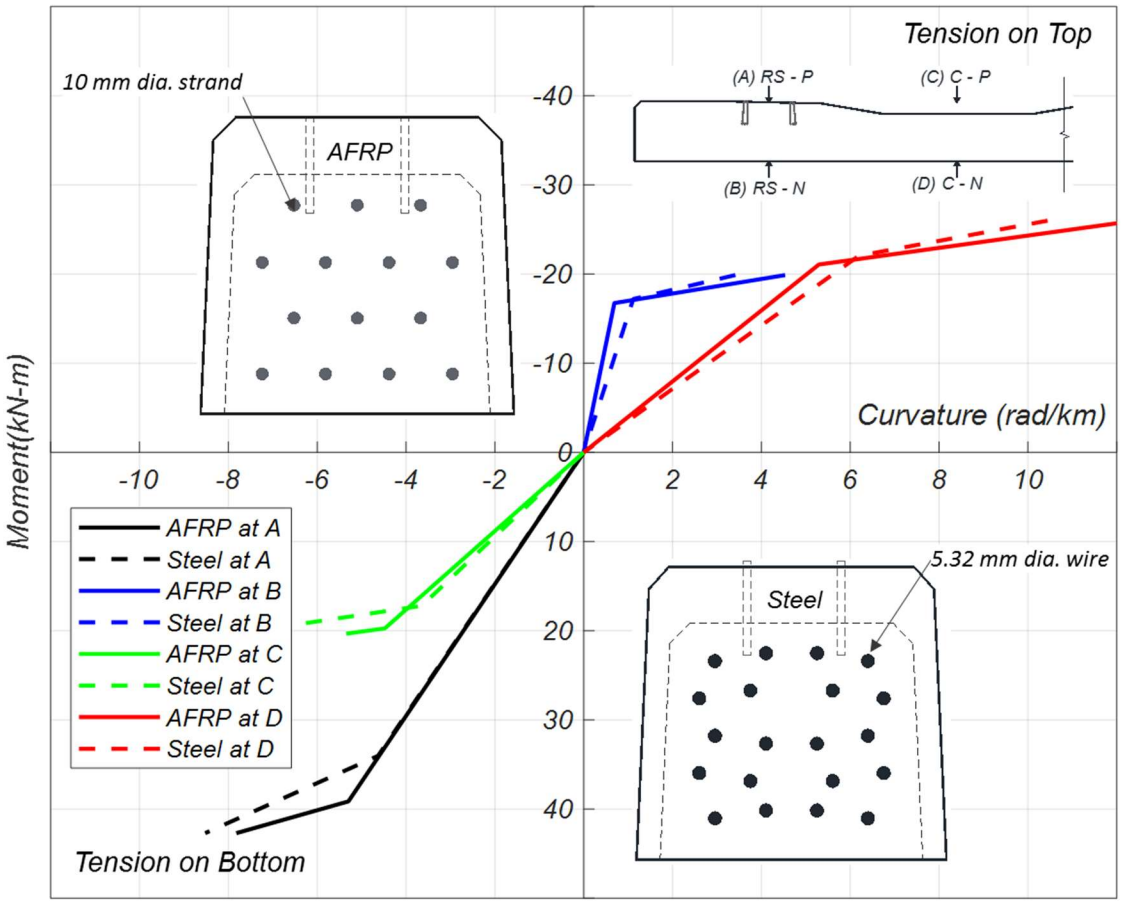

Figure 5.3 Theoretical Moment-Curvature Plots for AFRP tendons and steel wires

5.5. Experimental Investigation

In order to maintain cross-sectional properties from the conventional ties to the new ties, negative polymer molds were built using a urethane rubber. Urethane rubber was selected due to its high level of stiffness. Having a stiffer material means that it will hold its form better when concrete is poured into it. Since conventional ties have a complicated shape, the stiffness of the rubbers plays a significant role. Four boxes were constructed to make four molds to allow for four new ties to be cast at the same time.

To enable the construction of the four ties, a prestressing bed also constructed at the RELLIS Campus of Texas A&M University. The procedure to stress AFRP was adopted from the study of Gar et al. [61]. Each strand required the use of a 38 mm Schedule 80 steel pipe (inner diameter of 38 mm, outer diameter of 48 mm, and wall thickness of 5.1 mm) filled with an expansive grout. Gar et al. [58] used 457 mm long pipes while Gar et al. [61] used a 914 mm long pipe in conjunction with a threaded rod. For this research, 914 mm pipes were adopted used for prestressing AFRP strands. All 14 strands were placed at once and their dead ends grouted in one day, and they were left to cure for 2 days before grouting and stressing the live ends.

To accelerate the stressing process, two center-hole jacks were used simultaneously with 150 mm stroke. The elongation of each strand was calculated using an approximate modulus of elasticity of 69 GPa [61]. The calculated elongation was 117 mm and was used as a field check to determine that if the desired stress had been reached without relying solely on the pressure gauges on the jacks themselves.

Oil pressure was applied to the jacks to achieve the desired 49 kN. During the stressing process, three strands were replaced due to fracture, and the applied load was reduced to 35.6 kN to prevent further strand failure. Overall, an average prestressing force of strands was 38.5 kN, which resulted in 431 kN of a total initial prestressing force with the assumption of 25 percent loss.

On completion of prestressing, concrete was poured into the molds. The concrete mix design was self-consolidating (SCC) with a specified strength of 55MPa. Based on ASTM C1611 [80], a slump flow test was conducted in the field. Twenty-four standard 100 mm x 200 mm test cylinders were also cast for compressive strength tests. According to the average of three compressive strength tests on cylinders, the concrete achieved a 28-day strength of 75.6 MPa.

After at least 48 hours passed and the concrete exceeded the transfer strength of 33 MPa, the AFRP strands were cut and removed from their molds.

5.6. Experimental Tests and Results

To evaluate the new tie, laboratory testing was conducted to ensure whether the ties met minimum specified requirements as set forth in AREMA [37]. In this study, only flexural tests were conducted to determine whether the new tie design is adequate for the expected loads in the field [37]. The flexural tests consisted of two parts: serviceability and ultimate strength.

5.6.1. Serviceability Tests (Static and Fatigue Test)

The serviceability tests include both static and dynamic loading tests to simulate in-service ties. Static tests were conducted on four critical sections while the fatigue test was only conducted on the rail seat in positive bending direction.

5.6.1.1. Vertical Load (Static) Tests

Figure 5.4 shows the test setups and the instrumentation detail to infer section curvatures. To determine if the concrete ties meet cracking strength, a series of vertical load tests were conducted on a set of four specimens for each test: rail seat vertical load tests (positive and negative moment tests) as depicted in Figure 5.4(a) and (b), center negative and positive bending moment tests as illustrated in Figure 5.4(c) and (d). Setup for these tests followed AREMA [37] (Chapter 30 Sections 4.9.1.4, 4.9.1.6, and 4.9.1.7). During testing, some adjustments were made to enable the completion of the experiment. First, the 25.4 mm x 12.7 mm rubber strips, supporting the actuator applied load, were replaced with 12.7 mm x 12.7 mm strips to increase the stability of the load. Second, the hardness of both actuator support strips and tie support pads was increased from 50A as prescribed by AREMA [37] to a stiffer 70A to be more efficient with the materials, as it was formed the 50A rubber would splinter and tear after only a few tests and would need near constant replacement.

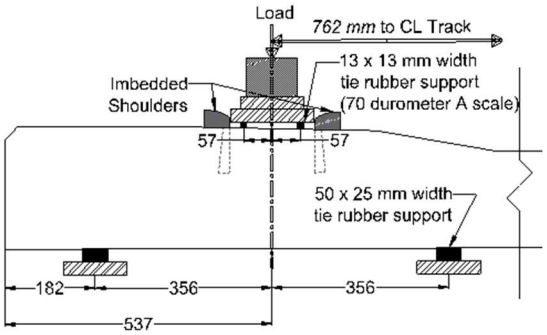

(a) Rail seat positive moment test

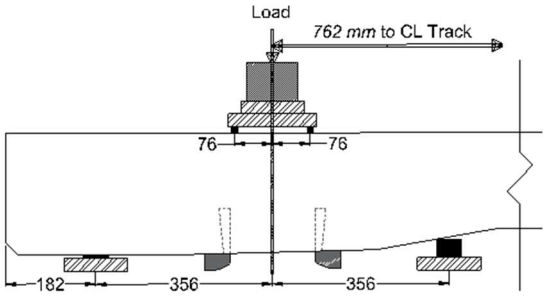

(b) Rail seat negative moment test

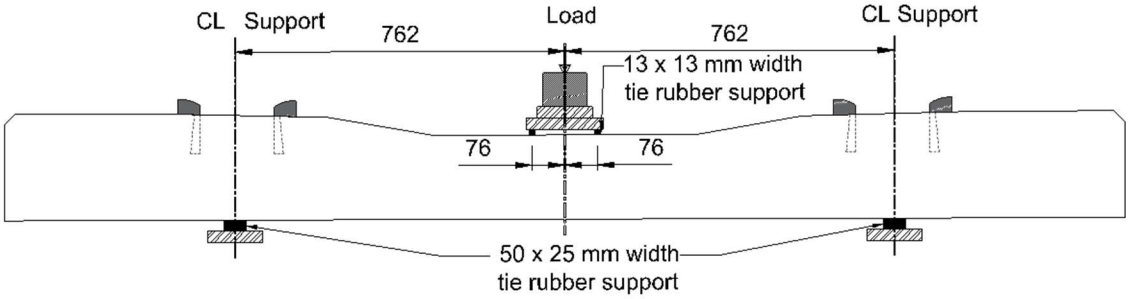

(c) Center positive moment test

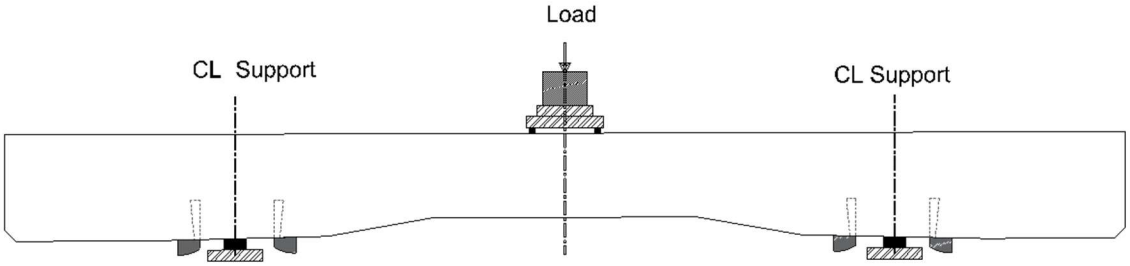

(d) Center negative moment test

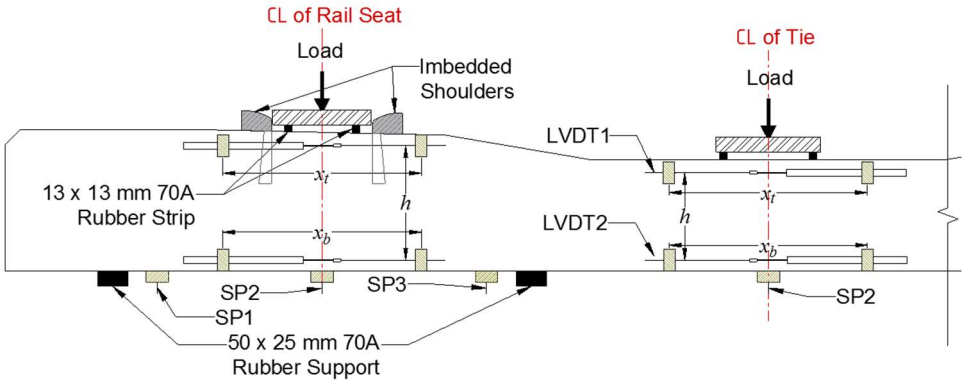

(e) Positive moment test instrumentation to infer section curvatures

Figure 5.4. Test Setups and Instrumentation at Four Critical Sections; (a) and (b) Rail Seats; (c) and (d) Center; and (e) Instrumentation

The load, P, was continuously increased until the design moment, M, achieved as given in Table 5.3. The vertical load tests were terminated at P typically at or above the specified load, P_s, determined from the design moment, M_{cal}. The provided values for design moment, M, test termination load, P, and the specified load, P_s, at each position are listed in Table 5.3.

Curvatures were observed during testing using two Linear Variable Differential Transducers (LVDTs) and three String Potentiometers (string pots) were installed on the tie as shown in Figure 5.4(e). Curvatures were inferred from the measurement differences for xt and xb. The LVDTs were placed along the side of the tie, one at the top and one at the bottom to measure differential displacement along the lateral face of the tie. String pots were placed beneath the tie to measure the vertical deflection of the tie: two adjacent to the supports and the third under the loading point. Data collected from these sensors were used to infer when cracking had occurred during testing.

Table 5.3 Test termination loads for the vertical load test.

Position and direction	Specified load, P_s (kN)	Provided moment, M_p (kNm)	Termination load, P (kN)
Rail seat +	+ 216	+ 43	+ 275
Rail seat -	- 114	- 20	- 128
Center -	- 66	- 26	- 76
Center +	+ 46	+ 16	+ 46

Figure 5.5 presents the inferred moment-curvature behavior for each test with the theoretical bilinear moment-curvature plots. The inferred moment-curvature plots may be used to identify whether the structural cracking occurred or not before the load reaches the specified required load, Ps, which is shown with the black dotted horizontal line in Figure 5.5(a) and (b). Figure 5.5(a) shows the tie behavior under load at central region, while Figure 5.5(b) shows the behavior under load at rail seat region. The theoretical bilinear curves for each position were obtained by using measured material properties. Based on the theoretical curves, all tests meet AREMA [37] requirements except center negative moment test (Figure 5.5(a)). This can explain that either concrete strength or prestressing force has more effect on the tie behavior under vertical load at the central region than at the rail seat region.

According to AREMA [37], if there is no structural cracking, the tie meets the design requirements for each test. Therefore, during each test, a visual inspection was made to determine if structural cracking was observed. Only hairline cracks or no visible crack was found at the specified load, Ps, during all tests except rail seat negative moment tests (0.1 mm average crack width). It should be noted that the tests were not terminated at Ps as specified in AREMA [37] but terminated at P, which is higher than Ps. This resulted in more damage on the specimens than expected and may have had an adverse effect on the following tests.

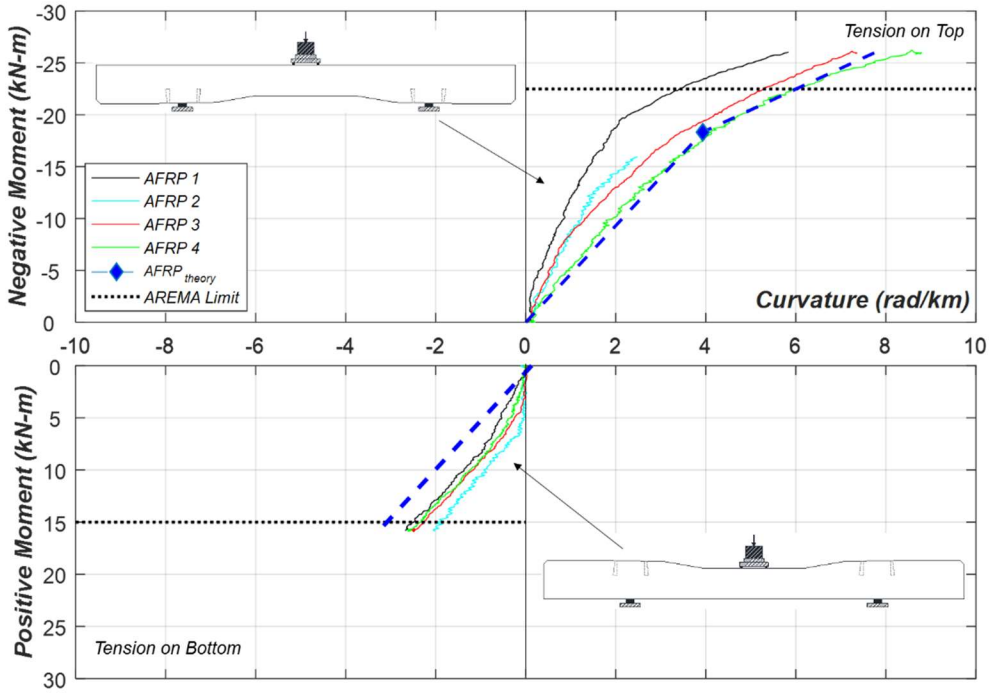

(a) Loaded at central region

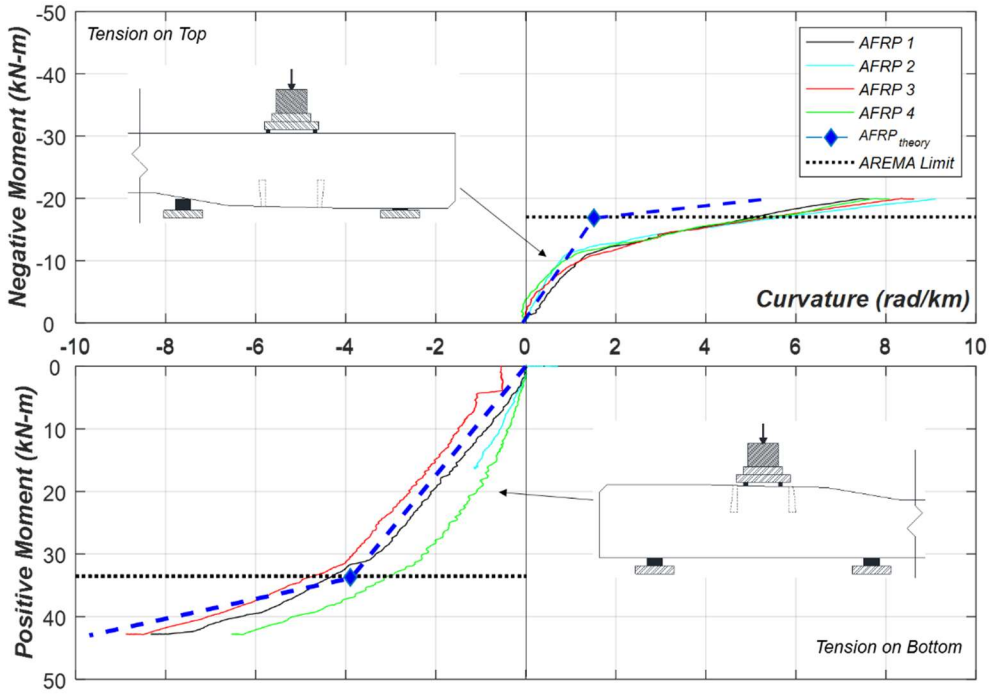

(b) Loaded at rail seat region

Figure 5.5 Vertical load test set up and the result for tie with AFRP tendons

5.6.1.2. Fatigue Test

Repeated load tests are intended to simulate fatigue loading on the ties with a setup as given in AREMA [37]. Figure 5.6 demonstrates schematic fatigue test setup and condition of the railroad ties after fatigue tests. Herein, fatigue tests were only performed at the rail seat and in the positive moment direction. The test setup was similar to the setup for the static positive rail seat vertical load test (Figure 5.4(a)) but with the 203 mm wide and 25 mm thick 70A rubber sheets instead of 51 mm x 25 mm 50A rubber strips. The sheets are far superior to the strips, being able to withstand the repetitive load due to the lack of compression seen by the thicker rubber strips. Another change that was made was to replace the load supporting rubber with 6 mm thick birch hardwood. Also, to prevent the tie from 'walking' while load cycling proceeded, the two rocker supports were tack welded to the floor a piece of sheet metal securely fastened to the strong floor of the lab.

When performing the repeated load test, the cracking load, P_{cr}, was determined first. In this instance, the cracking load is defined as the load in which a crack has formed and propagated from the tension face to the outermost layer of reinforcement [37]. For specimens AFRP 1 and AFRP 2, P_{cr} = 309 kN and 303 kN, respectively. Following initial cracking, the load was lowered to 17.8 kN, and cyclic loading was conducted from 17.8 kN to $1.1P_{cr}$ = 339 kN and 333 kN for AFRP 1 and AFRP 2, respectively. Approximately 3 million cycles were applied at a rate of 3.5 Hz. To meet AREMA [37] requirements, the tie needs to support a static load of $1.5P_{cr}$, applied at the same location of the repetitive load; no tendon slippage above 0.025 mm, concrete compression failure, shear cracking, or tendon rupture once the repetition of the load was complete is permitted. For AFRP 1

and AFRP 2 specimens, the static loads at $1.5P_{cr}$ = 463 kN and 454 kN, respectively. Since the requirements are specified for a prestressed concrete tie with steel wires, the maximum specified slippage of 0.025 mm needs to be modified by multiplying by the modular ratio, $n = E_s/E_{AFRP} = 2.83$, where E_s = modulus of elasticity for steel = 200 GPa and E_{AFRP} = modulus elasticity for AFRP = 70.5 GPa. Thus, the maximum specified tendon slippage for AFRP strands may be specified as 0.071 mm instead of 0.025 mm.

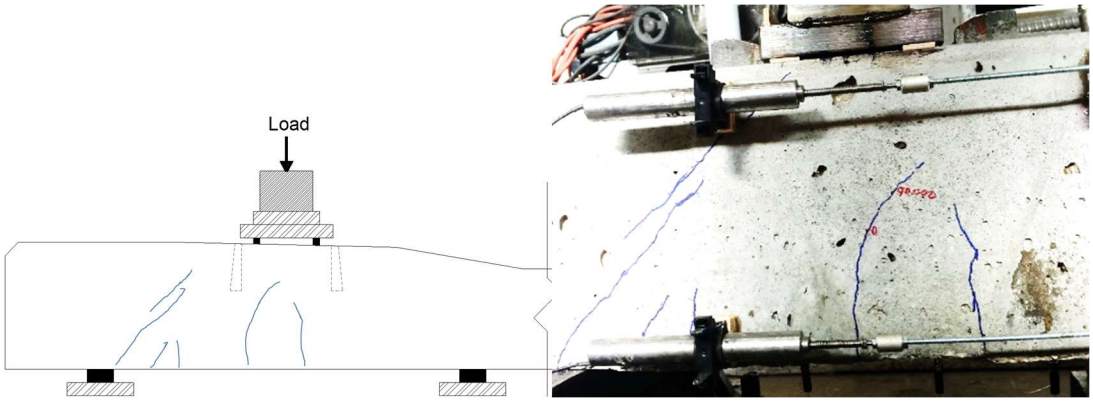

(a) Specimen AFRP 1

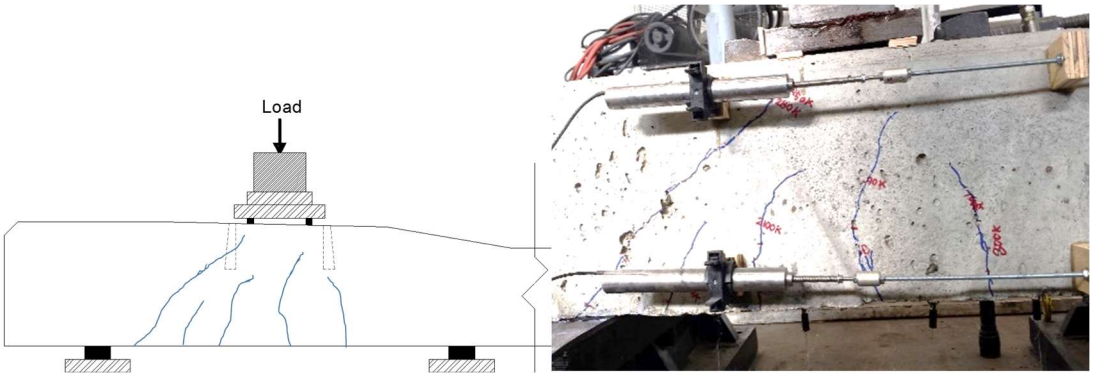

(b) Specimen AFPR 2

Figure 5.6 Fatigue tests showing nature of cracks at the end of test

Both specimens were able to support a rail seat load of 1.5Pcr with tendon slippage less than 0.071 mm, and no concrete compressive failure or tendon failure. Some concrete shear cracks were observed. For both specimens AFRP 1 and AFRP 2, flexure-shear cracks were found during the repetitive tests at approximately 1 million and 800,000 cycles, respectively. No additional cracks were formed while a static load of $1.5P_{cr}$ was loading, but the existing flexural and shear cracks grew slightly. The maximum width for shear cracks after holding the static load was measured as 0.45 mm and 0.41 mm for AFRP 1 and AFRP 2, respectively.

5.6.3. Ultimate Strength Test

A code-based ultimate load test is intended to establish the maximum load and failure mode of the ties [37]. A static load of 1.5P was applied to another positive rail seat region, where the fatigue test was not conducted. The load held for at least 3 minutes, while the bottom layer of reinforcement was checked for tendon slippage. If the slippage was less than 0.071 mm (for AFRP strands), then the tie was deemed to meet bond requirements. Subsequently, the specimen was then loaded until failure. Once failure commenced, tendon slippage, maximum load, and the failure mode were documented. Table 5.4 and Figure 5.7 show the ultimate test results with the minimum required load ($1.5P$) and the allowable tendon slippage (0.071 mm).

Table 5.4 Ultimate strength test result

Specimen	Min. required load (kN)	Max. load (kN)	Slip at 412 kN (mm)	Slip at max load (mm)
AFRP 1	412	629	0.044	0.102
AFRP 2		657	0.014	0.025

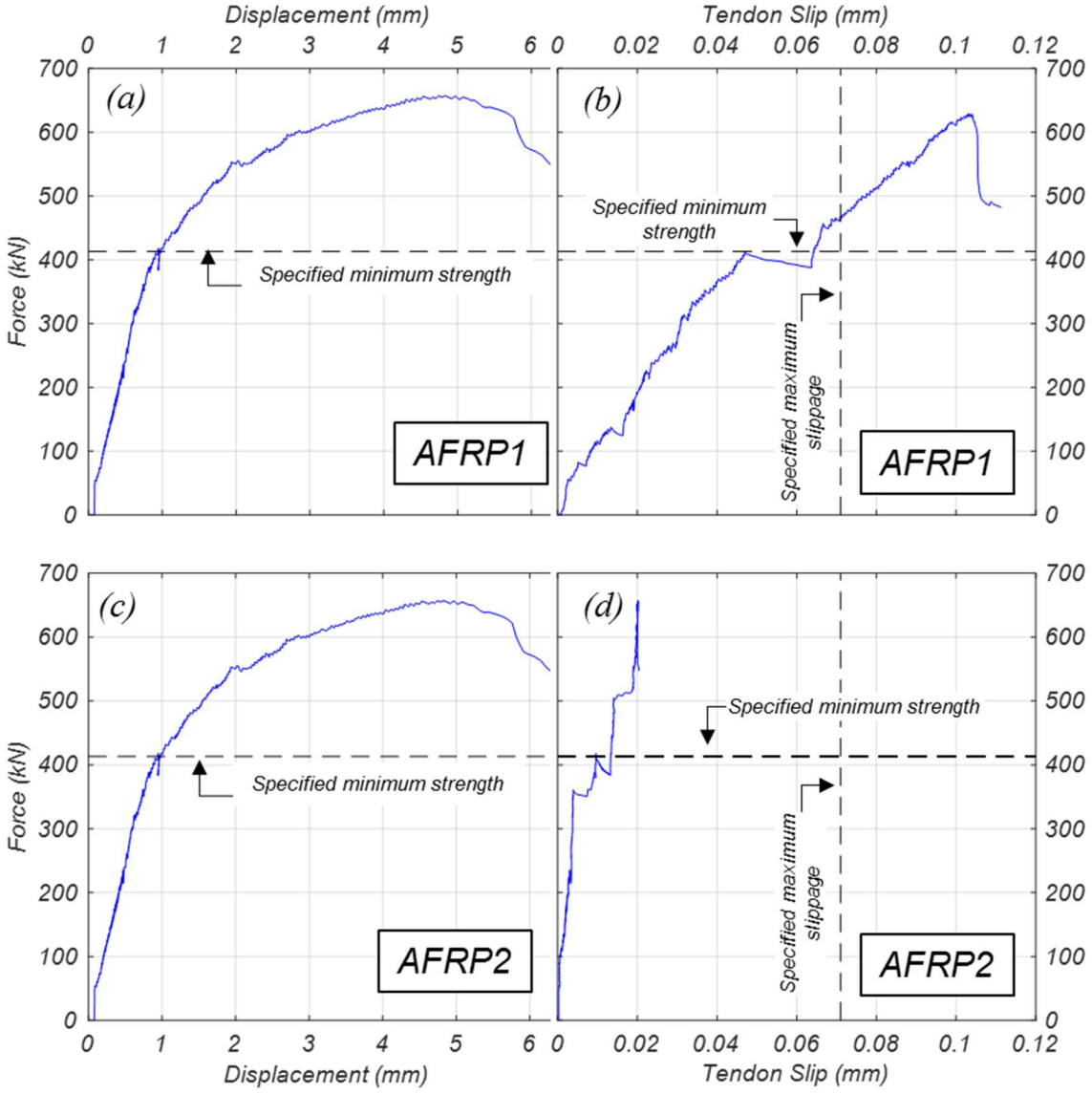

Figure 5.7 Results for ultimate strength tests: (a) and (c) are load-deflection curves for AFRP 1 and AFRP 2, respectively; (b) and (d) show tendon slippage for AFRP 1 and AFRP 2, respectively

When the static load of $1.5P = 412$ kN was held for 3 minutes, no tendon slippage larger than 0.071 mm, no shear crack, and no concrete nor tendon failures were observed. For specimen AFRP 1, the strands slipped while the load was held at 1.5P, but that slippage did not exceed 0.071 mm. The strand slippage was observed to be larger than the 0.071 mm specified maximum at a load of 620 kN which is greater than the 412 kN minimum strength as shown in Figure 5.7(b). Sudden tendon slip was observed at loads of approximately 350 kN and 510 kN for specimen AFRP 2. However, the maximum tendon slip of the specimen was 0.014 mm, which is somewhat smaller than the maximum specified slippage of 0.071 mm, at the ultimate strength. Thus, the tie with AFRP strands met bond development and ultimate strength requirements in accordance with AREMA [37].

5.7. Discussion

The new tie with AFRP strands was designed in accordance with AREMA [37] and PCI [79], and several tests were conducted to evaluate the tie. According to the tests, the new tie with AFPR strands met most of the AREMA [37] requirements with the exception of the small hairline cracks during fatigue test and the vertical load test under negative bending moment near the rail seat region. Even though all test results could not fully meet AREMA [37] requirements due to the premature cracks, the new ties with AFRP strands show promise in replacing conventional ties because of noncorrosiveness and nonconductive material property of AFRP. Unlike prestressing steel, AFRP will not lead to corrosive damage caused by minor cracking.

To overcome these minor deficiencies, there are three major factors that should be considered to improve tie performance with AFRP strands: concrete strength, prestressing force on AFRP strands, and diameter and bond length of AFRP strands. These factors are explained in what follows.

First, self-consolidating concrete (SCC) was used in this investigation. The design of the prestressed concrete members requires an estimation for the properties of SCC. Existing design equations to predict the properties of SCC provide up to 30% error [81]. Therefore, further study for the design of PSC ties with SCC is needed; however, stronger concrete is recommended.

Second, several AFRP strands fractured during stressing and required replacement during construction. The prestress losses became difficult to quantify and the effect on the behavior of the ties remains unclear. It is believed this problem could be more easily overcome in a full length long-line commercial prestressing bed.

Third, the required transfer length to accomplish the transfer from prestressing strands to the concrete by bond highly depends on the diameter of the strands [79]. The used AFRPs in this investigation had a diameter that was twice that of steel wires used in comparative analysis as shown in Figure 5.1. Therefore, smaller diameter strands are recommended for future AFRP application to successfully replace prestressing steel wires. It is recommended that further verification tests using smaller diameter of AFRP strands to be conducted.

5.8. Closing Remarks

Based on the research present herein, the following conclusions are drawn:

1) Crack-free performance is essential for the corrosion mitigation and preservation of ties which use prestressing steel. The use of AFRP prestressing strands to mitigate corrosion potential shows promise. And although crack-free performance may remain desirable, it is contended that it may not be essential as corrosion is not a significant concern.
2) The ties with 10 mm diameter AFRP strands met the minimum strength and bond development requirements, although some minor cracks were observed during the tests near the rail seat where was within the bond length region. Improved crack-free AFRP ties should be further investigated, and it may be achievable by using smaller diameter strands that have a shorter bond length.
3) The adoption of AFRP prestressing strands may achieve better track fault-free signaling. Although the shoulders, which are imbedded into the ties, may touch the AFRP prestressed strands due to a tie deterioration, an electrical short is less likely for AFRP strands because they are nonconductive in nature. Such verifications of insulation attributes should be the subject of future research.

6. SUMMARY, CONCLUSIONS, AND RECOMMENDATIONS

6.1. Summery

In-service concrete infrastructure commonly has faced problems related to increasing load demands by heavy haul traffic. Such concrete structures have experienced increasing crack widths as well as unexpected new cracks. Together, these cracks may decrease service life and are possible signs of structural deficiencies. Concepts for improving the performance of inverted-T bent caps and railroad ties were developed and experimentally validated.

First, for inverted-T bent caps, a conceptual design of eighteen alternative retrofit solutions were developed to address the ledge flexure, hanger, and/or punching shear deficiencies which were identified in previous studies based on the current design specification. The different solutions included both metallic and fiber reinforced polymer materials, which are applied either with or without prestress. To identify which retrofit solutions are most viable, a weighted sum decision making model was used based on six criteria: (i) strength-increase, (ii) cost, (iii) constructability, (iv) dimensional/clearance constraints, (v) durability, and (vi) ease of monitoring. Among the most highly ranked solutions, through-web post-installed post-tensioning threadbar with catcher channel (and end-region stiffener) and load balancing post-tensioning solutions were selected for further investigation and experimental validation. Based on one-half scale experimental tests, results demonstrated that the specimens are strengthened and the solutions were capable of restraining any pre-existing cracks thereby delaying failure. Design and retrofit recommendations were provided, including their limitations.

Second, using non-metallic aramid fiber reinforced polymer instead of the usual steel strands for prestressing concrete railway sleepers (ties) was explored. Such a switch in prestress materials may help in reducing electric leakage when in service; however, the strength, stiffeness, and crack resistance due to the material change should not be inferior. Test results on sleepers prestressed by aramid fiber reinforced polymer strands demonstrated that the strands were capable of providing sufficient strength and stiffness. Recommendations were made on how the performance could be improved by using smaller diameter strands to delaying further cracking beneath the rail seats.

6.2. Conclusions

With the concepts of improving the performance of inverted-T bent caps and railroad ties, their effectiveness was experimentally investigated. Based on the investigations, the following conclusions are drawn:

1. In-service inverted-T bent caps have shown signs of distress through a series of disquietening cracks observed in the field (Figure 3.1). When evaluated against current standards, such inverted-T bent caps often possess marginal strength capacities. To economically retrofit such deficient structures, augment load paths are necessary. Therefore, eighteen alternative retrofit solutions for in-service inverted-T bent caps are developed to improve performance in terms of serviceability and ultimate strength. The solutions were assessed using a multi-criteria decision making (MCDM) method to identify most viable solutions for further investigation. The current objective, to rate and rank diversity of retrofit solutions to improve serviceability of inverted-T bent caps, was achieved in a robust fashion. Weighted sum model efficiently considered all

six criteria (strength increase, cost, constructability, dimensional and clearance constraints, durability, and ease of monitoring) while providing flexibility to consider different weight factors for each criterion depending on their importance. With the given rank-order of the criteria, top half solutions are determined to be viable with any reasonably defendable combination of weights.

2. Based on the analysis results, the most critical criteria and measure was '*Strength'* followed by '*Cost'*. The results represent that the weights for '*Strength*' and '*Cost'* criteria are highly contributed to the ranking of the alternative solutions, and thus, it should be carefully decided based on the condition of the bridges. For this study, a load balancing PT solution (Solution 14), concrete infill with partial- and full-depth FRP wrap with waling solutions (Solutions 16 and 17), enlarged bearing pad solution (Solution 18), and through-web post-installed PT threadbar with catcher channel (Solution 8) are deemed the most viable.
3. The experimental investigations were conducted to evaluate the effectiveness of these solutions. This study focused on the retrofit solutions utilizing post-tensioning techniques: (i) Through-web post-tensioning PT threadbar with catcher channel (Solution 8) to provide supplemental hanger and ledge capacity via bolts drilled through the web of the inverted-T section and connected to a catcher channel. The end region of a cantilever inverted-T bent cap beam is also often deficient and this can be retrofitted by bonding and bolting a steel end-plate system. (ii) Load-balancing external PT (Solution 14) balancing the dead load reactions at or nearby the girder seats using PT to improve both serviceability and the ultimate limit state conditions.

Experiments, conducted as proof-of-concept tests, demonstrated that both serviceability and the ultimate limit state conditions may be markedly improved by providing augment load paths.

4. For both the straddle (interior) and cantilever (exterior) parts of the inverted-T specimens, the through-web post-installed PT threadbar with catcher channel solution successfully postponed and reduced cracking. That is, the retrofitted specimens remained in a serviceable condition below the *serviceability* limit and without significant cracking until the *ultimate* limit was approached. The end-region stiffener solution also successfully delayed cracking and provided additional strength to the cantilever (exterior) part of the inverted-T bent cap specimens. With the proposed rational modification, this solution may be the most efficient approach for end-region capacity deficient or cracked cantilever inverted-T bent caps.
5. The PT *retrofit* solution successfully postponed cracking and failure for both the cantilever and straddle parts of the inverted-T specimens. That is, the retrofitted specimens remained in a serviceable condition beyond the *SLS* limit and without significant cracking until the *ULS* limit was approached. By repairing the specimen using external PT solution, pre-existing cracks were successfully restrained, and the ultimate strength was improved to provide similar performance obtained for the uncracked specimen that was retrofitted. Thus, both retrofit and repair of deficient inverted-T bent caps using external PT are a simple and effective means to extend the service life.

6. It was also demonstrated that the code-based serviceability and ultimate strength capacity predictions are somewhat conservative based on the experimental analysis. For the serviceability limit, the crack control approach proposed by (Zhu and Hsu, 2005) is applicable to conservatively estimate the serviceability limit of inverted-T bent caps without and with the PT retrofit. To predict more practical ultimate strength capacity, it is recommended to adopt the modified tributary width as proposed in Figure 3.9, and conduct a limit analysis.
7. Crack-free performance is essential for the corrosion mitigation and preservation of ties which use prestressing steel. The use of AFRP prestressing strands to mitigate corrosion potential shows promise. And although crack-free performance may remain desirable, it is contended that it may not be essential as corrosion is not a significant concern. The ties with 10 mm diameter AFRP strands met the minimum strength and bond development requirements, although some minor cracks were observed during the tests near the rail seat where was within the bond length region. Improved crack-free AFRP ties should be further investigated, and it may be achievable by using smaller diameter strands that have a shorter bond length. The adoption of AFRP prestressing strands may achieve better track fault-free signaling. Although the shoulders, which are imbedded into the ties, may touch the AFRP prestressed strands due to a tie deterioration, an electrical short is less likely for AFRP strands because they are nonconductive in nature. Such verifications of insulation attributes should be the subject of future research.

6.3. Recommendations

Based on the findings from this study, recommendations to extend the results of this research include the followings:

1. Selection of retrofit solutions should be based primarily on the deficiencies of in-service inverted-T bent caps, with additional consideration for obstacles to implementation, initial costs, and life-cycle costs. Ultimately, selection of the retrofit solutions may depend on the unique characteristics of a project (bent configuration, location, and bridge purpose), typical practices of local jurisdictions, and importance assigned to each selection criterion. Although one-half scaled test results demonstrated that the retrofit solutions improved overall performance of the bet caps in terms of serviceability and ultimate strength, experimental investigation for full -scale retrofit solutions need to be conducted to consider the superstructure of a bridge and limitations for field application.
2. To improve tie performance with AFRP strands, three major factors may need to be considered: (i) self-consolidating concrete (SCC) was used but some errors may be provided when predicting the properties of SCC using existing design equations for normal concrete. Therefore, further study for the design of PSC ties with SCC is needed; however, stronger concrete is recommended. (ii) Use of a full length long-line commercial prestressing bed is recommended for prestressing AFRP strands to quantify the effect on the behavior of the ties. (iii) Smaller diameter strands are recommended for future AFRP applications to successfully replace prestressing steel wires to accomplish the transfer from prestressing strands to the concrete by bond

without premature cracks beneath the rail seats. Further verification tests using smaller diameter of AFRP strands need to be conducted.

3. Retrofit solutions using prestressing techniques show promise to improve serviceability and ultimate strength capacities of inverted-T bent caps. However, as noted in this study, the conventional steel PT strand (and threadbar) has a potential issue related to corrosion when it is exposed to crucial environment, and thus, use of a greased and sheathed strand is recommended for external retrofitting to prevent potential corrosion. Whereas, AFRP strands, which is noncorrosive and nonconductive material, may also be an option to replacing conventional steel PT strands. This study demonstrated that replacing usual steel strands for concrete railroad sleepers to AFRP strands help in reducing a potential of corrosion while the strength, stiffness, and crack resistance was not inferior. In addition, AFRP strand application to the deficient inverted-T bent caps does not require any bond length, which was a minor issue in railroad tie application. Therefore, further investigation on application of AFRP strands to inverted-T bent caps to improve performance is recommended to be conducted.

7. REFERENCES

[1] Sussmann, T., and Thompson, H., "Track structural design for maintenance and rehabilitation with automated track inspection data," presented at the International Heavy Haul Association, Cape Town, South Africa, 2017.

[2] Furlong, R.W., Ferguson, P.M., and Ma, J.S., "Shear and anchorage study of reinforcement in inverted T-beam bent cap girders," Center for Highway Research, the University of Texas at Austin, Research Report 113-4, 1971.

[3] Furlong, R., and Mirza, S., "Strength and Serviceability of Inverted T-Beam Caps Subject to Combined Flexure, Shear, and Torsion," Center for Highway Research, the University of Texas at Austin, Research Report l53-1F, 1974.

[4] Zhu, R.R.H., Dhonde, H., and Hsu, T.T.C., "Crack Control for Ledges in Inverted'T'Bent Caps," University of Houston, Department of Civil & Environmental Engineering, Research Report 0-1854-5, October 15 2003.

[5] Larson, N., Gomez, E.F., Garber, D., Bayrak, O., and Ghannoum, W., "Strength and serviceability design of reinforced concrete inverted-T beams," Center for Transportation Research, The University of Texas at Austin, FHWA/TX-13/0-6416-1, June 2013.

[6] Hurlebaus, S., Mander, J.B., Birely, A.C., Terzioglu, T., Cui, J., and Park, S.H., "Strengthening of existing inverted-T bent caps. Volume 1: Preliminary design," Texas A&M Transportation Institute, Texas A&M University System, FHWA/TX-18/0-6893-R1-Vol1, 2018.

[7] Mirza, S.A., and Furlong, R.W., "Design of reinforced and prestressed concrete inverted T beams for bridge structures," *PCI Journal,* vol. 30, no. 4, pp. 112-137, 1985.

[8] Garber, D.B., Varney, N.L., Gómez, E.F., and Bayrak, O., "Performance of Ledges in Inverted-T Beams," *ACI Structural Journal,* vol. 114, no. 2, 2017.

[9] Deifalla, A., and Ghobarah, A., "Behavior and analysis of inverted T-shaped RC beams under shear and torsion," *Engineering structures,* vol. 68, pp. 57-70, 2014.

[10] AASHTO, *AASHTO LRFD Bridge Design Specifications*, 8th ed. Washington DC: American Association of State Highway and Transportation Officials (AASHTO), 2017.

[11] AASHTO, *AASHTO LRFD Bridge Design Specifications*, 7th ed. Washington DC: American Association of State Highway and Transportation Officials (AASHTO), 2014.

[12] Deifalla, A., Awad, A., and Elgarhy, M., "Effectiveness of externally bonded CFRP strips for strengthening flanged beams under torsion: An experimental study," *Engineering structures,* vol. 56, pp. 2065-2075, 2013.

[13] Mirza, S., Furlong, R., and Ma, J., "Flexural shear and ledge reinforcement in reinforced concrete inverted T-girders," *ACI Structural Journal,* vol. 85, no. 5, pp. 509-520, 1989.

[14] Mirza, S.A., and Furlong, R.W., "Serviceablity Behavior and Failure Mechanisms of Concrete Inverted T-Beam Bridge Bentcaps," *ACI Journal,* Technical Paper vol. 80, no. 4, pp. 294-304, 1983.

[15] Zhu, R.R.H., and Hsu, T.T.C., "Crack Width Prediction for Exterior Portion of Inverted'T'Bent Caps," University of Houston, Department of Civil & Environmental Engineering, Research Report 0-1854-4, April 1 2003.

[16] Zhu, R.R.H., and Hsu, T.T.C., "Crack width prediction for ledges in inverted 'T'bent caps," *ACI Special Publication,* vol. 225, pp. 179-196, 2005.

[17] Zhu, R.R.H., Wanichakorn, W., Hsu, T.T.C., and Vogel, J., "Crack width prediction using compatibility-aided strut-and-tie model," *Structural Journal,* vol. 100, no. 4, pp. 413-421, 2003.

[18] Zhu, R.R.H., and Hsu, T.T.C., "Crack Width Prediction for Ledges in Inverted 'T' Bent Caps," *ACI Symposium Publication,* vol. 225, 3/1/2005.

[19] Galal, K., and Sekar, M., "Rehabilitation of RC inverted-T girders using anchored CFRP sheets," *Composites Part B: Engineering,* vol. 39, no. 4, pp. 604-617, 2008.

[20] Higgins, C.C., Howell, D.A., Smith, M.T., and Senturk, A.E., "Shear repair methods for conventionally reinforced concrete girders and bent caps: final report, December 2009," School of Civil and Construction Engineering, Oregon State University, FHWA OR-RD-10-09, 2009.

[21] Goebel, J.H., Johnson, B.A., and Higgins, C., "Strength and durability of near-surface mounted CFRP bars for shear strengthening reinforced concrete bridge girders," Oregon Department of Transportation, Research Section, FHWA-OR-RD-12-12, 2012.

[22] Chaallal, O., Mofidi, A., Benmokrane, B., and Neale, K.J.J.o.c.f.c., "Embedded through-section FRP rod method for shear strengthening of RC beams: Performance and comparison with existing techniques," vol. 15, no. 3, pp. 374-383, 2011.

[23] Breveglieri, M., Aprile, A., and Barros, J.A., "Embedded Through-Section shear strengthening technique using steel and CFRP bars in RC beams of different percentage of existing stirrups," *Journal Composite Structures,* vol. 126, pp. 101-113, 2015.

[24] Woods, E.A., "Shear strengthening and model testing of concrete bridge headstocks," Bachelor of Engineering, Civil Engineering, University of Southern Queensland, Toowoomba, Australia, 2004.

[25] Aravinthan, T., and Suntharavadivel, T., "Effects of existing shear damage on externally posttensioned repair of bent caps," *Journal of Structural Engineering,* vol. 133, no. 11, pp. 1662-1669, 2007.

[26] Multco.us. (2018, February). *Hawthorne and Morrison Bridges Bent Cap Strengthening Project*. Available: https://multco.us/bridges/hawthorne-and-morrison-bridges-bent-cap-strengthening-project

[27] Bank, L.C., *Composites for construction: structural design with FRP materials*. Hoboken, NJ: John Wiley & Sons, 2006.

[28] Daly, A.F., and Witarnawan, W., "A method for increasing the capacity of short and medium span bridges," in *Proceedings of the 10th REAAA Conference*, Tokyo, Japan, September 2000.

[29] Yang, J.-M., Min, K.-H., Shin, H.-O., and Yoon, Y.-S., "Effect of steel and synthetic fibers on flexural behavior of high-strength concrete beams reinforced with FRP bars," *Composites Part B: Engineering,* vol. 43, no. 3, pp. 1077-1086, 2012.

[30] Khaloo, A.R., "Shear Repair of Reinforced Concrete Beams Using Post-Tensioning," *ACI Special Publication,* Symposium Paper vol. 193, pp. 519-550, 8/1/2000.

[31] Martinola, G., Meda, A., Plizzari, G.A., and Rinaldi, Z., "Strengthening and repair of RC beams with fiber reinforced concrete," *Cement and concrete composites,* vol. 32, no. 9, pp. 731-739, 2010.

[32] Nordin, H., "Fibre reinforced polymers in civil engineering: flexural strengthening of concrete structures with prestressed near surface mounted CFRP rods," Master of Science, Department of Civil Engineering, Luleå University of Technology, Luleå, Sweden, 2003.

[33] Rojob, H., and El-Hacha, R., "Self-prestressing using iron-based shape memory alloy for flexural strengthening of reinforced concrete beams," *ACI Structural Journal,* vol. 114, no. 2, p. 523, 2017.

[34] Tanarslan, H., "Flexural strengthening of RC beams with prefabricated ultra high performance fibre reinforced concrete laminates," *Engineering Structures,* vol. 151, pp. 337-348, 2017.

[35] ACI Committee 364.2T, *Increasing Shear Capacity Within Existing Reinforced Concrete Structures* (Technical Documents). 2008.

[36] White, J.G., "Concrete tie track system," *Transportation Research Record,* vol. 953, pp. 5-11, 1984.

[37] AREMA, "Concrete Ties," in *Manual for railway engineering*, vol. 1Landover,MD: American Railway Engineering and Maintenance-of-Way Association (AREMA), 2015.

[38] Venuti, W., "Concrete Railroad Ties in North America," *Concrete International,* vol. 2, no. 1, pp. 25-32, 1980.

[39] AAR, "Class I Railroad Statistics," ed: Association of American Railroads, 2015.

[40] Van Dyk, B.J., Dersch, M.S., and Edwards, J., "International concrete crosstie and fastening system survey–final results," RailTEC, University of Illinois at Urbana-Champaign, Technical Report, 2012.

[41] NTSB, "Metro-North Railroad Derailment," in "Railroad Accident Brief," The National Transportation Safety Board, NTSB/RAB-14/11, 2014, Available: https://www.ntsb.gov/investigations/AccidentReports/Reports/RAB1411.pdf.

[42] Zeman, J.C., Edwards, J.R., Barkan, C.P., and Lange, D.A., "Failure mode and effect analysis of concrete ties in North America," in *Proceedings of the 9th International Heavy Haul Association Conference*, 2009, pp. 270-278.

[43] Ferdous, W., and Manalo, A., "Failures of mainline railway sleepers and suggested remedies–review of current practice," *Engineering Failure Analysis,* vol. 44, pp. 17-35, 2014.

[44] Rezaie, F., and Farnam, S., "Fracture mechanics analysis of pre-stressed concrete sleepers via investigating crack initiation length," *Engineering Failure Analysis,* vol. 58, pp. 267-280, 2015.

[45] Soltanian, H., Firouzi, A., and Mohammadzadeh, S., "Time dependent reliability analysis of railway sleepers subjected to corrosion," *Structural Concrete,* vol. 19, no. 5, pp. 1409-1418, 2018.

[46] Sengul, O., and Gjørv, O.E., "Effect of embedded steel on electrical resistivity measurements on concrete structures," *ACI Materials Journal,* vol. 106, no. 1, p. 11, 2009.

[47] Mindess, S., Yan, C., and Venuti, W.J., "Impact Resistance of Fibre Reinforced Prestressed Concrete Railroad Ties," *Special Publication,* vol. 128, pp. 183-200, 1991.

[48] Donovan, B., "Development of a durable concrete railroad tie," Master of Science, Civil Engineering, University of Nevada, Reno, Ann Arbor, 1997.

[49] Zeitouni, A.I., Rizos, D.C., and Qian, Y., "Benefits of high strength reduced modulus (HSRM) concrete railroad ties under center binding support conditions," *Construction and Building Materials,* vol. 192, pp. 210-223, 2018.

[50] Li, Z., Khennane, A., Hazell, P.J., and Remennikov, A.M., "Performance of a hybrid GFRP-concrete beam subject to low-velocity impacts," *Composite Structures,* vol. 206, pp. 425-438, 2018/12/15/ 2018.

[51] Selvachandran, P., Anandakumar, S., and Muthuramu, K., "Deflection of prestressed concrete beam using fiber reinforced polymer (FRP) tendon," *Australian Journal of Structural Engineering,* vol. 17, no. 3, pp. 188-196, 2016.

[52] Lutch, R.H., Harris, D.K., and Ahlborn, T.M., "Prestressed concrete ties in North America," in *Proceeding of AREMA Annual Conference*, 2009, pp. 1-39.

[53] Harris, D.K., Lutch, R.H., Ahlborn, T.M., and Duong, P., "Optimization of a prestressed concrete railroad crosstie for heavy-haul applications," *Journal of Transportation Engineering,* vol. 137, no. 11, pp. 815-822, 2011.

[54] ACI Committee 440, *ACI-440.4R-04 Prestressing Concrete Structures with FRP Tendons (Reapproved 2011)*. 2011, p. 35.

[55] Noël, M., and Soudki, K., "Fatigue behavior of GFRP reinforcing bars in air and in concrete," *Journal of Composites for Construction,* vol. 18, no. 5, p. 04014006, 2014.

[56] El Refai, A., "Durability and fatigue of basalt fiber-reinforced polymer bars gripped with steel wedge anchors," *Journal of Composites for Construction,* vol. 17, no. 6, p. 04013006, 2013.

[57] Younes, T., Al-Mayah, A., and Topper, T., "Fatigue performance of prestressed concrete beams using BFRP bars," *Construction and Building Materials,* vol. 157, pp. 313-321, 2017.

[58] Gar, S.P., Head, M.H., and Hurlebaus, S., "Computational Modeling of Aramid Fiber-Reinforced Polymer Prestressed Girder in Composite Action with Bridge Deck," *ACI Structural Journal,* vol. 110, no. 6, 2013.

[59] McKay, K., and Erki, M., "Aramid tendons in prestressed concrete applications," in *Proceedings of 1st International Conference on Advanced Composite Materials in Bridges and Structures*, 1992, pp. 221-230.

[60] Gar, S.P., "Structural performance of a full-depth precast bridge deck system prestressed and reinforced with AFRP bars," Ph.D., Department of Civil Engineering, Texas A&M University, College Station, Texas, 2012.

[61] Gar, S.P., Hurlebaus, S., Mander, J.B., Cummings, W., Prouty, M.J., and Head, M.H., "Sustainability of Transportation Structures Using Composite Materials to

Support Trade and Growth," Texas A&M Transportation Institute, College Station, Texas, SWUTC/14/600451-00009-1, June 2014.

[62] Ho, W., "Integrated analytic hierarchy process and its applications–A literature review," *European Journal of operational research,* vol. 186, no. 1, pp. 211-228, 2008.

[63] Chauhan, A., and Vaish, R., "Magnetic material selection using multiple attribute decision making approach," *Materials & Design (1980-2015),* vol. 36, pp. 1-5, 2012.

[64] Zavadskas, E.K., Turskis, Z., and Kildienė, S., "State of art surveys of overviews on MCDM/MADM methods," *Technological and economic development of economy,* vol. 20, no. 1, pp. 165-179, 2014.

[65] Mardani, A., Jusoh, A., Md Nor, K., Khalifah, Z., Zakwan, N., and Valipour, A., "Multiple criteria decision-making techniques and their applications – a review of the literature from 2000 to 2014," *Economic Research-Ekonomska Istraživanja,* vol. 28, no. 1, pp. 516-571, 2015/01/01 2015.

[66] Fishburn, P.C., "Letter to the editor—additive utilities with incomplete product sets: application to priorities and assignments," *Operations Research,* vol. 15, no. 3, pp. 537-542, 1967.

[67] Peng, Y., "Regional earthquake vulnerability assessment using a combination of MCDM methods," *Annals of Operations Research,* vol. 234, no. 1, pp. 95-110, 2015.

[68] Terzioglu, T., Karthik, M.M., Hurlebaus, S., and Hueste, M.B.D., "Systematic Assessment of Nondestructive Evaluation Techniques for Post-Tensioning and Stay Cable Systems," *Journal of Infrastructure Systems,* vol. 25, no. 2, p. 04019015, 2019.

[69] Butler, J., Jia, J., and Dyer, J., "Simulation techniques for the sensitivity analysis of multi-criteria decision models," *European Journal of Operational Research,* vol. 103, no. 3, pp. 531-546, 1997/12/16/ 1997.

[70] Triantaphyllou, E., and Sánchez, A., "A Sensitivity Analysis Approach for Some Deterministic Multi-Criteria Decision-Making Methods*," *Decision Sciences,* vol. 28, no. 1, pp. 151-194, 1997/01/01 1997.

[71] AISC Committee 360, *Specification for structural steel buildings (ANSI/AISC 360-10)*. Chicago, IL: American Institute of Steel Construction, 2010.

[72] ACI Committee 318, *Building code requirements for structural concrete (ACI 318-14) and commentary*. Farmington Hills, MI: American Concrete Institute, 2014.

[73] Suntharavadivel, T.G., and Aravinthan, T., "Overview of external post-tensioning in bridges," in *Proceedings of the 2005 Southern Region Engineering Conference (SREC 2005)*, 2005, pp. 29-38: Engineers Australia, Toowoomba Local Group.

[74] Yu, H., Jeong, D., Marquis, B., and Coltman, M., "Railroad concrete tie failure modes and research needs," in *2015 Transportation Research Board 94th Annual Meeting, TRB15-0311*, 2015.

[75] Gar, S.P., Head, M., Hurlebaus, S., and Mander, J.B., "Comparative experimental performance of bridge deck slabs with AFRP and steel precast panels," *Journal of Composites for Construction,* vol. 17, no. 6, p. 04013014, 2013.

[76] Gar, S.P., Head, M., Hurlebaus, S., and Mander, J.B., "Experimental performance of AFRP concrete bridge deck slab with full-depth precast prestressed panels," *Journal of Bridge Engineering,* vol. 19, no. 4, p. 04013018, 2014.

[77] Posluszny, R.D., "Applications of prestressed AFRP bars in concrete railroad ties," Master of Science, Civil Engineering, Texas A&M University, Collge Station, Texas, 2016.

[78] ACI Commitee 318, *Building Code Requirements for Structural Concrete (ACI 318-14) and Commentary*. American Concrete Institute (ACI), 2014.

[79] PCI, H. Wilden, Ed. *PCI Design Handbook: Precast and Prestressed Concrete*. Precast/Prestressed Concrete Institute, 2010.

[80] *ASTM C1611/C1611M-09 Standard Test Method for Slump Flow of Self-Consolidating Concrete*, 2009.

[81] Kim, Y.H., Trejo, D., Atahan, H.N., and Hueste, M.B.D., "Mechanical property prediction for high early strength self-consolidating concrete," *Journal of materials in civil engineering,* vol. 24, no. 12, pp. 1501-1512, 2012.

APPENDIX A

This appendix provides scores that used in Section 2 for evaluation retrofit solutions for in-service inverted-T bent caps.

Table A.1. Scores for Strength Increase Criteria

		Location and Deficiency							Retrofit System		Avrg. Score
		Interior			Exterior			Score	System	Score	
	Retrofit Solution	LF	P	H	LF	P	H				
1	Prestressed high strength threadbar	3	3	0	0	0	0	4.0	Strengthening system	6	5.0
2	Steel hanger bracket	3	3	0	1	1	0	5.3	Alternative load path	8	6.7
3	End region stiffener	0	0	0	1	1	2	2.7	Passive support system	4	3.3
4	Clamped cross threadbar	3	3	0	2	2	0	6.7	Passive support system	4	5.3
5	Grouted cross threadbar	3	3	0	2	2	0	6.7	Passive support system	4	5.3
6	Upper seat brackets	3	3	0	1	1	0	5.3	Alternative load path	8	6.7
7	Threadbar hanger with steel bracket	3	3	0	1	1	0	5.3	Passive support system	4	4.7
8	Through-web post-installed PT threadbar with catcher channel	3	3	3	2	2	2	10.0	Alternative load path	8	9.0
9	Grouted threadbar anchored with channel	3	3	0	2	2	0	6.7	Passive support system	4	5.3
10	Anchored FRP wrap	3	3	3	2	2	2	10.0	Passive support system	4	7.0
11	Concrete infill with prestressing threadbar	3	3	1	1	1	1	6.7	Alternative load path	8	7.3
12	Concrete infill with hanger threadbar	3	3	3	2	2	2	10.0	Alternative load path	8	9.0
13	Concrete masonry piers	3	3	3	2	2	2	10.0	Alternative load path	8	9.0
14	Load balancing post tensioning (PT)	3	3	3	2	2	2	10.0	Active support system	10	10.0
15	Concrete infill with FRP anchored by FRP anchors	3	3	0	2	2	2	8.0	Passive support system	4	6.0
16	Concrete infill with partial-depth FRP anchored by steel waling	3	3	0	2	2	2	8.0	Alternative load path	8	8.0
17	Concrete infill with full-depth FRP anchored by steel waling	3	3	3	2	2	2	10.0	Alternative load path	8	9.0
18	Enlarged bearing pad	0	3	0	0	1	0	2.7	Active support system	10	6.3

Table A.2. Scores for Total Cost Criteria

No	Retrofit Solution	Total Cost	Score
1	Prestressed high strength threadbar	$39K	7
2	Steel hanger bracket	$17K	9
3	End region stiffener	$10K	10
4	Clamped cross threadbar	$39K	7
5	Grouted cross threadbar	$31K	7
6	Upper seat brackets	$25K	8
7	Threadbar hanger with steel bracket	$21K	8
8	Through-web post-installed PT threadbar with catcher channel	$19K	9
9	Grouted threadbar anchored with channel	$22K	8
10	Anchored FRP wrap	$35K	7
11	Concrete infill with prestressing threadbar	$28K	8
12	Concrete infill with hanger threadbar	$63K	4
13	Concrete masonry piers	$83K	2
14	Load balancing post tensioning (PT)	$24K	8
15	Concrete infill with FRP anchored by FRP anchors	$62K	4
16	Concrete infill with partial-depth FRP anchored by steel waling	$35K	7
17	Concrete infill with full-depth FRP anchored by steel waling	$39K	7
18	Enlarged bearing pad	$6K	10

Table A.3. Scores for Constructability Criteria

No.	Retrofit Solution	Risk of Damaging Reinforcement		Accessibility Requirements		Lane closure below the bridge		Lane closure above the bridge		Total weight to be lifted		Avrg. Score
		Risk	Score	Accessibility	Score	No. of days	Score	No. of days	Score	kips	Score	
1	Prestressed high strength threadbar	Low	6	Sides and/or Ends	10	12	6	0	10	18.0	0	6.4
2	Steel hanger bracket	Very low	8	Behind the girders	2	5	9	0	10	2.2	8	7.4
3	End region stiffener	High	2	Sides and/or Ends	10	3	9	0	10	1.0	9	8.0
4	Clamped cross threadbar	Very High	0	Web and/or Ledges	6	17	5	0	10	1.1	9	6.0
5	Grouted cross threadbar	High	2	Bottom	8	16	5	0	10	0.60	10	7.0
6	Upper seat brackets	Very Low	8	Web and/or Ledges	6	7	8	0	10	3.2	7	7.8
7	Threadbar hanger with steel bracket	Medium	4	Web and/or Ledges	6	7	8	0	10	2.0	8	7.2
8	Through-web post-installed PT threadbar with catcher channel	High	2	Deck and/or Bottom	4	7	8	7	8	4.4	6	5.6
9	Grouted threadbar anchored with channel	Medium	4	Bottom	8	15	5	0	10	5.1	5	6.4
10	Anchored FRP wrap	Medium	4	Diaphragm and Web	0	13	6	0	10	1.9	9	5.8
11	Concrete infill with prestressing threadbar	Low	6	Deck and/or Bottom	4	12	6	6	9	1.3	9	6.8
12	Concrete infill with hanger threadbar	Medium	4	Deck and/or Bottom	4	23	3	7	8	1.8	9	5.6
13	Concrete masonry piers	No Risk	10	Bottom	8	> 30	0	0	10	4.5	6	6.8
14	Load balancing post tensioning (PT)	Medium	6	Behind the girders	2	3	9	4	9	5.8	5	6.2
15	Concrete infill with FRP anchored by FRP anchors	Medium	4	Web and/or Ledges	6	10	7	6	9	1.9	9	7.0
16	Concrete infill with partial-depth FRP anchored by steel waling	Medium	4	Web and/or Ledges	6	16	5	0	10	1.5	9	6.8
17	Concrete infill with full-depth FRP anchored by steel waling	Medium	4	Web and/or Ledges	6	10	7	6	9	1.9	9	7.0
18	Enlarged bearing pad	Very low	10	Under the Girders	0	2	10	2	10	0.9	10	8.0

Table A.4. Scores for Dimensional and Clearance Constraint Criteria

No.	Retrofit Solution	Dimensional and Clearance Constraint (in.)	Score
1	Prestressed high strength threadbar	0.0	10
2	Steel hanger bracket	0.0	10
3	End region stiffener	0.5	9
4	Clamped cross threadbar	5.5	3
5	Grouted cross threadbar	5.5	3
6	Upper seat brackets	0.0	10
7	Threadbar hanger with steel bracket	2.8	7
8	Through-web post-installed PT threadbar with catcher channel	4.5	5
9	Grouted threadbar anchored with channel	4.5	5
10	Anchored FRP wrap	0.0	10
11	Concrete infill with prestressing threadbar	0.0	10
12	Concrete infill with hanger threadbar	3.8	6
13	Concrete masonry piers	> 9	0
14	Load balancing post tensioning (PT)	0.5	9
15	Concrete infill with FRP anchored by FRP anchors	0.0	10
16	Concrete infill with partial-depth FRP anchored by steel waling	0.0	10
17	Concrete infill with full-depth FRP anchored by steel waling	0.0	10
18	Enlarged bearing pad	0.0	10

Table A.5. Scores for Durability/Longevity Criteria

No.	Retrofit Solution	Corrosion		Debonding		Risk of Fatigue and Fracture		Avrg. Score
1	Prestressed high strength threadbar	Directly exposed to environment below the bent	2	No risk of debonding	10	None	10	7.3
2	Steel hanger bracket	Directly exposed to environment on the web/ledges	0	Large diameter epoxy anchor bolts	6	Very high	0	2.0
3	End region stiffener	Directly exposed to environment on the web/ledges	0	Small diameter epoxy anchor bolts	8	Very low	8	5.3
4	Clamped cross threadbar	Fully enclosed	6	No risk of debonding	10	None	10	8.7
5	Grouted cross threadbar	Enclosed and grouted	8	Grouted thread bars under concentric loading	4	None	10	7.3
6	Upper seat brackets	Directly exposed to environment on the web/ledges	0	Small diameter epoxy anchor bolts	8	High	2	3.3
7	Threadbar hanger with steel bracket	Directly exposed to environment on the web/ledges	0	Small diameter epoxy anchor bolts	8	High	2	3.3
8	Through-web post-installed PT threadbar with catcher channel	Fully enclosed	6	No risk of debonding	10	Very low	8	8.0
9	Grouted threadbar anchored with channel	Enclosed and grouted	8	Grouted thread bars under concentric loading	4	Very low	8	6.7
10	Anchored FRP wrap	Noncorrosive material	10	Anchored FRP installation using epoxy	2	None	10	7.3
11	Concrete infill with prestressing threadbar	Enclosed and grouted	8	No risk of debonding	10	None	10	9.3
12	Concrete infill with hanger threadbar	Enclosed and grouted	8	No risk of debonding	10	None	10	9.3
13	Concrete masonry piers	Noncorrosive material	10	No risk of debonding	10	None	10	10.0
14	Load balancing post tensioning (PT)	Enclosed and grouted	8	No risk of debonding	10	Medium	4	7.3
15	Concrete infill with FRP anchored by FRP anchors	Enclosed and grouted	8	Anchored FRP installation using epoxy	2	None	10	6.7
16	Concrete infill with partial-depth FRP anchored by steel waling	Directly exposed to environment on the web/ledges	0	Anchored FRP installation using epoxy	2	None	10	4.0
17	Concrete infill with full-depth FRP anchored by steel waling	Directly exposed to environment on the web/ledges	0	Anchored FRP installation using epoxy	2	None	10	4.0
18	Enlarged bearing pad	Noncorrosive material	10	No risk of debonding	10	None	10	10.0

Table A.6. Scores for Ease of Monitoring Criteria

No.	Retrofit Solution	Ease of Monitoring	Score
1	Prestressed high strength threadbar	Borescope testing	4
2	Steel hanger bracket	Visual inspection using a lift	8
3	End region stiffener	hands on inspection	6
4	Clamped cross threadbar	Borescope testing	4
5	Grouted cross threadbar	Inspection using NDT	2
6	Upper seat brackets	Visual inspection using a lift	8
7	Threadbar hanger with steel bracket	Borescope testing	4
8	Through-web post-installed PT threadbar with catcher channel	Borescope testing	4
9	Grouted threadbar anchored with channel	Inspection using NDT	2
10	Anchored FRP wrap	Detailed hands-on inspection	6
11	Concrete infill with prestressing threadbar	Inspection using NDT	2
12	Concrete infill with hanger threadbar	Inspection using NDT	2
13	Concrete masonry piers	Visual inspection from ground	10
14	Load balancing post tensioning (PT)	Visual inspection using a lift	8
15	Concrete infill with FRP anchored by FRP anchors	Inspection using NDT	2
16	Concrete infill with partial-depth FRP anchored by steel waling	Borescope testing	4
17	Concrete infill with full-depth FRP anchored by steel waling	Inspection using NDT	2
18	Enlarged bearing pad	Visual inspection using a lift	8